VICTORIA UNIVERSITY OF WELLINGTON
Te Whare Wānanga o te Ūpoko o te Ika a Māui

ANTARCTIC RESEARCH CENTRE

Antarctic Data Series No 25

OCEANOGRAPHY AND SEDIMENTATION BENEATH THE MCMURDO ICE SHELF IN WINDLESS BIGHT, ANTARCTICA

2005
(Revised August 2007)

P.J. Barrett[1], L. Carter[1], D. Damiani[2], G.B. Dunbar[1], E. Dunker[3], G. Giorgetti[2], M.A. Harper[1], R.M. McKay[1], F. Niessen[3], U. Nixdorf[3], A.R. Pyne[1], C. Riesselmann[4], N. Robinson[5], C. Hollis[6] and P. Strong[6]

[1] Antarctic Research Centre, Victoria University of Wellington, PO Box 600, Wellington, NZ.
[2] Dipartimento di Scienze della Terra, Università di Siena, 8 via Laterina, Siena 52100, Italy.
[3] Alfred Wegener Institut fur Polar- und Meerforschung, Columbusstrasse, Bremerhaven, Germany.
[4] Department of Geological & Environmental Sciences, Stanford University, Stanford, CA 90425, USA.
[5] National Institute of Water and Atmospheric Research, PO Box 14-901, Kilbirnie, Wellington, NZ.
[6] Institute of Geological and Nuclear Sciences, PO Box 30-368, Lower Hutt, NZ.

in association with the

SCHOOL OF EARTH SCIENCES
Te Kura Tātai Aro Whenua

Cover image: Field Camp at Windless Bight with Mt Erebus on the right.

Contents

Figures

Tables

ABSTRACT

This report presents new data on oceanographic conditions and sedimentation beneath the McMurdo Ice Shelf south of Ross Island, in preparation for deep drilling as part of the ANDRILL project. The goal was to survey two potential drill sites in order to help plan for the drilling system and to understand the present day sedimentation regime. Field data were gathered in January 2003, through access holes 0.6 m wide made with the AWI hot water drilling system. The two sites lie 5 and 12 km east of the shelf edge near Scott Base. They were covered by ice 70 and 143 m thick, and the sea floor was 926 and 923 m below sea level respectively.

Water column measurements from the two locations show that the net current direction is to the east from McMurdo Sound through to the Ross Ice Shelf, with speeds averaging 5 to 7 cm/sec but at times reaching 17 cm/sec. Flows at a third and shallower location at the ice shelf edge below the sea ice off Scott Base were in the same net direction but much stronger – up to 60 cm/sec. Water column profiles of salinity and temperature show the first parameter is fairly conservative but temperature exhibits marked fine scale variability over a tidal cycle. Nevertheless, the water column structure is similar to that found 25 years ago at the first ever hole drilled through the Ross Ice Shelf 400 km south at Site J9. These waters are some of the coldest and densest in the world, helping to drive the global thermohaline circulation system.

The sea floor at both sites is soft mud with diatoms and calcareous microfossils. Diatoms are abundant in open Ross Sea surface waters, and mostly sink to the sea floor as pellets but some are swept under the ice shelf by currents. Calcareous microfossils are found locally in shallower depths, and were not expected here because of the cold and deep corrosive waters. One of the cores passed down into a stony glacial deposit representing sediment released from basal ice grounded 20,000 years ago when ice filled most of the Ross Sea after the last glaciation. However penetration of low energy (3.5 kHz) seismic waves 300 m into the soft sea floor suggests that the sites were too deep to have been overcompacted or eroded by grounded ice. This observation, together with the fine-grained nature of the sediment confirms the basin's suitability for the planned 1000-m-deep ANDRILL hole for recovering a long and sensitive record of Ross Ice Shelf history. Current speeds in the water column also indicate its technical feasibility.

1 INTRODUCTION

Peter Barrett

This project was designed both to investigate the little explored sub-ice shelf environment and to provide essential site data for coring 1000 m into the sea floor by ANDRILL (Lacy et al., 2002) for a history of the McMurdo-Ross Ice Shelf (MRIS). The weight of Ross Island has been depressing the crust for at least the last million years, resulting in a depression over 900 m deep around the island in which sediment has been accumulating (Figure 1). These sediments have recorded periods of Ross Ice Shelf stability, along with past episodes of both more extensive ice (with possible grounding) during glacial periods and less extensive ice (with sea ice or open water in place of the present shelf ice) during warmer interglacials. The texture of the sea floor sediments also reflects variations in the current regime beneath the ice shelf.
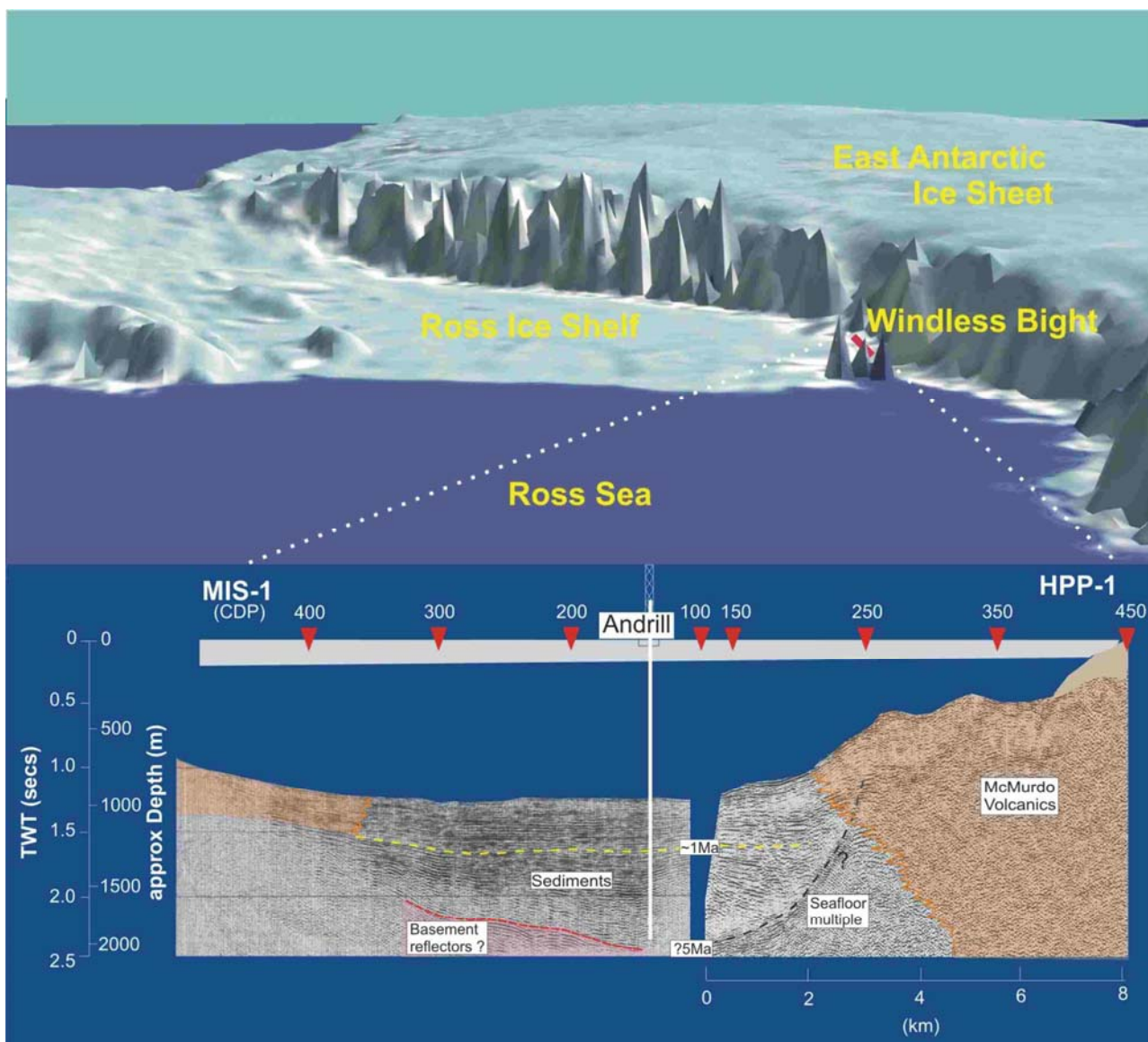
Figure 1. The Ross Embayment (image from NASA) and a composite seismic section beneath the ice shelf in Windless Bight just south of Ross Island. The two sites described in this report, and a third ancillary site for current data, are shown in Figure 2. Seismic data are from Bannister and Naish (2002) on the left and Melhuish et al. (1995) on the right.

Field work was carried out from late December to early February, 2003, and is described in scientific and logistics reports to AntarcticaNZ by Barrett (2003) and Pyne (2003). The project ran well with two access holes drilled and kept open through the ice shelf for up to nine days. All instruments and sampling devices deployed through the access holes functioned and were recovered. Data on location, ice thickness and water depth for the two ice shelf sites are given in Table 1. A third site was occupied at the edge of the ice shelf and monitored over a period of three weeks for currents in the upper 2/3 of the water column.

Table 1. Basic data for the two sites occupied in January 2003, on the McMurdo Ice Shelf in Windless Bight.

Site 1 - 5 km from edge of shelf	*Jan 13 to 22*
Position	77° 53.308'S 167° 05.067'E
Ice Shelf thickness	70.5+-0.1 m
Datum - Ice Shelf surface	0 m
Firn-ice transition	27.0+-0.5 m
Sea level depth	17.3+-0.2 m
Sea floor depth by wire line	937 m (920 m bsl)
Site 2 - 12 km from edge of shelf	*Jan 28 to Feb 2*
Position	77° 50.111'S 167° 20.209'E
Ice Shelf thickness	143.7+-0.1 m
Datum - Ice Shelf Surface	0 m
Firn-ice Transition	27.2 +-0.2 m
Sea level depth	27.6 m
Sea floor depth by wire line	950.7 m (923 m bsl)

The field operations comprised the following activities:

i) Camp setup: This involved locating the sites identified from earlier seismic lines, the primary sites being on or close to line intersections (Figure 2). Site 1 was originally located on the intersection of lines MIS-1 and MIS-2, but was on the flight path for Williams Field and the rig represented a hazard. The site was relocated to the position shown. Once the site was located with GPS, the various camp units were towed out – the camp kitchen and sleeping wanagans, workshop and science wanagans, and the sled with the hot water drilling system mounted. Camp setup typically took around two days.

ii) Hot water drilling operation: This was provided by the Alfred Wegener Institute for Polar and Marine Research, and had been delivered by ship in a container to Scott Base at the end of the previous summer. This is described in more detail in the next section. Drilling the hole through the ice shelf and reaming it to a uniform diameter also took around two days.

iii) Winch operations (including oceanographic measurements and sediment sampling): Once the access hole was available, the winch was used to measure water depth and then water column properties through a tidal cycle (conductivity, temperature, current speed, current direction) before sampling the sea floor by grab and gravity corer. This took four and nine days at Sites 1 and 2 respectively. The routine is outlined in more detail below and in Table 2.

iv) Camp breakdown and move/return to base, took around two days.
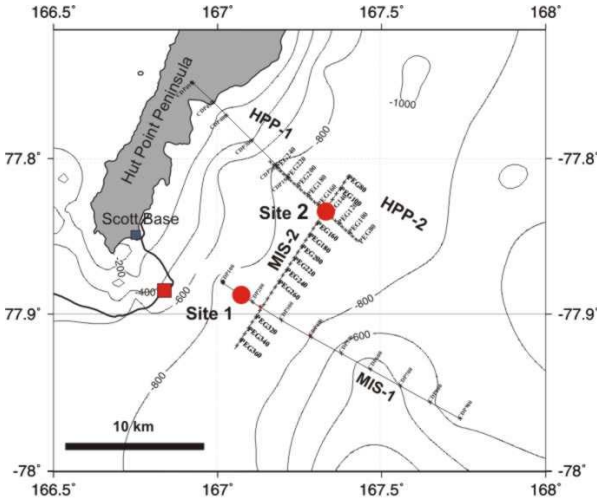
Figure 2. Hut Point Peninsula and the McMurdo Ice Shelf to the SE, showing the bathymetry of the broad channel connecting the waters of McMurdo Sound to the NW with those beneath the Ross Ice Shelf to the east. The intersecting lines mark seismic surveys run by the Institute of Geological & Nuclear Sciences (Melhuish et al., 1995; Bannister and Naish, 2002; Horgan et al., 2003) for imaging the geometry of the strata filling the basin (see Figure 1). The square west of Site 1 is a third site occupied for current monitoring at the shelf edge.

The first measurements at each site were to establish water depth and nature of the sea floor. A 3.5 kHz transducer was lowered and set 2 m below the base of the ice shelf to obtain a high quality acoustic record of the sea floor and sub-surface sediment. At Site 1, water depth was determined to be 855 m below the base of the ice shelf (908 m bsl, 926 m below the ice shelf surface, a convenient reference point for all subsequent oceanographic measurements). However, the water depth was determined by weighted line to be 938 m, 12 m deeper than the acoustic estimation. This depth was used for operational purposes on oceanographic casts. A similar procedure was followed for Site 2.

Table 2. Measurements and samples taken beneath the McMurdo Ice Shelf at Sites 1 and 2 in Windless Bight.

Device	Measurements or samples taken	Site 1	Site 2
3.5 kHz sounder	First estimate of water depth and sub-seafloor stratigraphy	Penetration to ~300 m	Ice too thick for cable
S4	Current speed and direction profiles through the water column	Casts 1 to 13 from 1400 Jan 14	Casts 1 to 10 from 1110 Jan 28
CTD	Conductivity and temperature profiles through the water column	to 1700 Jan 16	to 1240 Jan 29.
NIO bottles (1 litre)	Water samples for chemistry and suspended particulate matter	~20 samples taken at 6 levels	~20 samples taken at 6 levels
ADCP array	Current speed and direction measured simultaneously through the water column for at least 48 hours	Deployed for 87 hours on Jan 18-22	Deployed for 47 hours on Jan 31 to Feb 1
Gravity cores	48 mm diameter sediment cores – at least 3 from each site more than 50 cm long	Cores 7, 11, 13, 50, 60 and 61 cm	Cores 29, 42, 61 and 63 cm
Grab	Top 3-5 cm from sea floor	Grabs 1, 2 empty. Grab 3 30% full	Grabs 1 & 2 empty. Grab 3 full

1.1 References

Bannister, S. and Naish, T.R. 2002. ANDRILL Site Investigations, New Harbour and McMurdo Ice Shelf, Southern McMurdo Sound, Antarctica. *Institute of Geological and Nuclear Sciences Report 2002/01*, 24 p.

Domack, E.W., Jacobson, E.A., Shipp, S., and Anderson, J.B. 1999. Late Pleistocene-Holocene retreat of the West Antarctic Ice Sheet system in the Ross Sea: Part 2 – sedimentologic and stratigraphic signature. *Geological Society of America Bulletin* 111, 1517-1536.

Horgan, H., Naish, T., Bannister, S., Balfour, N., Wilson, G., Finnemore, M., and Pyne, A. 2003. Seismic stratigraphy of the Ross Island flexural moat under the McMurdo-Ross Ice Shelf, Antarctica. Immediate Scientific Report to AntarcticaNZ.

Lacy, L., Harwood, D., and Levy, R. 2002. *Future Antarctic Margin Drilling: Developing a Science Program Plan for McMurdo Sound*. Andrill Contribution 1. University of Nebraska-Lincoln, Lincoln, NE, 316 pp.

Meluish, A, Henrys, S.A., Bannister, S., and Davey, F.J. 1995. Seismic profiling adjacent to Ross Island: Constraints on Late Cenozoic stratigraphy and tectonics. *Terra Antartica* 2, 127-136.

2   HOT WATER DRILLING

Uwe Nixdorf and Erich Dunker

2.1   Introduction

Drilling with a water-heated probe has proved to be a very energy- and time-efficient means of penetrating thick ice bodies, such as glaciers, ice streams and ice shelves, even in the low temperatures of the polar regions, and has been in use now for more than 25 years. Hot water drilling through 420 m of floating ice by Browning et al. (1979) led to the first study of sea water from beneath the Ross Ice Shelf (Clough & Hansen, 1979). A similar system led to the discovery of a basal marine ice layer of the 600-m-thick Filchner Ronne Ice Shelf by Engelhardt & Determann (1987). Hole diameters for these systems were typically around 0.6 m, with drilling taking around a day. Subsequently oceanographic conditions beneath this ice shelf were revealed using this method (e.g. Nicholls et al., 2001), which has provided a means of making direct field observations on ice flow in Greenland (e.g. Lüthi et al., 2002) and in the Antarctic (e.g. Engelhardt & Kamb, 1998). A large and sophisticated hot water drilling equipment was used at the South Pole, Antarctica, in order to drill holes 1 m in diameter and 1000 m deep in order to deploy a muon and neutrino detector array (Koci, 1994).

The hot water drilling system used for this project was that developed by the Alfred Wegener Institute for studies beneath the Filchner-Ronne Ice Shelf (Nixdorf et al., 1994). The hot water capacity of the system (Figure 3) is in total 90 l/min from six JP8 fuelled burners, with a heat power of 125 kW per burner. The temperature of the feed water is close to 0° C. Each burner has a feed water hose and a low pressure feed pump. The water temperature at the outflow of each burner is about 95°C, normal working pressure is about 80 bar (1200 psi). The water of the six individual pressurised hot water lines is collected in a junction box. At this box the driller controls two valves, one regulating the flow of water to the drill winch, and the other controlling the flow to the melt water tank in order to melt snow. At the gauges by the junction box the driller can monitor the rate of penetration, the depth of the drill nozzle and the actual weight of the downhole drill nozzle and drill hose. The latter is a critical parameter in order to produce vertical access holes.

The system uses a combination of melted snow from a temporary water storage tank (5000 l) and re-circulated melt water in order to increase the rate of energy yield (latent heat of ice). The first step in drilling is to melt a cavern to build up a large pool of water below the firn-ice transition. The second is to drill the actual access hole through this cavern so that the upwelling drilling water is collected in the cavern and pumped back by a submersible pump. This concept was pioneered at J9 (Browning et al., 1979). The access hole is drilled first as a narrow pilot hole 150 mm diameter with a typical penetration rate of 30 m/hr. This is then widened to >600 mm diameter using a reamer with a slightly slower rate. Additional time and fuel consuming reaming is needed at the bottom of the hole as hot water is lost to the ocean beneath the ice shelf. After each drilling operation the water in all hoses, burners and pumps is replaced with food grade glycol to prevent them from freezing.
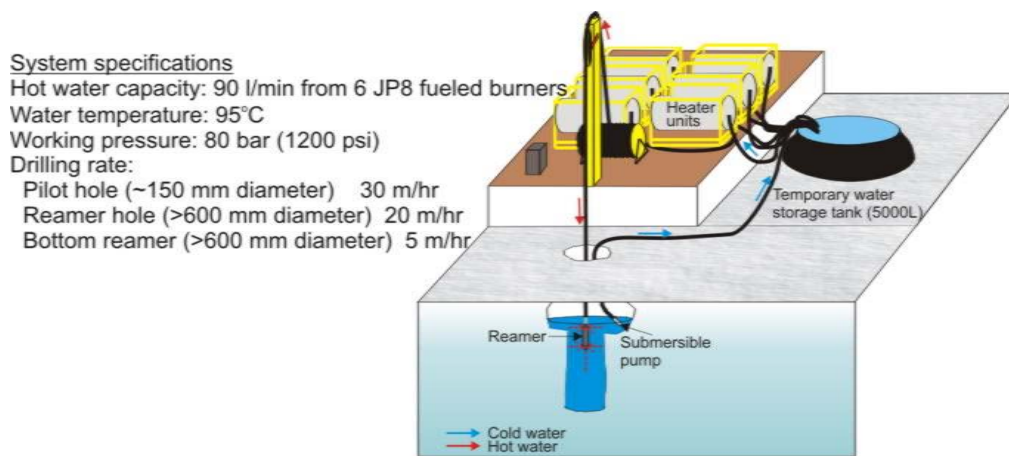
Figure 3. The hot water drilling system. This system uses a combination of melted snow and recirculated meltwater to produce a jet of hot (95°C) water to melt a hole through the ice shelf. First a vertical pilot hole (~150 mm) is made through the ice shelf. This is then widened to >600 mm using a reamer. Additional reaming is usually needed at the bottom of the hole, as hot water is lost to the ocean beneath.

The Scott Base winter-over staff extended the sledge deck in order to increase the available space on the drill sledge. The hot water drilling equipment was unpacked, assembled on the sled and tested in the period December 31 to January 4, and found to work well despite the long transit from Bremerhaven and storage over the winter.

2.2 Site 1

Hot water drilling began at Site 1 on January 7 by melting snow in order to fill the 5000 l water tank (Table 3). A cavern was drilled on January 8 from 14:20 until 18:45. During this first period of use all people in the group were made familiar with the operation and its potential dangers (high pressure, hot water/steam). A first pilot hole was started on January 9, 10:55 and the bottom of the 70.5 m thick ice shelf reached at 13:15. Reaming this hole lasted from 13:40 to 16:55 and a caliper log was recorded. In order to check the log the caliper sonde was recalibrated in the field. On January 10, the reaming work went on and for the first time a special designed reaming deflector that was attached to the reamer nozzle was used. Unfortunately, this deflector was lost at a depth of about 15 m and could not be recovered in subsequent attempts.

It was decided to give up this hole, so as to not risk the damage or loss of instruments that might be trapped if the deflector shifted further down the hole. On January 11, the sledge was backed up about 2 m in order to minimise the additional effort, so that the cavern could still be used. The access hole at Site 1 was drilled on January 11. The pilot hole was drilled from 11:25 to 13:55. Reaming took place from 14:15 to 19:00. A caliper log showed that the diameter of the hole was >56 cm from top to a depth of 68.2 m. However from there to the bottom of the ice shelf, the diameter narrowed almost linearly to 18 cm. On January 12, the reaming attempts lasted from 10:00 to 14:00 and with a wooden deflector from 16:00 to 18:00, but with little effect. A new reamer was built from two flanged steel salad bowls ~50 cm in diameter and bolted with a narrow gap around the flange to force the hot water against the sides of the hole. The device worked well, with reaming starting at 20:30 and finishing at 02:00. The hole was then made available for measurements and sampling from January 13-22 supplemented by a number of caliper logs and further reaming on January 17-18 from 21:25 to 01:00.

Having experienced some difficulty in reaming near the bottom of the ice shelf, it was decided not to freeze in the oceanographic array as originally planned. Instead, it was ensured that the access holes were reamed wide enough so that after 48 hours the mooring could be recovered without further hot water drilling. In fact bad weather delayed recovery until a total of 86 hours had passed, but hole diameter had not yet reduced significantly, and the array was recovered uneventfully.

2.3   Site 2

The hot water drilling work started here on January 25 by melting snow in order to fill the 5000 l water tank (Table 3). A cavern was drilled on January 26 from 11:05 until 14:45. A pilot hole was drilled from 15:55 until 21:00. Reaming this hole lasted from 12:00 to 18:20 and 21:00 until 22:00 using the reamer nozzle and from 22:10 until 02:00 using the bottom reamer. The reaming process was hampered by falling temperatures that caused some problems in starting the burners and a frozen hose from the junction box to the melt water tank. A subsequent caliper log proved that the diameter of the hole was >56 cm from top to bottom of the ice shelf. Measurements and sampling through the hole took place from January 28 to February 02, supplemented by a number of caliper logs and a reaming effort on January 30 from 13:40 to 20:00.

Table 3. Hours for Hot Water Drilling operations at Sites 1 and 2 in Windless Bight.

	SITE 1	*SITE 2*
Cavern	4 hrs 25 mins	3 hrs 40 mins
Pilot hole	2 hrs 30 mins	5 hrs 5 mins
Reamer	4 hrs 45 mins; 4 hrs; 2 hrs	6 hrs 20 mins; 1 hr
Bottom Reamer	5 hrs 30 mins; 3 hrs 35 mins	3 hrs 50 mins; 6 hrs 20 mins
TOTAL	**26 hrs 45 mins**	**26 hrs 15 mins**

Additional time was needed to replace water with glycol after each period of drilling activity, and vice versa. This took between 1 to 2 hours (and more in cold temperatures). The fuel consumption for hot water drilling, the vehicles and the camp generator added up to 35 drums of JP8 and 8 drums of gasoline for the whole season's operation.

2.4   Site 3 - Sea ice mooring

A mooring in the sea ice at Site 3 was freed using two burners, a subset of the hot water drilling equipment and a new designed cylindrical nozzle on February 03 between 13:30 and 16:00.

In summary, the project ran extremely well with access holes drilled and kept open through the ice shelf for 10 days (Site 1) and 5 days (Site 2). This was critical for the success of the project. With the success of the steel basin reamer the time required for hot water drilling at Site 2 was reduced considerably, even taking into account the much thicker ice at that site. All instruments and sampling devices deployed through the access holes functioned and were recovered. The two most central of the four proposed sites were occupied, and a third site at the edge of the ice shelf monitored over a period of three weeks for currents in the upper 2/3 of the water column. In the course of the ANDRILL project, a cylindrical shaped reaming nozzle will be designed and built that will allow to redrill and thus recover moorings that have been frozen in. This will be of value for future oceanographic measurements beneath ice shelves.

2.5 Ice shelf observations

Uwe Nixdorf

Ice shelves are largely flat plates of mostly meteoric ice floating in equilibrium with the ocean water and make up about 44% of the Antarctic coast line (Drewry et al., 1982). They play an important role for the Antarctic system in at least two respects: Firstly most of the Antarctic ice that is discharged towards the coast enters ice shelves. The two largest ice shelves alone, the Ross and the Filchner-Ronne, account for about half of the ice discharge (Thomas, 1979). They not only drain the largest part of the West Antarctic Ice Sheet (WAIS), but a substantial fraction of the East Antarctic Ice Sheet as well. They also figure prominently in debate on the stability of the WAIS in context of global climate change (Mercer, 1978; De Angelis & Skvarca, 2003; see also review by Oppenheimer, 1998).

Secondly, a quantitative knowledge of ice shelf-ocean interactions is crucial for mass balance estimations of Antarctica (Jacobs et al., 1992) as well as for the formation of Antarctic bottom water (e.g. Fahrbach et al., 1991) and thus for the global ocean circulation. Besides the bottom melting processes of ice shelves mostly occurring at their grounding zones, accretional processes of platelet ice that form so-called marine ice layers (Oerter et al., 1992) can also be observed. A first concept of the relevant processes was given by Lewis & Perkin (1986).

An overview of the glaciological and geophysical field data evidence for the Ross Ice Shelf is given by Bentley & Jezek (1981) and for the northwest corner by McCrae (1984). From their investigations ice thickness of the McMurdo Ice Shelf at Site 1 was expected to be 60-80 m and at Site 2 approximately 140 m. These values are in good agreement with those that we recorded with our calliper log after drilling (Table 2).

More remarkably, however, we observed the presence of platelet ice below the ice shelf at both sites. The first hints that platelets might be present occurred during drilling, when some buoyancy remaining in the drill nozzle was found after having drilled several times for some metres below the ice-ocean interface. Moreover it was known from the deployment of the sea ice mooring at Site 3 that here there is a 3-4 m thick layer of platelet ice. These thin platelets (thickness approx 1-2 mm) are elliptically shaped with a radius of about 10 cm.

The first retrieval of platelet ice occurred when the oceanographic instruments were brought up from beneath the ice shelf to the surface. A sampler was built for platelet ice, which was lowered several times approx. 3-5 m below the ice-ocean interface at both sites. The ice platelets were observed to have the same thickness and shape as the ones found at the sea ice mooring but with smaller radius. At Site 1 the radius was in the range of 2-3 cm; at Site 2 the platelets were even smaller. These shapes distinguish them from slush that might have built in the borehole. The questions that remain are: Where are the platelets formed? Do the platelets accumulate beneath the ice shelf or are the platelets carried in from open water in winter? Measurement of ablation/freezing rates at the bottom of the ice shelf would help resolve these questions.

2.6 References

Bentley, C.R. and Jezek, K.C. 1981. RISS, RISP and RIGGS; post-IGY glaciological investigations of the Ross Ice Shelf in the US programme. *Journal of the Royal Society of New Zealand* 11, 355-372.

Browning, J.A., Bigl, R.A., Somerville, D.A., 1979. Hot-water drilling and coring at Site J-9, Ross Ice Shelf. *Antarctic Journal of the United States* 14, 60-61.

Clough, J.W. and Hansen, B.L. 1979. The Ross Ice Shelf Project. *Science* 203, 433 – 434.

De Angelis, H. and Skvarca, P. 2003. Glacier Surge after Ice Shelf collapse. *Science* 299, 1560-1562.

Drewry, D.J., Jordan, S.R., Jankowski, E. 1982. Measured properties of the Antarctic ice sheet: Surface configuration, ice thickness, volume and bedrock characteristics. *Annals of Glaciology* 3, 83-91.

Engelhardt, H. and Determann, J. 1987. Borehole evidence for a thick layer of basal ice in the central Ronne Ice Shelf. *Nature* 327, 318-319.

Engelhardt, H. and Kamb, B. 1998. Basal sliding of Ice Stream B, West Antarctica. *Journal of Glaciology* 44, 223-230.

Fahrbach, E., Knoche, M., Rohardt, G. 1991. An estimate of water mass transformation in the southern Weddell Sea. *Marine Chemistry* 35, 25-44.

Jacobs, S.S., Hellmer, H.H., Doake, C.S.M., Jenkins, A., Frolich, R.M. 1992. Melting of ice shelves and the mass balance of Antarctica. *Journal of Glaciology* 38, 375-387.

Koci, B. 1994. The AMANDA Project: Drilling precise, large-diameter holes using hot water. *Memoirs of National Institute of Polar Research* special issue 49, 203-211.

Lewis, E.L. and Perkin, R.G. 1986. Ice pumps and their rates. *Journal of Geophysical Research* 91 C, 11756-11762.

Lüthi, M., Funk, M., Iken, A., Gogineni, S., Truffer, M. 2002. Mechanisms of fast flow in Jakobshaven Isbrae, West Greenland: Part III. Measurements of ice deformation, temperature and cross-borehole conductivity in boreholes to the bedrock. *Journal of Glaciology* 48, 369-385.

McCrae, I.R. 1984. A summary of glaciological measurements made between 1960 and 1984 on the McMurdo Ice Shelf, Antarctica. Antarctic Division of DSIR Report No 360, 93p.

Mercer, J.H. 1978. West Antarctic Ice Sheet and CO2 greenhouse effect: A threat of disaster. *Nature* 272, 321-325.

Nicholls, K.W., Osterhus, S., Makinson, K., Johnson, M.R. 2001. Oceanographic conditions south of Berkner Island, beneath Filchner-Ronne Ice Shelf, Antarctic. *Journal of Geophysical Research C, Oceans* 106, 11,481-11,492.

Nixdorf, U., Oeter, H., and Miller, H. 1994. First access to the ocean beneath Ekströmisen, Antarctica, by means of hot-water drilling. *Annals of Glaciology* 20, 110-114.

Oerter, H., Kipfstuhl, J., Determann, J., Miller, H., Wagenbach, D., Minikin, A., Graf, W. 1992. Evidence for basal marine ice in the Filchner-Ronne ice shelf. *Nature* 358, 399-401.

Oppenheimer, M. 1998. Global warming and the stability of the West Antarctic Ice Sheet. *Nature* 393, 325-332.

Thomas, R.H. 1979. Ice shelves: A review. *Journal of Glaciology* 24, 273-286.

3   WATER COLUMN DATA

After water depth had been determined at each site, the hole was made available for gathering oceanographic data. The first cast was run with the S4 current meter, set in conductivity-depth profiling mode and positioned 1 m above the weighted end of the line and the CTD (conductivity-depth-temperature) probe 5 m above that. Subsequent casts included water sampling with two National Institute of Oceanography (NIO) 1 litre bottles set to sample a total of 6 levels in the water column in the 13 and 10 casts made through a full tidal cycle at each of the two sites. The S4 data were found to be erratic and are not reported here. However the CTD data were consistent, and are described in the following section. After the oceanography casts an array of three Acoustic Doppler Current Profilers (ADCPs) was set for several tidal cycles at each site for characterising the water flow throughout the water column, and these data are also presented and reviewed. The section concludes with a report on water chemistry and suspended sediment data from water sampling programme.

3.1   Physical oceanography from CTD data
Lionel Carter

Ultimately, all Ross Sea shelf waters are derived from Circumpolar Deep Water that has upwelled along the Antarctic Slope in the vicinity of the Antarctic Slope Front (e.g. Jacobs et al., 1985). Through a range of processes involving the introduction of brine, precipitation and melt water, as well as cooling and mixing, the following shelf water masses are generated; their properties being summarised in Figure 4 and Table 4.

- Antarctic Surface Water (AASW),

- High and Low Salinity **Shelf Water** (HSSW and LSSW),

- **Ice Shelf Water** which has shallow and deep components (SISW and DISW).
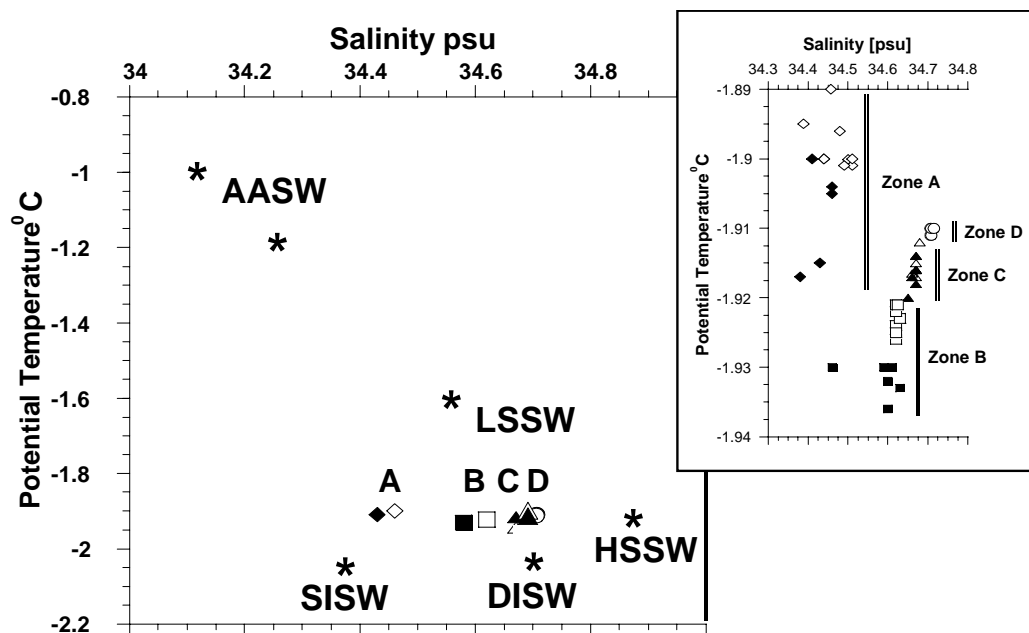
Figure 4. T/S plot of main shelf water masses including Antarctic Shelf Water [AASW], Low Salinity Shelf Water [LSSW], High Salinity Shelf Water [HSSW], Shallow Ice Shelf Water [SISW] and Deep Ice Shelf

Water [DISW]. A, B C and D refer to water mass zones at Site 1 (solid symbols) and Site 2 (hollow symbols) with mean T/S for each cast plotted in inset.

Table 4. Physical oceanographic characteristics of Ross Sea shelf waters. Modified from Jacobs et al. (1970, 1985).

Water mass and boundary	Depth [m]	Potential Temperature θ [^0C]	Salinity [ppt]	Comments
Antarctic Surface Water – open shelf [**AASW**]	0 -100	0 - -1.5 x = -0.96 σ = 0.57	34.1-34.5 x = 34.12 σ = 0.18	Upwelled CDW; found in all Ross Sea in summer; mainly in mixed layer
Antarctic Surface Water near RIS [**AASW$_g$**]	~50-100	x = -1.17 σ = 0.33	x = 34.24 σ = 0.13	Not modified AASW but CDW affected by contact with RIS
Temperature Minimum	10-100	x = -1.64 σ = 0.18	x = 34.3 σ = 0.05	Lies in halocline at base of AASW
Low Salinity Shelf Water [L**SSW**]	~100-500	x = -1.59 σ = 0.21 with warm core of – 0.84	x = 34.53 σ =0.04	Also Ross Sea Shelf Water [RSSW] Most widespread shelf water; lies midway AASW and HSSW
High Salinity Shelf Water [H**SSW**]	~500 – 750	x = -1.91 σ = 0.02	x = 34.84 σ = 0.05	Densest water in Antarctic ocean with low T and high S
Ice Shelf Water				Associated with glacial ice and T < sea surface freezing
Shallow [S**ISW**]	~50 – 250 @ RIS	x = -2.04 σ = 0.04	x = 34.36 σ = 0.02	Probably formed from interaction ice shelf &/or sea ice with LSSW
Deep [D**ISW**]	~250 – 500 @ RIS	x = -2.03 σ = 0.08	x = 34.68 σ = 0.04	Probably formed from interaction ice shelf &/or sea ice with HSSW
Antarctic Slope Front	10-45 km seaward shelf break; strong T / S gradients and currents; separates CDW from shelf waters			
Circumpolar Deep Water [CDW]	Off-shelf upwelling to 100m	1.25 to –1.0 x = 1.17 σ = 0.25	34.5-34.72 x = 34.7 σ = 0.02	Upwells along slope and is source for all shelf waters by cooling, mixing and addition of brine, meltwater, precipitation

From a broad perspective, this shelf modification of Circumpolar Deep Water makes the Ross Sea a major contributor of cold, saline bottom water that helps drive the global thermohaline conveyor system. Cooling beneath the Ross Ice Shelf and sea ice, together with brine derived from freezing sea water, elevate the density sufficiently to contribute to bottom water (e.g. Jacobs et al., 1985). Thus, Hot Water Drill Sites 1 and 2 on the McMurdo Ice Shelf (MIS) sector of the Ross Ice Shelf in Windless Bight, encountered waters with very low temperatures and high densities.

3.1.1 Site 1 data acquisition

The access hole at Site 1, 5 km east of the shelf edge, showed the shelf there to be 70.5 m thick, with sea level within the hole at 17.3 m below the ice shelf surface. The distance from the shelf surface to the seabed was 937 m, making the water depth 919.7 m (937 m-17.3 m). All measurements are referred to sea level as formed in each ice hole, unless otherwise specified.

A total of 13 hydrological casts were made using a Seabird Electronics 37-SM CTD set to sample at 5s intervals on a winch wire travelling nominally at 0.5 m/s. Between 500 and 650 measurements were made on each downcast and upcast. Data were converted to salinity, potential temperature, density (θt) and depth using the Seabird Seaplot software. Water samples for salinity corroboration were collected with NIO water bottles.

Apart from cast #1, which was an isolated test run on the flood phase of the tide on 14.01.03, the remaining casts #2 to #13 were collected to continuously sample a full diurnal tidal cycle commencing near low water on 15.01.03. Casts were made at between 2h and 3.3h intervals and involved recording both up and down CTD data. The resultant up-down profiles are very similar for each of T and S in depths >200 m, but departures occurred in shallower depths especially with salinity, which exhibited diminished and irregular values on the down-profile compared to the up-profile (Figure 5). In contrast, differences in the up and down T profiles at these shallow depths were relatively minor. It is suggested that the variability in salinity is due largely to entrapment of ice near the CTD conductivity cell either during its descent through the ice shelf, where slush ice was observed at sea level, or at the base of the ice shelf where ice platelets had collected (see section 2.5 above). Accordingly, only the up-profile of T and S are presented here (Figures 6, 7). Converted CTD data are recorded on the compact disc accompanying this report.
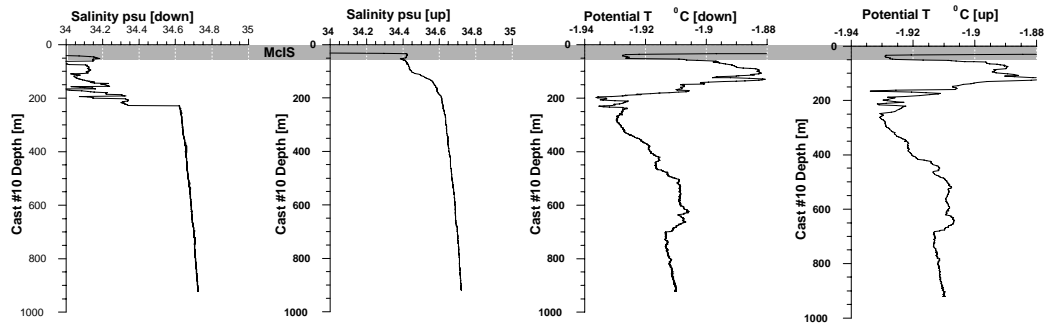
Figure 5. Comparison of up and down casts highlighting the variability of the salinity down profile, which is probably the result of ice entrapment in the CTD as it passes through the ice hole or beneath the McMurdo Ice Shelf [MIS].
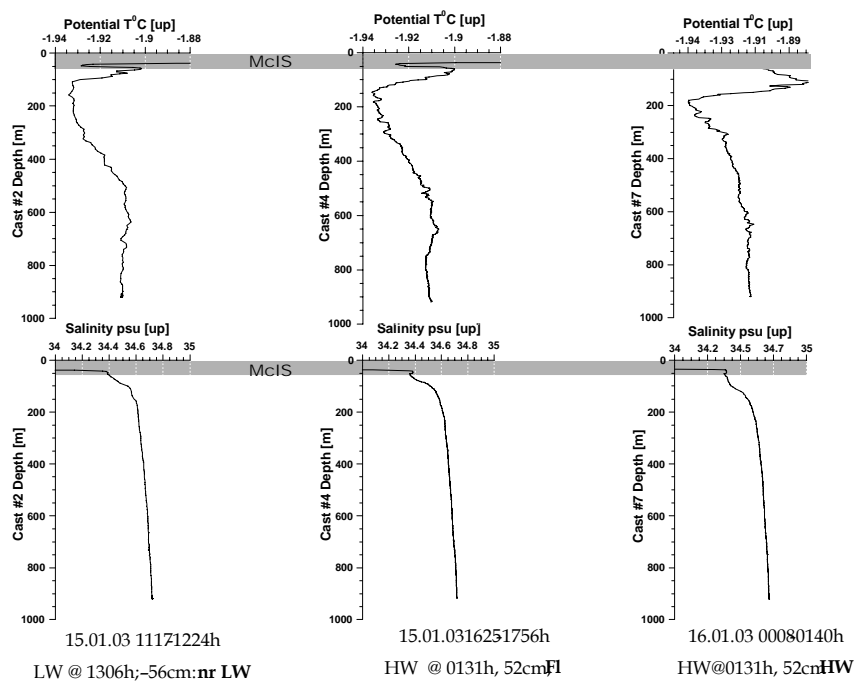
Figure 6. T and S on the flood phase at Site 1. McIS= McMurdo Ice Shelf.
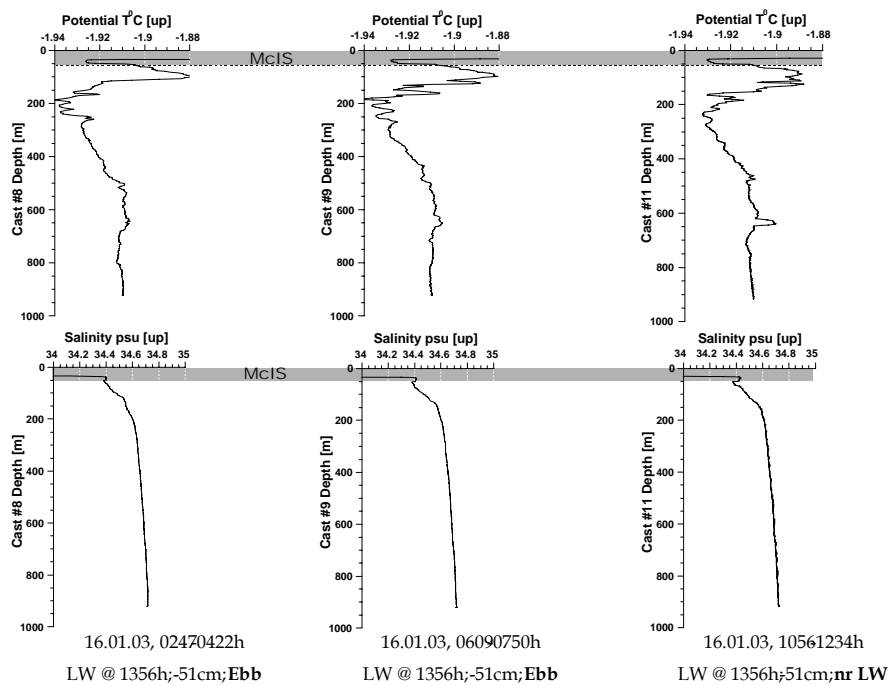
Figure 7. T and S for the ebb phase at Site 1. McIS = McMurdo Ice Shelf.

3.1.2 Site 2 data acquisition

The access hole at Site 2, 12 km east of the shelf edge, showed the shelf there to be 143.7 m thick. Sea level was found to be 27.6 m below the ice shelf surface, making the water depth with respect to sea level 950.7 m (seabed depth from ice shelf surface) - 27.6m = 923.1 m.

Ten hydrological casts were run using the same equipment as deployed for Site 1. Sampling protocols were also the same, with the exception that for Site 2, the winch was stopped for two minutes each 100 m to allow the S4 current meter to produce stabilised data. Casts were run over a diurnal tidal cycle that began 1203h, 28.01.03 and was completed at 1109h, 29.01.03 (Figures 8, 9). Again, only the upcast data are presented to eliminate anomalously low salinity values resulting from ice capture by the CTD on the downcast.
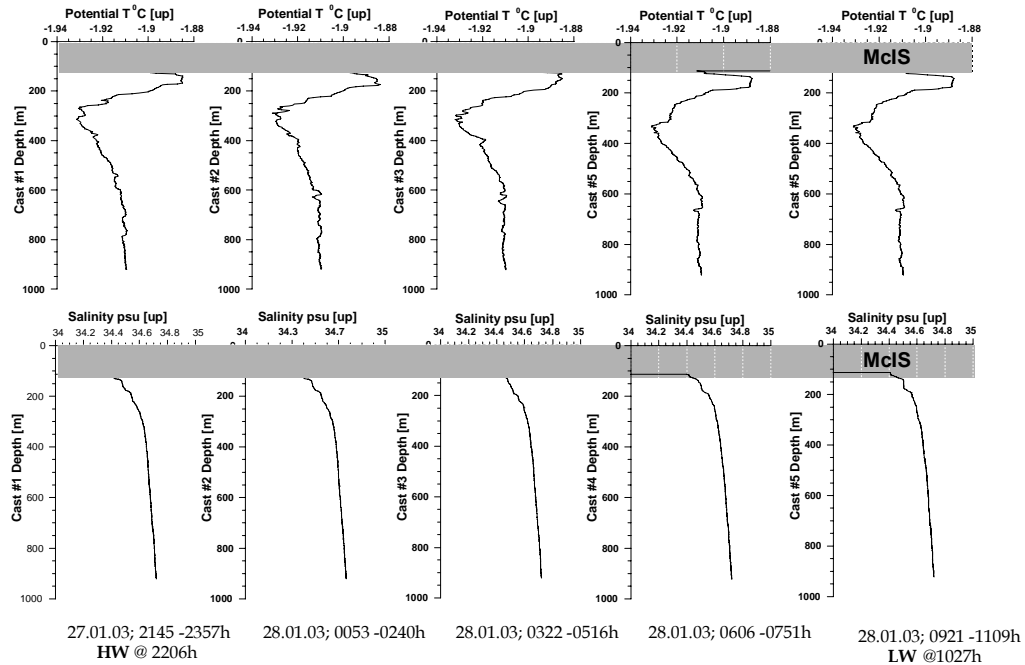
Figure 8. T and S on the ebb phase at Site 2. McIS = McMurdo Ice Shelf.
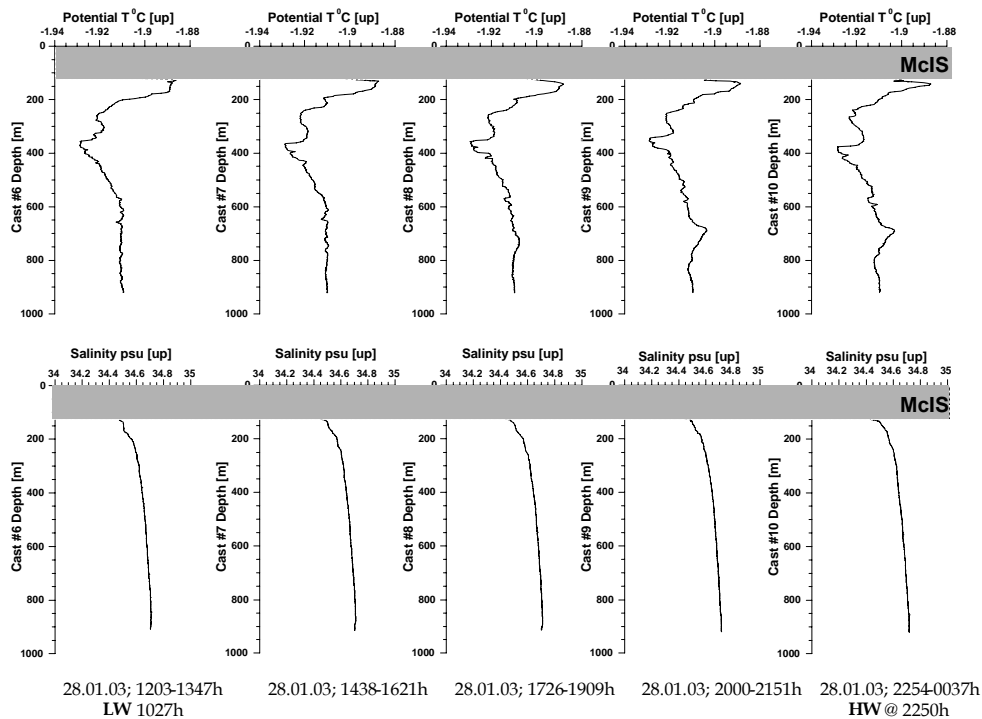
Figure 9. T and S on the flood phase at Site 2. McIS = McMurdo Ice Shelf.

3.1.3   Site 1 results

3.1.3.1   *Water mass structure*

Salinity profiles are simple comprising a sharp gradient in the 50-90 m thick layer immediately underlying the McMurdo Ice Shelf (water depth 53-140 m). There, salinity increases rapidly from 34.36 to 34.5 psu. Thereafter, values increase gradually to reach a maximum of 34.72 psu at 922 m (Figures 6-7). In contrast, the temperature profiles show considerable structure that persists in a basic form throughout the tidal cycle of measurements. The 60-100 m of water below the ice shelf (110-150 m water depth) encompasses a relatively warm tongue with temperatures reaching –1.88^{0}C. The tongue is underlain by a colder zone with range of –1.936 to –1.93^{0}C, the coldest waters encountered. The cold spike occurs around 111 to 275 m below which the waters warm to reach a zone of near-isothermal water of –1.91^{0}C at 500 to 660 m depth. This temperature, together with a restricted salinity range of 34.70 to 34.71 psu, are maintained to the seabed, apart from a small but persistent tongue of warm water ~ 650 m depth (Figures 6, 7). Using the temperature structure, four zones of water are recognised below the ice shelf (Table 5).

Table 5. Water column zones recognised beneath the McMurdo Ice Shelf at Site 1 in Windless Bight.

Zone	Depth range [m]	Salinity [psu]	Temperature [^{0}C] Mean ranges of casts
A	53 - 150	34.38 to 34.46	-1.915 to -1.90
B	111- 275	34.59 to 34.63	-1.930 to -1.936
C	260 - 660	34.65 to 34.67	-1.918 to -1.914
D	660 - 922	34.70 to 34.71	-1.911

In terms of the shelf water masses outlined by Jacobs et al. (1985) (Figure 4), the T/S plots for the Zones B, C and D are closest to Deep Ice Shelf Water, whereas Zone A seems more allied to Shallow Ice Shelf Water, which would be in keeping with its position immediately beneath the Ross Ice Shelf although it is 0.1^{0}C warmer than classical Ice Shelf Water (Table 4).

16

3.1.3.2 Water mass variability
Even over the short span of a diurnal tidal cycle, water masses varied as evinced by the time series presented in Figures 6 and 7. Commencing around low water of 15.01.03, the relatively warm tongue immediately below the ice shelf began to expand and warm slightly over the ensuing flood phase. Expansion continued through the following ebb phase and it was only around low water of the 16.01.03 that the tongue receded slightly as indicated by a slightly cooler temperature and reduced thickness. As this event appeared to be independent of the tidal phase suggesting that the incursion was driven by another mechanism; perhaps the mean flow bringing in slightly warmer, Lower Salinity Shelf Water from the open ocean.

At depth, the tidal cycle witnessed an ebb cooling of the cold spike of Zone B to ~ -1.936°C (Figure 7). There appeared to be considerable shear with the expanding less cold waters above. Finally, the warming waters of Zone C contracted in thickness over the flood phase from ~ 470 m at low water on the 15.01.03 to less than 375 m at high water on the 16.01.03, before returning to 425 m thickness during the following ebb phase. Such variability was accompanied by an appropriate expansion and contraction of the Zone D.

3.1.4 Site 2 results
3.1.4.1 Water mass structure
Like the first site, CTD profiles from Site 2 exhibit the same simple salinity structure of steeply increasing values in the 200 m of water immediately underlying the ice shelf, followed by a more gradual increase to the seabed (Figures 8, 9). Likewise, Site 2 has the same basic tetrapartite thermal structure with well-defined Zones A to D.

Table 6. Water column zones recognised beneath the McMurdo Ice Shelf at Site 2 in Windless Bight.

Zone	Depth range [m]	Salinity [psu]	Temperature [°C]
			Mean ranges of casts
A	116 - 230	34.29 to 34.51	-1.901 to -1.882
B	210 - 440	34.62 to 34.63	-1.926 to -1.921
C	380 - 850	34.66 to 34.68	-1.917 to -1.912
D	570 - 923	34.70 to 34.71	-1.911 to -1.910

Compared to Site 1, Zone A has a similar thickness, but Zone B is more substantial. Furthermore, Zone B is deeper than its counterpart at Site 1, possibly because of displacement under the thicker ice shelf. Zone D is similar at both sites but overlying Zone C is thinner at Site 2.

A comparison of the water mass properties reveals that the shallow Zones A and B of Site 2 are slightly warmer and more saline than their counterparts recorded nearer to the ice shelf edge (Figure 4, inset). This difference suggests either a shorter residence time for the waters at Site 2 or more pronounced inflow of shelf waters as suggested by the deeper influence of warmer water intrusions in Zone B (see *Water mass variability)*. By comparison, the deep Zones C and D of both sites are very similar.

3.1.4.2 Water mass variability
Apart from very small fluctuations (<±0.03 psu) in the 100 m of water immediately below the ice shelf, salinity profiles remained unchanged throughout the diurnal tidal cycle. By comparison,

the thermal structure varied along lines similar to those recorded at Site 1 (cf. Figures 6, 7 with 8, 9). The relatively warm intrusion immediately beneath the ice shelf (Zone A) persisted throughout the tidal cycle (Figures 8, 9). It was most pronounced, in terms of thickness at low water, whereas the intrusion reached a maximum temperature of -1.884^{0}C at the early part of the ebb phase.

The underlying cold Zone B was disrupted during the flood phase by an intrusion of marginally warmer (0.05^{0}C warmer) water that occurred around depths of 300-350 m (Figure 9). A similar incursion affected the upper reach of Zone D at depths of ~700 m, developing from the middle part of the flood phase and continuing to high water. A slightly warmer incursion also affected Zone D at Site 1, but this time it occurred during the ebb phase and at ~630 m depth – about 70 m shallower than at Site 2, which is the difference in ice shelf thickness at the two sites.

3.1.5   Comparison with J9 near the head of the Ross Ice Shelf
The only other hole through the Ross Ice Shelf is Site J9 at 82^0 22.5′S; 168^0 37.5′W (Figure 10). Located about 450 km south of the ice shelf edge, the hole passed through 420 m of ice before reaching the 237 m-thick water column beneath (Clough and Hansen, 1979). Temperature profiles run by Gilmour (1979) revealed a very cold (-2.16 to -2.14^{0}C) layer about 50 m thick, directly beneath the ice shelf. Further down, waters gradually warmed (-2.14 to -1.87^{0}C) before passing into a well-mixed basal layer. The temperature and salinity of the basal zone at Site J9 as measured from water bottles and reversing thermometers, are ~ -1.9 to -1.86^{0}C and 34.68 to 34.84 psu respectively, with recorded mean values of 34.74 psu (Jacobs et al., 1979).

The general thermal structure at Site J9 is similar to that recorded at HWD03 sites (Figure 10) with the caveats that:

-   Sites 1 and 2 have, in addition, a relatively warm tongue intruding immediately below the ice shelf, and;

-   the temperature scale and hence thermal structure at the HWD03 sites is exaggerated by a factor of 5.

Nevertheless, the J9 and Hot Water Drill sites exhibit a cold Zone B, underlain by relatively warmer Zone C that finally passes into a well-mixed Zone D. The shallow waters at J9 are colder than the cold spikes observed at Sites 1 and 2, but the underling transitional Zone C has similar properties. Zone D itself is very similar to the basal waters at J9.

Of course, the physical oceanography at the three sites is based on "snap shots" and any comparison is made with caution, but it appears that there is continuity between J9 and the McMurdo Ice Shelf sites, as evinced by the similar thermal structure, notably Zones C-D. Differences in water temperatures immediately underlying the ice shelf between the two McMurdo Ice Shelf sites may relate to (i) the intrusion of warm Low Salinity Shelf Water from the nearby shelf, perhaps in a local flow from the east of Ross Island and out through McMurdo Sound (e.g. Heath, 1971), and (ii) and shorter residence times.
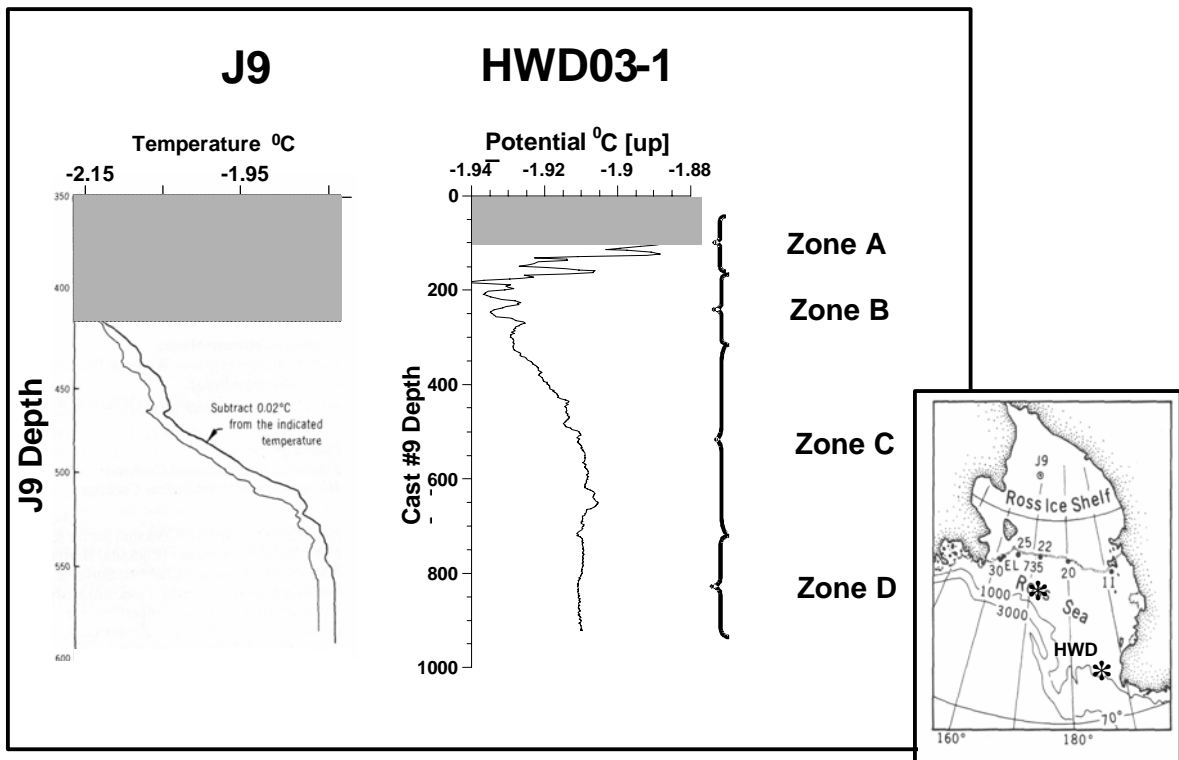
Figure 10. Comparison of data from J9 and MIS sites.

3.1.6   References

Clough, J.W. and Hansen, B.L. 1979. The Ross Ice Shelf Project. *Science* 203, 433-434.

Gilmour, A.E. 1979. Ross Ice Shelf sea temperatures. *Science* 203, 438-439.

Heath, R.N. 1971. Circulation and hydrology under the seasonal ice in McMurdo Sound, Antarctica. *New Zealand Journal of Marine and Freshwater Research* 5, 497-515.

Jacobs, S.S., Amos, A.F., Bruchhausen, P.M. 1970. Ross Sea oceanography and Antarctic Bottom Water formation. *Deep-Sea Research* 17, 935-962.

Jacobs, S.S., Fairbanks, R.G., Horibe, Y. 1985. Origin and evolution of water masses near the Antarctic continental margin: evidence from $H_2^{18}O/H_2^{16}O$ ratios in seawater. *In:* Jacobs, S.S. (ed.) Oceanology of the Antarctic Continental Shelf. *Antarctic Research Series* 43, 59-85.

Jacobs, S.S., Gordon, A.L., Ardai, J.L. 1979. Circulation and melting beneath the Ross Ice Shelf. Science 203, 439-443.

19

3.2 Current velocity patterns from ADCP data
Natalie Robinson

Four RD Instruments Ltd Acoustic Doppler Current Profilers (ADCPs) were used at three different locations, two of them through the ice shelf at Sites 1 and 2, and one through the sea ice at the ice shelf edge (Figure 11). The instrument deployed at this site was an RDI "Broadband" long-range (154 kHz) instrument. At the other two sites an array was assembled with two RDI "Sentinel" medium-range (307 kHz) instruments and a short-range, high-resolution (614 kHz) "Navigator". The raw data from each instrument were extracted using proprietary RDI software (*WinADCP*) and are included in the CD-ROM appended to this volume. Note that all dates/times are given in UTC – Universal Time Co-ordinate.

In order to correlate the current flows at the three sites, the data are referenced to the tidal cycle. It is not known whether there is a significant lag in the tide between Scott Base and these sites.
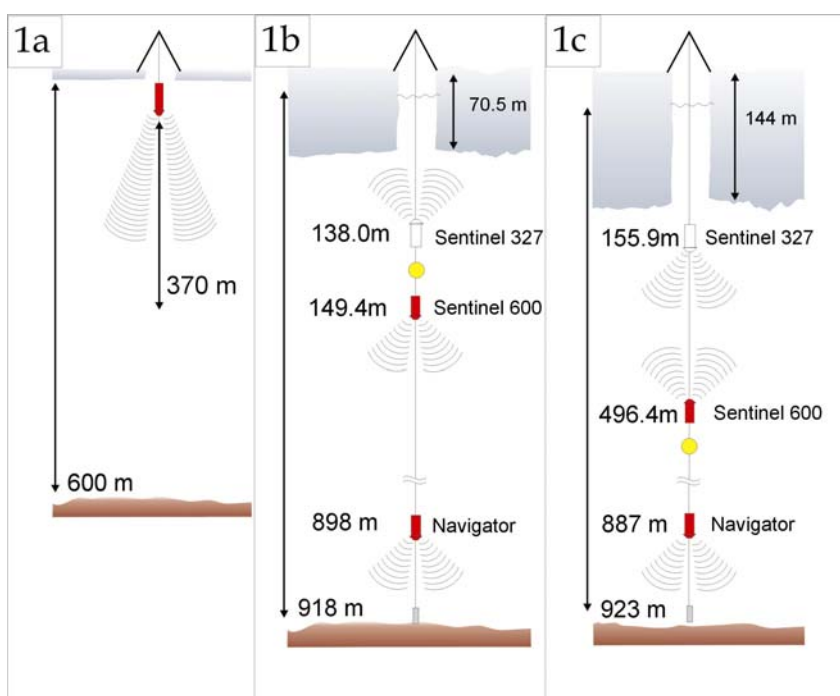
Figure 11. Mooring array for the (a) sea ice site, (b) Site 1 and (c) Site 2. Map locations are shown in Figure 1. In each case, around 50% of the available water column was surveyed by the array of instruments. The configuration of the ADCPs was changed for Site 2 because the Sentinel 327 was depth-rated to only 200 m bsl, and the new arrangement increased the proportion of the water column surveyed.

3.2.1 Sea ice site
The Broadband ADCP was deployed on January 10 through a hole cut in 3-m-thick sea ice using a Kässbohrer hydraulic arm. The instrument was suspended at a water depth of 5 m and was programmed to collect 48 readings 2 seconds apart at the start of every ten-minute period. Measurements were taken at all depths simultaneously, with the first "bin" at 23 m water depth and below this in 8 m bins. Useful information was recovered from the first 48 of 60 bins, giving a usable depth range of 23 to 400 mbsl. The ADCP was recovered 19 hrs later to enable a longer-term mooring frame to be installed (data from the first deployment are in the file "datatst.000" and are shown in Figure 12).

20
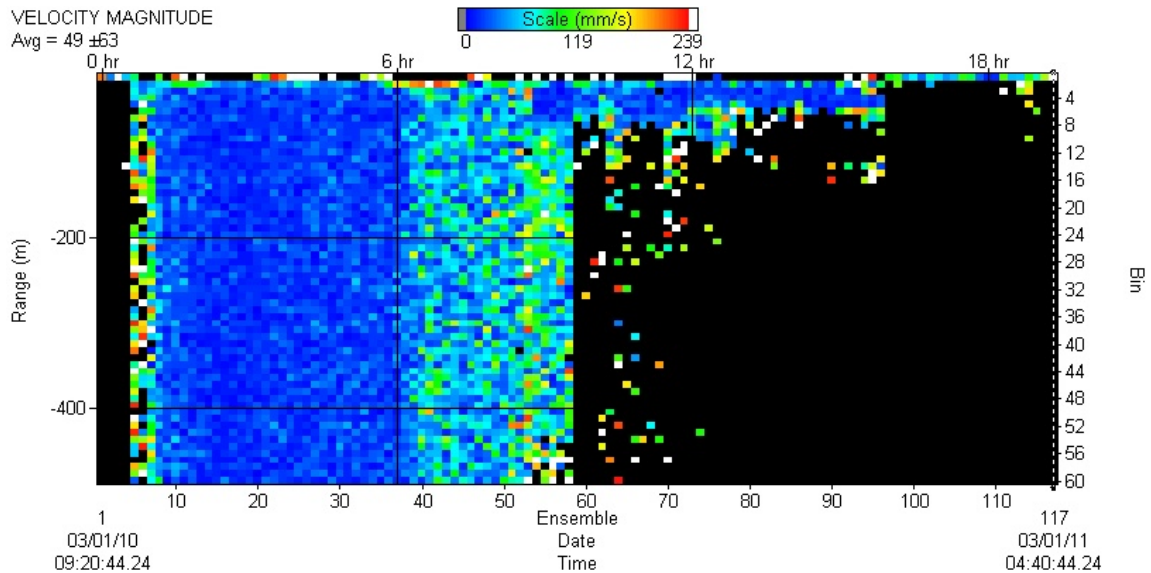
Figure 12. Screen image from the WinADCP software showing the loss of data after ~9 ½ hours of the initial deployment. This is attributed to platelet ice covering the transducers.

A check on the underside of sea ice using a submersible video camera showed an accumulation of 4.3 m of platelet ice. The loss of data after ~9 ½ hrs is attributed to this platelet ice swamping the transducers. The ADCP was then redeployed at a depth of 10 m on the 11 January and remained in place until the 3 February (24 days). These data are in the file "BB-DATA.000" and a copy of the deployment log, including the command script is included in the file "BB-deployment log.txt". Note that the raw data are not corrected for a magnetic declination of 155°. However, this correction has been applied to the results in the extracted files and those shown in Figure 13.

The duration of this mooring makes it possible to see a clear relation between the current velocity and the phase of the tide, both daily and lunar cycles (Figure 13). The largest daily variation in current direction occurs during the spring tide, with little variation during neap tide. This also means that the structure in the water column has greater definition during the spring tide. In general, the faster currents are seen on the flood tide, with flow in a south-easterly direction, while slower currents flow north on the ebb tide. Mean speeds of ~20 cms-1 were observed, with maximum speeds of up to 52 cm.s-1. Daily variations in both magnitude and direction are consistent through most of the depth range of the instrument. Overall, net transport is to the southeast.
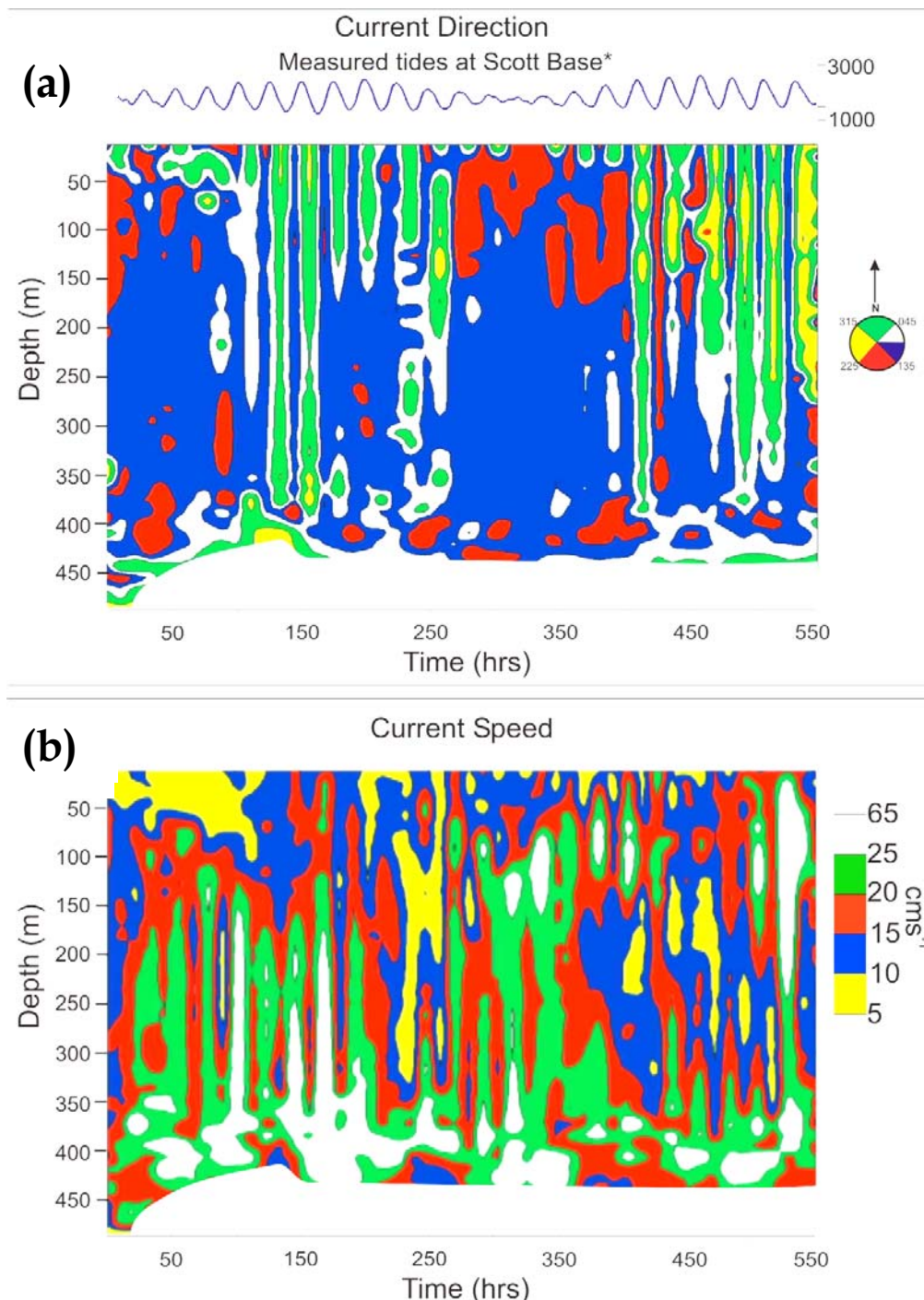
Figure 13. Current meter data from the sea ice site showing (a) current direction, and (b) current speed, with depth below sea level (mbsl). Both magnitude and direction show a strong correlation with tidal fluctuations, with strongest flows on the flood tide in SE direction. The structure is consistent through the water column to a depth of ~350 mbsl, which is assumed to be the limit for the instrument.

3.2.2 Site 1 results

Three ADCPs were deployed at this site, with Sentinel #327 at a depth of 138.0 m, looking up to the base of the ice shelf. Sentinel #600 looked down from a depth of 149.4 m while the Navigator looked down from 898 m, 20m above the sea floor in order to capture the flow structure of the benthic boundary layer (Figure 11). Both the Sentinels were programmed to collect 200 readings

22

3 seconds apart at the start of every ten-minute period. A bin size of 4 m was used in #327, but this was increased to 10 m in #600 in an attempt to gain more range. The Navigator was set to record 175 readings 0.62 seconds apart with a bin size of 0.5 m. Useable data cover the range 70-132 mbsl (#327 – 327H1000.000), 176-295 mbsl (#600 – 600H1000.000, although we have interpolated between the two datasets in Figure 14) and 900-918 m for the Navigator (H1NAV000.000). All three instruments were corrected for a magnetic declination of 155° before deployment.
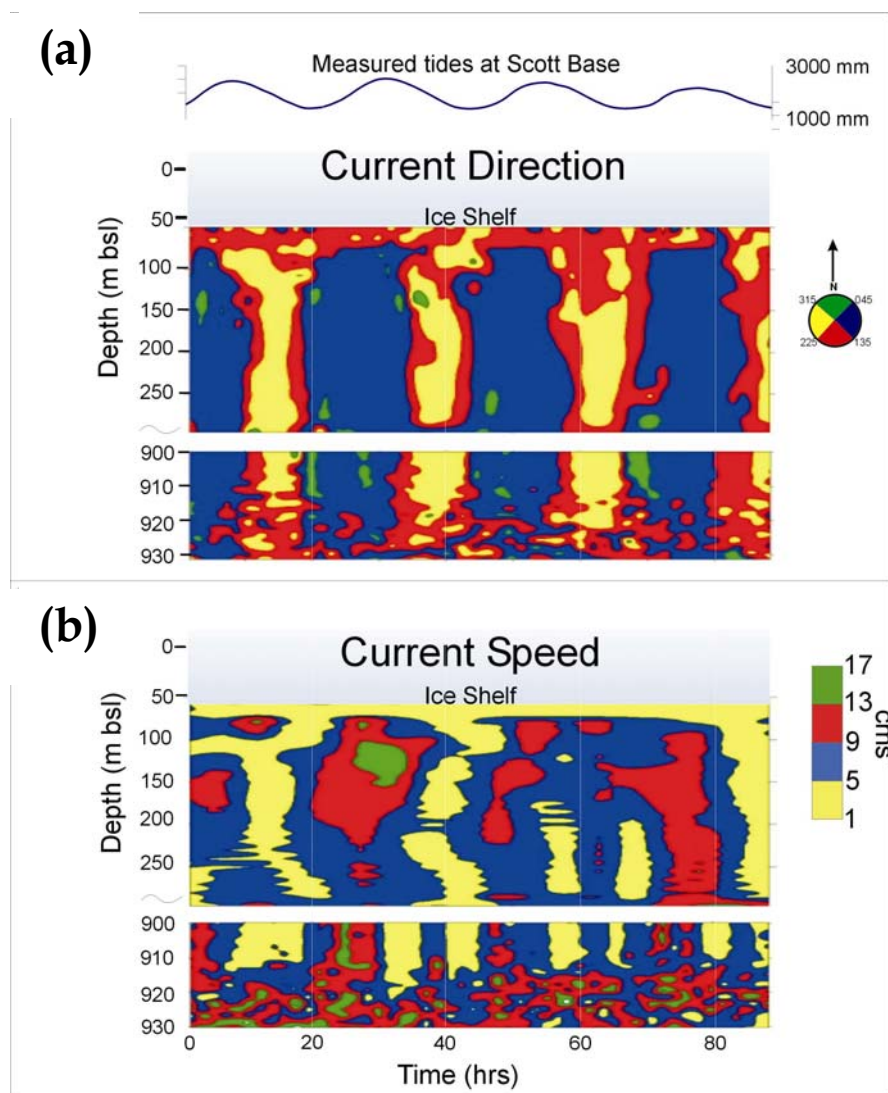
Figure 14. Current meter data from Site 1, showing (a) current direction, and (b) current speed at depth below sea level (mbsl) over the period of the mooring. The records from the Sentinel 327 (depth 138 mbsl) and the Sentinel 600 (depth 149 mbsl) have been interpolated to form one record. A gap of ~600 m exists between these and the Navigator, although the structure in the water column is consistent throughout. A clear correlation between tide and current velocity can be seen, with maximum flows on the flood tide up to 22 cms-1 in an easterly direction. The most likely cause of the disorder at the bottom part of the Navigator record is the depth range of the instrument continuing beyond the sea floor.

Data collection began at 0730 on 18 January 2003 and ended at 2220 on 21 January 2003, providing a total of 87 hours of information, beginning at the maximum of the spring tide. A clear correlation between current velocity and tidal cycle was observed throughout the water

column, with faster, easterly flows on the flood tide, and slower south to west flows on the ebb tide. Mean speeds of ~6.5 cm.s^{-1} were observed with maximum speeds up to 22 cms^{-1}. The observations from the Sentinels is nearly continuous for the 225 m of water immediately below the ice shelf, and these data are generally consistent with the Navigator readings, although a gap of ~600 m existed between the ranges of the instruments.

3.2.3   Site 2 results

The same three ADCPs deployed at Site 1 were also deployed at this site. However, the greater thickness of the ice shelf at this location combined with a maximum pressure rating of 200 m for #327 meant a different mooring configuration had to be used. Here #327 was placed at a depth of 156 m, looking down, while #600 was placed at 496 m looking up. In this way, the two instruments profiled most of the water column to a depth of 480 m. The Navigator looked down from 887 m, 36 m above the sea floor. Both Sentinels were programmed to collect 150 readings 2 seconds apart at the start of every five-minute period. A bin size of 10 m was used in #327 and 12 m in #600 in order to gain maximum range. The Navigator was set to record 130 readings 0.62 seconds apart every 5 minutes with a bin size of 2 m. Useable data cover the range 170-300 m (#327 – 327H2000.000), 360-480 m (#600 – 600D2000.000) and 890-920 m for the Navigator (H2NAV000.000) (Figure 15). As above, all three instruments were corrected for a magnetic declination of 155° before deployment. Data collection began at 0930 on 30 January 2003 and ended at 0930 on 1 January 2003 for a total of 48 hours, covering the peak of the spring tide.

Again, a clear correlation between current velocity and tidal cycle was observed. Fastest flows, up to a maximum of 20 cms^{-1}, were observed on the flood tide, with predominant east to northerly direction. The Sn600 current direction data show a time lag that is not yet unexplained.

Again, significant correlation between the data from the Sentinels and the Navigator can be seen despite the gap of ~400 m between the depth ranges. This is a further indication of the strong tidal influence throughout the water column.
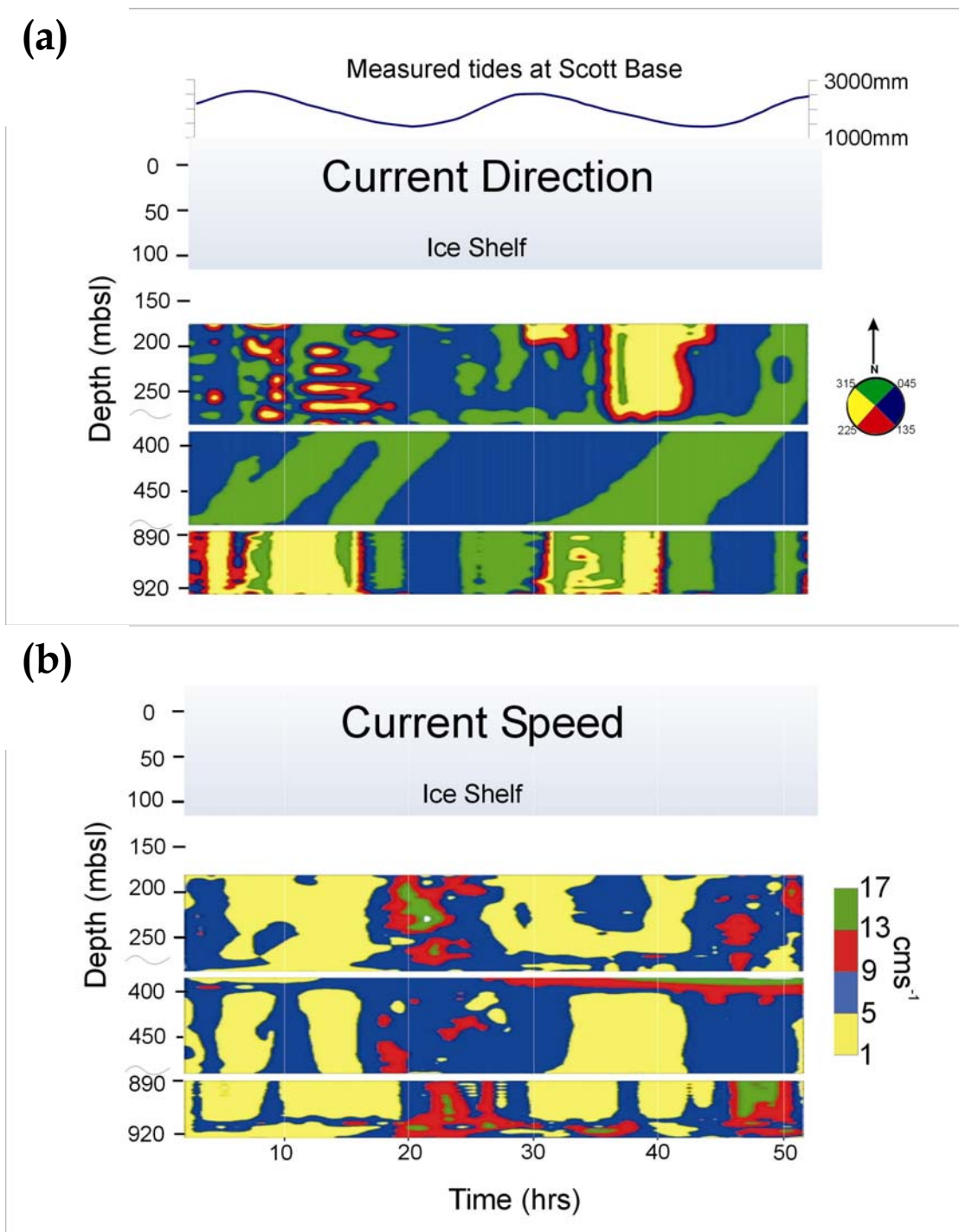
Figure 15. Current meter data from Site 2, showing (a) current direction and (b) current speed at depth below sea level (mbsl) over the period of the mooring. The records from the three instruments show strong correlation with the tides with maximum flows up to 20 cms^{-1} on the flood tide and predominant east to northerly direction. Strong correlation between the records in spite of the ~400 m gap between depth ranges demonstrates consistency in the water column.

3.2.4 Discussion and implications of the ADCP data

The predominant flows from the three sites reveal a net flow from McMurdo Sound, around Cape Armitage and into Windless Bight, with SE, E and NE net flows at sea ice and Sites 1 and 2

respectively (Figure 16). This is consistent with the composition of the seafloor sediment, which contains many diatom fragments, presumably advected under the ice shelf from the open water and seasonal sea ice cover in McMurdo Sound. Contrary to previous observations, McMurdo Sound may be a point of inflow beneath the Ross Ice Shelf, like the better known eastern and central sections of the ice shelf margin.

We also note that the McMurdo Sound region was experiencing anomalous sea ice conditions while these measurements were being recorded. In particular, the large iceberg B-15, which moved to block the strait between Ross Island and Beaufort Island, may have inhibited the annual breakout of sea ice. The same iceberg may have also been responsible for an increased flow around Cape Armitage as abundant oceanic plankton were observed much further south than usual (C. Evans, U Auckland, pers.comm., 2003).
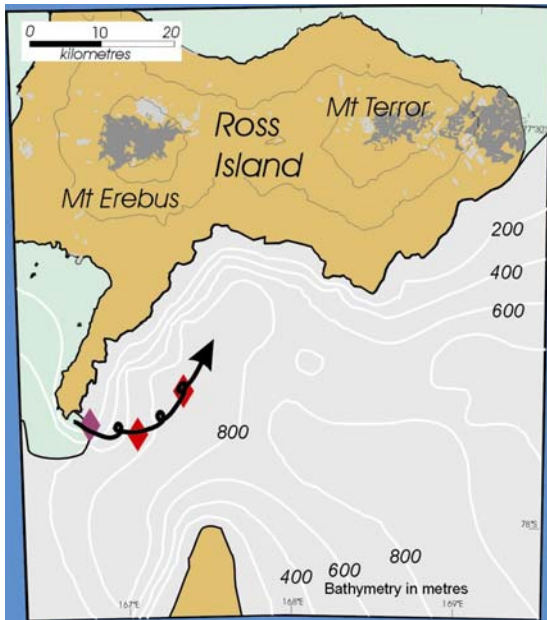
Figure 16. Bathymetry map showing the location of three sites and the predominant flows at each. A net flow from McMurdo Sound, around Cape Armitage and into Windless Bight is revealed, with flow along the axis of the deep basin surrounding Ross Island. This net flow is consistent with the composition of the sediment recovered from the sea floor, containing many fragments of diatom species, indicative of near-open-water conditions.

3.3 Water chemistry and suspended sediment data
Christina Riesselman

Water samples were obtained using pairs of 1L NIO bottles that were run with each of the two-hourly CTD casts. These were tripped to sample at six levels in the water column (Table 7). Sixty ml sub-samples were drawn and fixed with $HgCl_2$ for $\delta^{13}C$ and $\delta^{15}N$ analyses. Approximately 1.5L from each cast was filtered through a pre-combusted 21 mm diameter GF/C glassfibre filter for analysis of particulate organic matter (POM). POM samples are dried and stored, then placed in tin boats for analysis and combusted using a Carlo Erba NA1500 elemental analyser/Cono II device and a Finnigan Delta Plus mass spectrometer at Stanford University.

Elemental compositions are measured using the mass 44 beam intensity (V) on the Delta Plus, calibrated against the mass 44 beam intensity of standards that are analysed throughout the course of each run of 45 samples. Carbon isotopic compositions are standardised to NBS-21 (graphite). Reproducibility of the acetanilide standard normally averages 0.11% for N and 0.65% for C. Carbon isotopic reproducibility of NBS-21 averages 0.097 ‰. One hundred and fifty ml from each cast was filtered through a 45 μm filter for suspended sediment observations.

Table 7. Water column chemistry beneath the McMurdo Ice Shelf at Sites 1 and 2 in Windless Bight. Analyst: D A Mucciarone. Note: He 13.0, CO_2 15.0, N_2 20.0.

Date recovered	ID#1	DEPTH (m)	SITE	Wt (mg)	Amp(V) N	Amp(V) C	d15N Air	d13C PDB	C:N Atomic	mg N/L	mg C/L	Run
SITE 1												
10/28/03	P7 75-80m	75	HWD03-1	1.500	0.184	1.159	3.07	-28.35	7.81	6.889	46.126	16
10/28/03	P13 75-80m	75	HWD03-1	1.500	0.144	0.965	3.19	-28.95	8.30	5.294	37.698	22
10/27/03	P1 75-80m	75	HWD03-1	1.500	0.336	4.161	3.81	-27.81	16.20	12.181	169.191	11
10/28/03	P6 110-115m	110	HWD03-1	1.500	0.138	1.070	2.71	-29.29	9.54	5.193	42.490	15
10/28/03	P12 110-115m	110	HWD03-1	1.500	0.122	0.886	3.66	-29.39	8.85	4.585	34.787	21
10/27/03	P1 110-115m	110	HWD03-1	1.500	0.197		3.49			7.277		12
10/28/03	P5 370-375m	370	HWD03-1	1.500	0.079	1.023	8.20	-28.30	15.68	2.979	40.057	14
10/28/03	P11 370-375m	370	HWD03-1	1.500	0.045	0.610	5.22	-29.06	16.74	1.664	23.890	20
10/27/03	P1 370-375m	370	HWD03-1	1.460	0.167	2.512	4.06	-27.76	18.64	6.369	101.807	13
10/28/03	P4 626-631m	626	HWD03-1	1.500	0.300	2.153	5.08	-28.68	8.77	11.371	85.541	13
10/28/03	P10 626-631m	626	HWD03-1	1.500	0.080	0.729	9.46	-28.90	11.05	2.977	28.199	19
10/27/03	P1 626-631m	626	HWD03-1	1.320	0.111	1.618	2.64	-28.45	17.59	4.715	71.124	14
10/28/03	P3 886-891m	886	HWD03-1	1.500	0.143	1.305	3.21	-29.15	11.14	5.366	51.255	12
10/27/03	P1 886-891m	886	HWD03-1	1.390	0.244		3.14			9.771		15
10/28/03	P9 898-903m	898	HWD03-1	1.500	0.058	0.851	6.46	-29.62	17.66	2.194	33.230	18
10/28/03	P2 916-921m	916	HWD03-1	1.415	0.068	1.087	6.64	-28.55	19.68	2.734	46.124	11
10/27/03	P1 916-921m	916	HWD03-1	1.500	0.141	2.164	3.21	-28.57	18.99	5.277	85.908	16
10/28/03	P8 926-931m	926	HWD03-1	1.500	0.043	0.752	7.68	-31.75	21.47	1.622	29.856	17
10/28/03	P14 928-933m	928	HWD03-1	1.500	0.161	1.350	3.47	-29.10	10.38	5.925	52.728	23
SITE 2												
10/27/03	P7 149m	149	HWD03-2	1.100	0.115	0.829	3.02	-27.80	9.06	5.877	45.658	16
10/27/03	P11 149-154m	149	HWD03-2	1.810	0.119	0.819	4.68	-28.19	8.65	3.626	26.910	20
10/27/03	P6 184-189m	184	HWD03-2	1.760	0.086	0.748	4.05	-27.42	10.89	2.760	25.768	15
10/27/03	P12 184-189m	184	HWD03-2	1.755	0.102	0.776	4.59	-27.70	9.52	3.246	26.493	21
10/27/03	P5 427-432m	427	HWD03-2	1.800	0.068	0.635	4.58	-27.29	11.49	2.162	21.308	14
10/27/03	P13 427-432m	427	HWD03-2	2.000	0.097	0.810	2.92	-28.36	10.34	2.723	24.135	22
10/27/03	P4 670-675m	670	HWD03-2	1.840	0.180	1.135	4.13	-28.35	7.88	5.554	37.514	13
10/27/03	P10 670-675m	670	HWD03-2	1.855	0.066	0.629	6.15	-27.46	12.04	1.950	20.139	19
10/27/03	P2 910-915m	910	HWD03-2	1.721	0.179	1.281	4.32	-28.10	8.91	5.893	45.013	12
10/27/03	P9 910-915m	910	HWD03-2	1.575	0.062	0.729	6.11	-28.03	14.48	2.245	27.873	18
10/27/03	P8 936-941m	936	HWD03-2	1.760	0.061	0.684	4.64	-28.01	14.06	1.930	23.272	17
10/27/03	P1 943m	943	HWD03-2	1.125	0.143	1.096	3.37	-27.29	9.50	7.150	58.257	11
NOT PLOTTED												
10/27/03	C1 neph	Core water	HWD03-1	1.540	0.319	4.150	4.16	-26.59	16.89	11.298	163.632	17
10/27/03	C2 neph	Core water	HWD03-1	2.540	0.292	2.512	5.80	-26.64	10.87	6.324	58.956	18
10/27/03	C3 neph	Core water	HWD03-1	1.260	0.829	5.652	5.18	-25.88	8.97	35.433	272.610	19
10/27/03	C1	Core water	HWD03-2	1.500	0.328		5.62			11.902		20

4   SEA FLOOR DATA

Samples of the sea floor itself were taken initially by grab (the top 3-5 cm), and subsequently by a gravity corer built at AWI to operate through the 56-cm-wide hole in the ice shelf (Figure 17). The initial attempts yielded cores only a few cm long but by applying grease to the inside of the core liner cores more than 50 cm long were consistently recovered from both sites.

The general character of the sea floor of Windless Bight is inferred from new acoustic data reported in the following section. Following this we provide a brief description of the cores themselves, 10 radiometric ages from the cores, and grain size data. This is followed by micropalaeontological observations, petrographic and geochemical data, and physical properties of the cores. The section concludes with a depositional history inferred for the floor of Windless Bight from the data obtained from these two sites.

Figure 17. The Alfred-Wegener-Institut gravity corer deployed at HWD Sites 1 and 2. The hole through the ice sheet is covered by plywood in this image.

4.1   Sea floor sediment features from seismic data
Frank Niessen

Results from multi-channel seismic profiling through the ice shelf at Windless Bight carried out in the season 2001/02 (Horgan et al., 2005) suggested the presence of well-stratified sediments several hundred metres in thickness. In order to test the depth to which these sediments were unconsolidated, images of the sub-sea floor sediments were taken with a 3.5 kHz transducer placed 2 m below the base of the shelf ice. For very soft unconsolidated muds, acoustic penetration of 3.5 kHz pulses can be more than 100 m, whereas penetration can be only a few metres or less for highly lithified sediments. Total reflection or very limited penetration is also observed from sediment layers compacted by over consolidation from grounded glaciers (Rachor 1997). Our seismic experiment was to test whether sediments beneath the sea floor in the deep water of Windless Bight had been overcompacted, thus indicating that the Ross Ice Shelf had grounded there in the recent past.

Sediment echo sounding was carried out using an ORE Model 140 transceiver combined with a single 3.5 kHz Massa transducer. The transducer was connected to the transceiver by a 150-m-long cable, which allowed deployment of the transducer directly under the shelf ice at 70.5 m and 143.7 m below ice surface at both ice locations Sites 1 and 2, respectively. Echo soundings with pulse lengths of 4 ms were then carried out for at least 10 minutes at each location. The

receiving signals were plotted as analogue data on a chart recorder (Dowty Model 3710) and stored on DAT tape for future converting to SEG-Y data format and seismic processing.

Analogue data from Site 1 exhibits a clear reflector of the sea floor at 1205 ms 2-way travel time between the transducer under the shelf ice and the sediment surface (Figure 18). Assuming a constant p-wave velocity of 1447 m s^{-1} in seawater under the shelf ice (mean velocity for a salinity range of 33 to 34.8 ppt and temperature range of -1.5 to -2°C), a water depth of 871.8 m is calculated between the lower surface of the ice and the sea floor. Together with the shelf ice thickness the total distance from the ice surface to the sea floor is determined as 942.3 m. This depth is in relatively good agreement with the sea floor depth measured by wire line of 938 m. At Site 2, the high noise level did not allow the sea floor to be located in the acoustic analogue data printed on a chart recorder during the data acquisition.

In addition to the sea-floor echo, the 3.5 kHz echogram for Site 1 exhibits 38 distinct sub-bottom reflectors to 410 ms 2-way travel time below the sea floor (Figure 18). Below that level reflectors become weak and indistinct but are still visible down to about 820 ms 2-way travel time. Since 3.5 kHz pulses generally penetrate unconsolidated mud with relatively low p-wave velocities, we have used p-wave velocities measured in near-surface sediment core at Site 1 (Core 4, see section 4.12 on core physical properties) to convert travel time to sub-bottom depth. If the median of measured velocities (1571 m s^{-1}) is used, two-way travel times of 410 ms and 820 ms correspond to 322 m and 644 m below sea floor, respectively. Considering the fact that only one transducer was used and that considerable acoustic energy is lost in the water column of about 872 m, the sound penetration into sediments is surprisingly deep at Site 1. This implies that in the entire acoustic record down to travel times of 800 ms (or even more) consists of unconsolidated (and probably largely muddy) sediment. This record suggests that there was no significant shelf ice grounding during the deposition of the upper 650 m of sediments in Windless Bight (though there may well have been periods when muddy glacial debris was deposited, as indicated by the uncompacted diamicton forming the lower part of the core at Site 1).
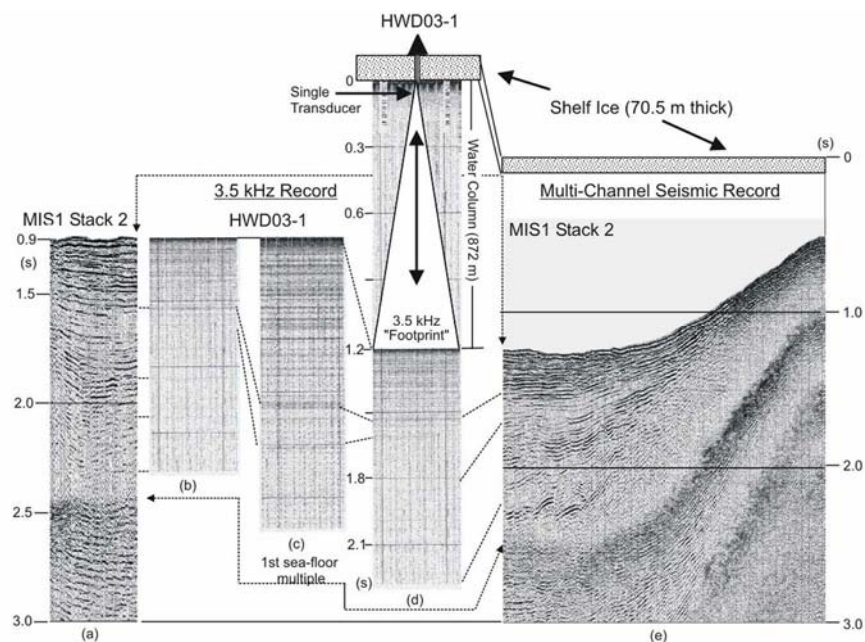
Figure 18. Seismic data (a, e) from Horgan et al. (2003) compared with 3.5 kHz data (b, c, d) recorded at Site 1. Note that travel time scales of seismic traces and 3.5 kHz traces have a vertical offset because the 3.5 kHz zero line is under the shelf ice. Sections (a) and (b) are presented on the same vertical scale for easier

comparison. Section (c) is enlarged for better presentation of high-resolution reflector pattern. Section (d) exhibits the entire 3.5 kHz reflection pattern including transducer "ringing" under the shelf ice, noise in the water column and sea floor as well as subbottom reflectors.

Figure 18 compares the 3.5 kHz records from Site 1 with the seismic line MIS-1, on which Site 1 is located. The comparison suggests that the entire seismic reflection record to 2.3 s of total 2-way travel time represents a muddy sedimentary sequence of relatively high porosity. It is interesting to note that in both the 3.5 kHz record and the MIS-1 seismic record numerous high-amplitude reflectors are visible in the upper 300 ms subbottom (Figure 1) suggesting that correlation of single reflectors in both records may be possible after further processing of the data.

One has to bear in mind that the transducer was stationary during the 3.5 kHz echo sounding. Thus, the recorded echograms represent the repetition of single traces similar in pattern and amplitude rather than a two-dimensional profile of a certain length indicative of horizontal layering as Figure 18 implies. Moreover, the noise-to-signal ratio of the analogue data is relatively poor as a consequence of the 150 m long transducer cable. Noise filtering after digitising of analogue data in the home laboratory could improve the reflection pattern shown for Site 1. No image is shown for Site 2 because the high noise level of the analogue data from that site does not allow an interpretation to be made without filtering.

4.1.1 References

Horgan, H., Naish, T., Bannister, S., Balfour, N., and Wilson, G. 2005. Seismic stratigraphy of the Plio-Pleistocene Ross Island flexural moat-fill: a prognosis for ANDRILL Program drilling beneath McMurdo-Ross Ice Shelf. *Global and Planetary Change* 45**,** 83.

Rachor, E. 1997. Scientific Cruise Report of the Arctic Expedition ARK-XI/1 of RV "Polarstern" in 1995. *Reports on Polar Research* 226, 157 pp.

4.2

Sediment description

Peter Barrett, Gavin Dunbar and Giovanna Giorgetti

Sea floor samples from both sites included grab samples (three from Site 1 and one from Site 2) and cores (six from Site 1 and four from Site 2, Table 8). One 60-cm-long core from each site (C4 in each case) was split and described with the aid of binocular and petrographic microscopes, and one half sampled for further analyses. The cores were described in terms of lithological units based on colour, sedimentary structures and texture, and a log is presented for each in Figures 19 and 20. A brief general description follows.

Table 8. List and location of grab and core material from Windless Bight Sites Site 1 and 2. Observations and analyses in this report were made mainly on Core 4 at each site.

Site 1	Length/Wt	Site 2	Length/Wt
Core 1	13 cm	Core 1	42 cm
Core 2	6.8 cm	Core 2	29 cm
Core 3	12.1 cm	Core 3	63 cm
Core 4	61 cm	Core 4	61 cm
Core 5	51 cm	Grab 1	10 gm
Core 6	60.8 cm	Grab 2	10 gm
Grab 1	1 kg	Grab 3	3 kg

4.2.1   Site 1 description

Unit 1 (0-8.5 cm) is a soft (at the top) to firm fine sandy mud (~40% sand) with minor coarse sand. The upper 1-2 cm contained small pebbles up to 16 mm long, mostly basaltic but containing exotic lithologies also. A small biogenic fraction includes sponge spicules and diatoms, which are more common and well preserved in the lower few cm.

Unit 2 (8.5-11 cm) is a firm bioturbated mud with less than 10% sand. Lower contact is gradational.

Unit 3 (11-16 cm) is a firm very fine sandy mud with 16 to 32% sand and a few sponge spicules and diatoms (<10%). It also has a small mollusc and worm tube along with several foraminifera (Figure 21). Lower contact is gradational.

Unit 4 (16-24 cm) is a firm mud (only 1-4% very fine sand). A few diatoms and rare forams were observed.

Unit 5 (24-31 cm) is a distinctive dark interval of soft muddy fine to very fine sand (63-97% sand), with mm-scale lamination including two or three mud layers. The unit looks to fine upwards, though analyses indicate some variability. The only biogenics are a few diatom fragments in the lower part. Lower contact is sharp with load features.

Unit 6 (31-36 cm), a firm mud with just 3-5% sand but with coarse sand grains and a few small pebbles in its lower part. It is moderately bioturbated and has a few diatom fragments. The upper contact with Unit 5 is sharp. Lower contact is gradational.

Unit 7 (36-61 cm) is a firm, slightly sandy mud with sparse scattered clasts (diamicton). The clasts are typically around 10 mm but up to 48 mm long, both angular and subrounded in shape, and all basic volcanic in composition. A few are striated (Figure 22).

SITE HWD03-1

CORE #: 4
Total length (m) 0.61

| Lat | 77°53.308 S |
| Long | 167°17.753 E |
| Water depth (m) 921 |

DATE: CORING/LOGGING

LOGGED BY: GG/GD
SCALE:
SHEET #: 1 of 1

REMARKS: grease used on the inside of the liner to aid core recovery. Core froze in storage.

Legend:
- }} Bioturbation (low, mod, high)
- Burrow
- Py Sulphide spots
- Load structures
- ..F.. Fining upwards
- — Gradational boundary
- ⊗ Foraminifera

BioStrat
- T Trace
- R Rare
- C Common
- F Frequent

Preservation
- P Poor
- G Good

Bio Strat columns: Section Number | Core Recovery | Depth (cm) | Foraminifers | Nannofossils | Sponge Spc | Diatoms | Preservation | Graphic Lithology | Colour | Description

Section 1:

Depth	Foram	Nanno	Sponge	Diatoms	Pres	Colour	Description
0	-	-	C	R	P	5Y3/2 Dk olive grey	0-8.5 cm Fine sandy mud (40% sand), dark olive grey. Pebbles up to 16 mm long in top 1 cm. Sub-angular to sub-rounded qtz, feldsp, volc glass and volc lithic grains. Biogenic content 1-5%, dominated by diatoms and sponge spicules. Rare benthic foraminifera. Moderately bioturbated.
	T	-	C	C	P/G		
5	T	-	C	F	P		
10	-	-	C	R	G	2.5Y4/2 Dk gyish brown / 5Y4/2 Olive grey	8.5-11 cm Sl sandy mud (>20% sand), dark greyish brown. Sub-rounded qtz, feldsp, volc glass and volc lithic grains. Biogenic content 2-3%, dominated by diatoms and sponge spicules. Rare calcareous foraminifera. Mod bioturbated.
15						5Y3/1 V. dk grey	11-16 cm V fine sandy mud (sand 16-32%). V dark grey to olive grey. Sub-rounded qtz, feldsp, and volc lithic grains. Biogenic content 2-3%, dominated by diatoms and sponge spicules. Strongly bioturbated.
20	T	-	C	R	G	5Y4/2 Olive grey	16-24 cm Mud (sand only 1-4 %). Olive grey.
25	-	-	T	-		5Y2.5/1 Black	24-31 cm Fine - v fine, well-sorted sand. Black. Sub-angular to sub-rounded qtz, feldsp and volc lithic grains. Trace occurrences of diatoms. Several mm-scale parallel, olive-coloured laminae in lower part of unit. Sand fines upwards, although irregular in lower 2 cm. Sharp lower boundary with load casts.
30	-	-	-	T	G	5Y4/2 Olive grey	31-36 cm Sl sandy mud (sand ~5%). Olive grey. Sub-angular coarse sand grains in muddy matrix. Trace occurrences of diatoms.
	T	-		T	G		
35						5Y3/1 V. dk grey	36-61 cm Sl pebbly sandy mud (diamicton) (sand 15-30%). V dark grey.
40	-	-	T	T	G		Clasts typically ~10 but up to 48 mm long. Sub-rounded phonolite, mafic volc, felsic volc, some with striated surfaces. Sand grains of qtz, feldspar, volc. glass and lithics.
45							Trace amounts of diatoms, sponge spicules and benthic foraminifers between 36-50cm. Biogenic material absent below 50 cm depth.
50	-	-	-	T	G		
55	-	-	-	-	G		
60							

Figure 19. Detailed log of Site 1 Core 4 from the floor of Windless Bight.

33

SITE HWD03-2
CORE #: 4
Total length (m) 0.62
Lat 77°50.111 S
Long 167°20.209 E
Water depth (m) 923

DATE: CORING/LOGGING 29-1-03

LOGGED BY: GG/GD
SCALE:
SHEET #: 1 of 1

REMARKS: Grease used on the inside of the liner to aid core recovery. Core froze in storage.

Bio Strat: Foraminifers, Nannofossils, Sponge Spc, Diatoms, Preservation

Graphic Lithology

Bioturbation (low, mod, high)
Burrow
Py Sulphide spots
Load structures
..F.. Fining upwards
— Gradational boundary
Foraminifera

BioStrat
T Trace
R Rare
C Common
F Frequent

Preservation
P Poor
G Good

Section Number / Core Recovery / Depth (cm)

Clay, Silt, Fine, Medium, Coarse, Granule

Colour

Description

5Y4/2 Olive grey — 0-3 cm V fine sandy mud (sand ~40%). Olive grey. Subangular pebbles to 16 mm long in top 1 cm. Sand and silt fraction is subangular to subrounded qtz, feldsp with volc lithic fragments and rare volc glass.

5Y5/1 grey — Visible biogenic silica 2-5%, mostly round and elongate diatoms and sponge spicules. Moderately bioturbated. Occasional 1-2 mm black sulphide? "blebs"

3-5 cm Irregular, bioturbated contact

7 cm sponge spicule-filled lens up to 20 mm in length

10Y5/1 Greenish grey — slightly stiffer layer

5-58 cm Sl v fine sandy mud (sand 3-12%). Grey to dark greenish grey.

10Y4/1 Dk. greenish grey — Subangular to subrounded qtz, feldsp, heavy minerals.

Variable biogenic silica in the mud fraction, predominantly diatoms and sponge spicules with some silicoflagellates (est 10% at 7 cm, 3% at 13 cm, 6% at 30 cm and 1% at 61cm). Highly bioturbated with burrows, spicule-filled lenses up to 10 mm in diameter and 50 mm in length.

10Y4/1 Dk. greenish grey

58-59 cm gradational contact

59-62 cm Sl pebbly sl sandy mud. Dark greenish grey. Common sub-angular granules and rare clasts up to 16 mm long in a muddy matrix.

Figure 20. Detailed log of Site 2 Core 4 from the floor of Windless Bight.

Figure 21. Features in the core from Site 1: Small mollusks, worm tube and foraminifera from 13 - 15 cm bsf. Scale in mm.

Figure 22. Features in the core from Site 1: Striae on pebble 20 mm across found at 35-37 cm bsf

4.2.2   Site 2 description

Site 2 is significantly different from Site 1 in being fine-grained (slightly) sandy mud throughout and lacking the basal diamicton.

Unit 1 (0-3 cm) is a soft very sandy mud (~40% sand), similar to the surface layer in Site 1 in having a little coarse sand and a few small pebbles up to 16 mm long.

Unit 2 (3-16 cm) is a firm sandy mud (20-50% sand) with little coarse sand and rare small pebbles and strongly bioturbated. Upper contact gradational.

Unit 3 (16-59 cm) is a firm slightly sandy mud (3-11% sand), 24-46% silt, 64-48% clay) with rare coarse sand above 20 cm and below 42 cm. Upper contact gradational.

Unit 4 (59-61 cm) is a slightly sandy mud (?diamicton) with a little fine to coarse sand and rare clasts up to 7 mm long (all angular/subangular and basic volcanic). Upper contact diffuse.

4.3   On-site petrography

Giovanna Giorgetti

Six sediment cores and one sediment grab were collected from Site 1, and four cores and three grabs from Site 2 (Table 8). Some cores were split and photographed, and after a visual description, smear slides were prepared for samples taken every 2 cm down the cores. These were studied using both a petrographic and an optical microscope to quantify the amount and nature of the biogenic content and the sand grain types in a preliminary way, and the results presented below.

Clasts of various sizes and compositions were found in all the split cores and in the grab (Table 9). Their depth of occurrence was noted and the pebbles sampled for further study. Some brief notes are tabulated in the last part of this section.

Table 9. Summary data for clasts recovered from Sites 1 and 2.

Site/depth	Number	Size (long axis)	Lithologies
Site 1 Core 1 0-1 cm	6	3-16 mm	Basic volcanic, quartz
Site 1 Core 1 12-13 cm	5	1-11 mm	Basic volcanic, quartz
Site 1 Grab 1	5	9-17 mm	Basic volcanic, metasediment, diamictite
Site 1 Core 4 1-3 cm	3	7-13 mm	Basic volcanic
Site 1 Core 4 31-60 cm	22	4-48 mm	Basic volcanic, metasediment, diamictite
Site 2 Core 4 0-1 cm	1	8 mm	Basic volcanic
Site 2 Core 4 58-60 cm	4	4-7 mm	Basic volcanic

The sediments largely consist of terrigenous material, mostly basaltic but with some basement and Beacon sandstone grains like the material making up the Transantarctic Mountains to the west. Siliceous biogenic material in cores from the Site 1 is in places common but mostly rare and in the lower part of the core virtually absent. In contrast, core from Site 2 has much more siliceous biogenic material which can be up to 50% in some intervals.

4.3.1   Site 1 Core 1

Core 1 is only 13 cm long, and comprises two lithological units that correspond to the upper two units of Core 4.

Unit 1 from 0 to 4 cm depth is comprised of very fine/fine muddy sand with pebbles up to 16 mm long (Table 9). The biogenic fraction is 5-10% and consists of sponge fragments and spiculae and diatom fragments. Sand grains consist of quartz, feldspar, volcanic glass, basic volcanic rocks and volcanic scoriae. Quartz grain content is high in the top sample (40%) but much lower below that (15%) with an increase of volcanic glass grains. Quartz grain shape varies from subangular to subrounded-rounded.

Unit 2, from 4 to 13 cm, is a very fine/fine muddy sand with a siliceous biogenic content around 20%. Grains in the sand fraction show the same petrographic characteristics as in the upper part of the core. However quartz grain content is lower (10-20%) while the volcanic glass content increases up to around 60%. A few small pebbles up to 11 mm long were noted from 12 to 13 cm (Table 9).

4.3.2 Site 1 Core 4

Core 4 has been subdivided into seven units based on lithological characteristics. Textural and compositional characteristics of these units based on smear slide description are summarised in Table 10.

The biogenic material comprises mainly diatoms, sponge spicules and fragments. Its content variation with depth is shown in Figure 23. The maximum content occurs at 2 cm depth where the diatoms are both preserved and fragmented. In all the other samples they are mainly fragmented. The biogenic content is low (~5%) down to 24 cm, and is virtually absent below this. In Unit 3, at 13-cm depth a bivalve and tubular carbonate shells have been recovered. In Unit 4, a few benthic foraminifera were found.

The sand fraction shows the same petrographic characteristics in all the units, but the relative abundance of quartz, glass and lithic grains varies (Figure 24 and Table 10). The quartz content decreases with depth in the upper two units and it shows a maximum in the third unit. In Unit 4, it increases again until it reaches relatively high constant values (ca. 20%) in Unit 5. In the two lower units, quartz content has the highest values ranging from 17 to 47%. Many of the quartz grains are subrounded to rounded, which is characteristic of sandstones of the Devonian Taylor Group (Beacon Supergroup) in the Transantarctic Mountains to the west. The glass content shows an opposite trend with respect to the quartz one. Some lithic grains have been recognised and consist of phonolites, basalts, and scoria.

Figure 23. Percentage of biogenic fraction vs depth in Site 1 Core 4.

Figure 24. Percentage of quartz (diamonds), glass (squares), and lithic (triangles) grains in the sand fraction vs depth in Site 1 Core 4.

Table 10. Summary of smear slide description for Site 1 Core 4. Biogenic content: percentage of biogenic (siliceous) component is with respect to the total sample. Quartz, glass, and volcanics percentage has been quantified in the sand fraction. Percentage of other minerals has not been quantified. Volcanics: mainly phonolite, scoria, basaltic rocks.

| Depth (cm) | Biogenics (%) | Biogenic material | | | | | Mineralogy | | | | Quartz grain roundness | Lithic | |
		Sponge	Diatoms	Bivalve	Forams	Tubular shells	Quartz (%)	Feldspar	Pyroxene	Olivine		Glass (%)	Volcanic (%)
0	5	Y	Y				27	Y		Y	subangular-subrounded	40	33
2	20	Y	Y				35	Y		Y	subangular-subrounded	31	34
4	6	Y	Y				20	Y		Y	angular-subangular	52	28
6	7	Y	Y				25	Y		Y	angular-subangular	50	25
8	7	Y	Y				21	Y		Y	subangular-subrounded	55	23
10	5	Y	Y				7	Y		Y	subrounded	67	26
12	T		Y				3	Y		Y	subangular	67	28
14	6	Y	Y	Y		Y	15	Y		Y	angular-subangular	68	17
16	5	Y	Y				10	Y	Y	Y	subangular-subrounded	70	20
18	9	Y	Y		Y		1	Y		Y	subangular-subrounded	69	30
20	3	Y	Y				0	Y	Y	Y	n/a	67	33
22	5	Y	Y				4	Y		Y	subrounded	62	34
24	-	-					19	Y	Y	Y	subangular-subrounded	30	51
26	-	-					14	Y	Y	Y	subangular-rounded	44	42
28	-	-					15		Y	Y	subangular-subrounded	41	44
30	T	Y	Y				20	Y	Y	Y	subangular-subrounded	40	40
32	T	Y			Y		7	Y		Y	subangular	18	75
34	T	Y					17	Y	Y	Y	subangular-subrounded	38	45
36	5	Y					41	Y	Y	Y	subangular-rounded	28	31
38	T	Y					30		Y	Y	subrounded-rounded	50	19
40	T	Y					46	Y	Y		subangular-subrounded	28	26
42	T	Y					31	Y	Y		subangular-subrounded	27	42
44	T	Y					42	Y		Y	subangular-subrounded	22	36
46	T	Y					40	Y		Y	subangular-subrounded	20	40
48	T	Y					43	Y		Y	angular-subrounded	15	42
50	-	-					38	Y		Y	subangular-rounded	22	40
52	-	-					47	Y		Y	subangular-rounded	15	38
54	-	-					32	Y		Y	subangular-subrounded	33	35
56	-	-					35	Y		Y	subangular-rounded	30	35
58	-	-					31	Y		Y	subangular	20	49
60	-	-					39	Y		Y	subangular-subrounded	22	39

4.3.3 Site 2 Core 4

Core 4 is divided into four lithologic units with slightly different colour and texture. Most of the core, from 3 cm down to 58 cm, is comprised of Units 2 and 3, which are similar in texture though with slightly different colouration and with Unit 2 showing stronger bioturbation. Textural and compositional characteristics of the units based on smear slide description are summarised in Table 11.

Biogenic content (diatoms, abundant sponge spicules and fragments) is shown in Figure 25. This is much higher at Site 2 than at Site 1. It clearly decreases with depth from 47% down to 12%. In Units 1, 2, 3, and upper Unit 4, sponge spicules are extremely abundant and are up to 3 mm in length. Through most of the core, diatoms are abundant and well preserved. In the lowest part of Unit 3 and Unit 4, biogenic content is almost absent and diatoms are fragmented.

As in cores from Site 1, the sand fraction comprises volcanic lithic fragments, glass and quartz, but their relative abundance varies with depth (Figure 26). The quartz content is usually lower than 20% and its trend is opposite to the glass one. Some lithic grains consist of phonolites, basalts, and scoria.
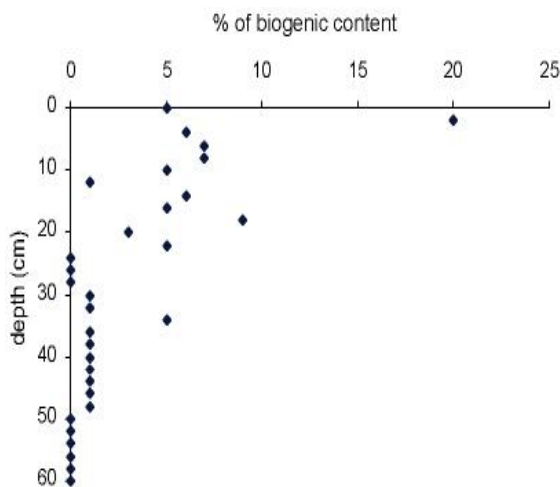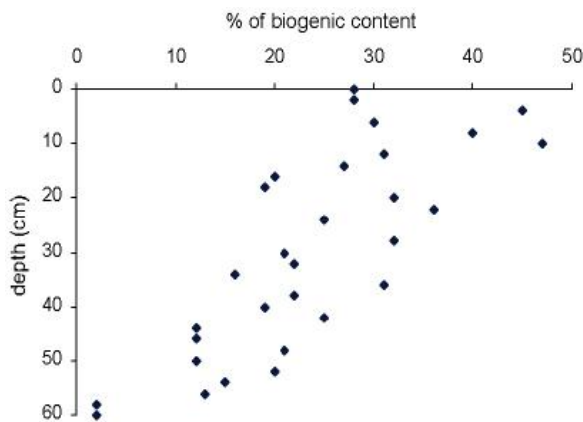

Figure 25. Percentage of biogenic fraction vs depth in Site 2 Core 4.

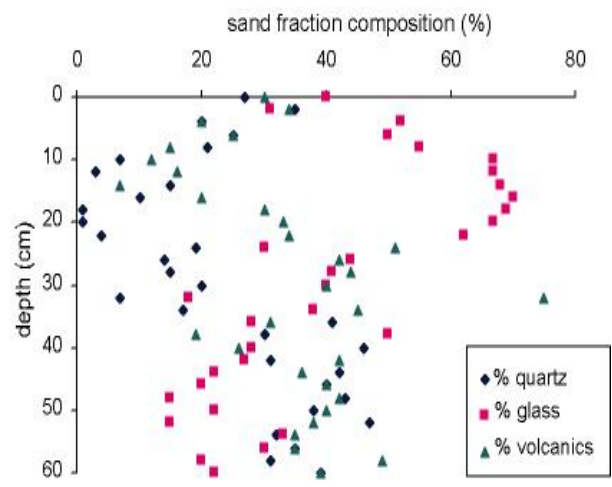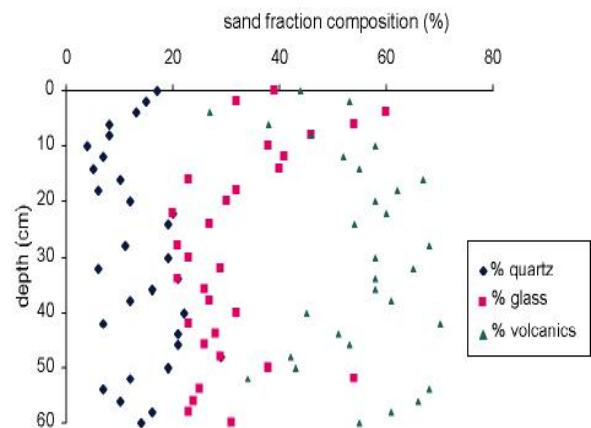*Figure 26.* Quartz (diamonds), glass (squares), and lithic (triangles) grains in sand fraction vs depth in Site 2 Core 4.

Table 11. Summary of smear slide description for Site 2 Core 4. Percentage of biogenic (siliceous) component with respect to the total sample. Quartz, glass, and volcanics percentages quantified for sand fraction. Volcanics mainly basic.

Depth (cm)	Biogenics (%)	Biogenic material					Mineralogy					Quartz grain roundness	Lithic	
		Sponge	Diatoms	Bivalve	Forams	Tubular shells	Quartz (%)	Feldspar	Pyroxene	Olivine	Biotite		Glass (%)	Volcanic (%)
0	28	Y	Y				17	Y				angular-subrounded	39	44
2	28	Y	Y				15	Y				subangular-subrounded	32	53
4	45	Y	Y		Y		13	Y	Y	Y		subangular-subrounded	60	27
6	30	Y	Y				8	Y	Y	Y	Y	subangular	54	38
8	40	Y	Y				8	Y		Y	Y	subangular-subrounded	46	46
10	47	Y	Y				4	Y		Y		angular-subrounded	38	58
12	31	Y	Y				7	Y		Y		subangular-subrounded	41	52
14	27	Y	Y				5	Y		Y		subangular-subrounded	40	55
16	20	Y	Y				10	Y		Y		subangular	23	67
18	19	Y	Y		Y		6	Y		Y		subangular	32	62
20	32	Y	Y		Y		12	Y		Y		subangular	30	58
22	36	Y	Y				20	Y		Y		subangular	20	60
24	25	Y	Y				19	Y		Y		subangular	27	54
28	32	Y	Y				11	Y		Y		subangular-subrounded	21	68
30	21	Y	Y				19	Y		Y		subangular-subrounded	23	58
32	22	Y	Y		Y		6	Y		Y		subangular-subrounded	29	65
34	16	Y	Y				21	Y		Y		subangular-subrounded	21	58
36	31	Y	Y				16	Y		Y		subrounded	26	58
38	22	Y	Y				12	Y		Y		subrounded	27	61
40	19	Y	Y				22	Y		Y		subrounded	32	45
42	25	Y	Y				7	Y		Y		subrounded	23	70
44	12	Y	Y				21	Y		Y		subangular-subrounded	28	51
46	12	Y	Y				21	Y		Y		subangular-subrounded	26	53
48	21	Y	Y				29	Y		Y		subangular-subrounded	29	42
50	12	Y	Y				19	Y		Y		subrounded	38	43
52	20	Y	Y				12	Y		Y		subrounded	54	34
54	15	Y	Y				7	Y		Y		subrounded	25	68
56	13	Y	Y				10	Y		Y		subrounded	24	66
58	<5	Y	Y				16	Y		Y		subangular-subrounded	23	61
60	<5	Y	Y				14	Y		Y		subangular-subrounded	31	55

4.3.4 Clasts from Sites 1 and 2

A total of 41 clasts were found in sediments from Site 1, though only five from Site 2 (Table 9). They occur mostly in the sandy mud just below the sea floor at both sites, and in the 30 cm of diamicton. Several clasts were also found 12-13 cm below the sea floor in Site 1 Core 1, and at the bottom of Site 2 Core 2.

The clasts are typically 5-15 mm in length, the largest being 48 mm long. They range from angular to rounded, and one or two have striae. Most are basic volcanic, and are presumed to be locally derived from the late Neogene volcanoes around Windless Bight. However, at least 8 are lithologies typical of the basement rocks of the Transantarctic Mountains to the west (meta-sandstone, meta-argillite, vein quartz), which we presume is their ultimate source. Two are diamictites with the coarser material mainly basic volcanic in origin. Thin section images of basic volcanics, metasediments and the two diamictites are shown in Figure 27. Table 12 and 13 provides basic data on the clasts themselves.

Table 12. Clasts sampled from Sites 1 and 2. **glacial pebble with striae. #7TS – thin-sectioned.

Clasts from Site 1 Core 1

Depth	Shape	Size	Lithology
0-1 cm	Rounded (cylindrical)	7x3x3 mm	-
0-1 cm	Rounded (spherical)	3 mm	Basic volcanic rock
0-1 cm	Subangular (platelet)	4x1x2 mm	Quartz vein
0-1 cm	Subangular (spherical)	4 mm	Dolerite
0-1 cm	Subangular	10x4x2 mm	Quartz-epidote vein
0-1 cm	Subangular	16x5x5 mm	Acid volcanic (tephrite?)
12-13 cm	Subrounded (spherical)	1 mm	volcanic scoria
12-13 cm	Subangular (platelet)	6x3x0.5 mm	Quartz vein
12-13 cm	Subrounded (cylindrical)	11x3x3 mm	Basic volcanic
12-13 cm	Subangular (spherical)	2 mm	Basic volcanic
12-13 cm	Angular	5x3x3 mm	Basic volcanic

Clasts from Site 1 Grab 1

Depth	Shape	Size	Lithology
0-3 cm #1 #8TS	Subangular (ellipsoidal)	17x4x7 mm	Volcanic scoria
0-3 cm #2 #9TS	Subangular (cubic)	10x8x9 mm	Metasediment
0-3 cm #3	Angular	9x5x6 mm	Quartz-feldspar vein
0-3 cm #4	Angular (platelet)	10x4x2 mm	Amphibolite
0-3 cm #5 #10TS	Subrounded (spherical)	13x10x8 mm	Diamictite

Clasts from Site 1 Core 4

Depth	Shape	Size	Lithology
0-1 cm #1TS	Subangular (spherical)	7x4x4 mm	Basalt
0-1 cm	Subangular (irregular)	13x11x6 mm	Basic volcanic
1-3 cm	Subangular (irregular)	8x5x4 mm	-
31-33 cm	Subangular (irregular)	9x6x5 mm	-
35-37 cm #2TS	Subrounded (prismatic)	34x19x14 mm	**Metasediment
39-40 cm	Angular (platelet)	9x6x0.5 mm	-
41-43 cm	Rounded (spherical)	5mm	Scoria

| 41-43 cm | Angular (platelet) | 4x4x3 mm | Basalt |

Table 12 (continued).

42-46 cm #3TS	Angular (irregular)	30x20x11 mm	Quartzite
47-49 cm	Subangular (prismatic)	8x4x1 mm	Basic volcanic
47-49 cm	Subangular (irregular)	6x2x3 mm	Scoria
47-49 cm	Angular (irregular)	6x4x3 mm	-
47-49 cm	Angular (prismatic)	8x6x4 mm	Basic volcanic
47-49 cm	Angular (irregular)	7x2x5 mm	-
49-51 cm	Angular (irregular)	11x10x5 mm	Basalt
49-51 cm #4TS	Angular (cylindrical)	7x4x3 mm	Contact metasediment
51-53 cm	Subrounded (irregular)	9x6x4 mm	-
51-53 cm #5TS	Subrounded (spherical)	48x21 mm	Basalt
51-53 cm #6TS	Subrounded (irregular)	19x13x8 mm	Diamictite
55-56 cm	Subrounded (spherical)	5 mm	Scoria
55-57 cm	Subangular (cylindrical)	14x6x6 mm	-
55-57 cm #7TS	Subrounded (prismatic)	8x6x3 mm	Basalt
55-57 cm	Angular (irregular)	8x5x3 mm	Basic volcanic
55-57 cm	Subangular (irregular)	11x7x6 mm	Basic volcanic
57-59 cm	Subrounded (platelet)	9x6x3 mm	-

Clasts from Site 2 Core 4

Depth	Shape	Size	Petrography
0-1 cm	Subangular (prismatic)	8x5x2 mm	Basic volcanic
58-60 cm	Angular	4x3x3 mm	Basic volcanic
58-60 cm	Angular	4x2x1 mm	-
59.5 cm	Subangular (spherical)	3x2x2 mm	Basic volcanic
60 cm	Angular (prismatic)	7x3x3 mm	Basic volcanic

Table 13. Clasts examined in thin-section from Site 1.

|	Depth	TS #	Shape	Lithology	Likely provenance
Site 1 Core 4	0-1 cm	# 1	Subangular	Basalt	McM Volcanic
Site 1 Core 4	35-37 cm	# 2	Subrounded	Metasediment	TAM Basement
Site 1 Core 4	42-46 cm	# 3	Angular	Metasediment	TAM Basement
Site 1 Core 4	49-51 cm	# 4	Angular	Metasediment	TAM Basement
Site 1 Core 4	51-53 cm	# 5	Subrounded	Basalt	McM Volcanics
Site 1 Core 4	51-53 cm	# 6	Subrounded	Diamictite	VLB strata
Site 1 Core 4	55-57 cm	# 7	Subangular	Basalt	McM Volcanic
Site 1 Grab 1	pebble 1	# 8	Subangular	Basalt	McM Volcanics
Site 1 Grab 1	pebble 2	# 9	Subangular	Metasediment	TAM Basement
Site 1 Grab 1	pebble 5	# 10	Subrounded	Diamictite	VLB strata
Site 1 Core 1	0-1 cm	# 11	Subangular	Micritic carbonate	TAM Basement
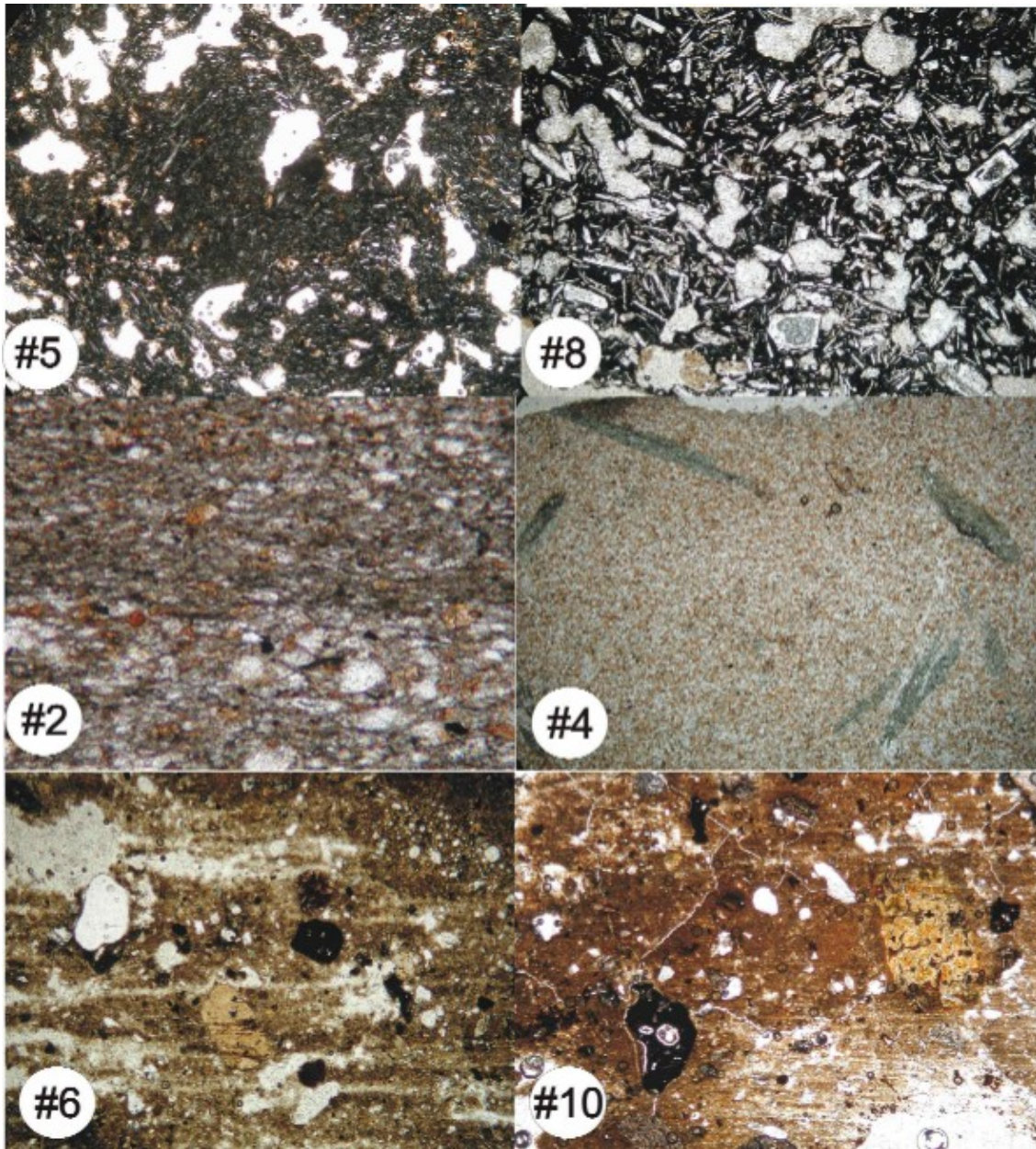
Figure 27. Photomicrographs of thin sections of clasts from Windless Bight cores. Numbers refer to thin section numbers in Table 13. The upper two are basalts, the middle two are metasedimentary rocks, #4 a hornfels with xenoblastic muscovite, and the lower two are volcanogenic diamictites.

4.4 Sediment organic geochemistry

Christina Riesselman

Sediment from both HWD03-1 and 2 cores were analysed at two centimetre intervals for the abundance of C, biogenic silica, $CaCO_3$, N, and isotopic ratios $\delta^{13}C$ and $\delta^{15}N$ (Table14) using the methods detailed in the Stanford Isotope Laboratory (SIL) on-line manual (http://pangea.stanford.edu/isotope/dam/manual.html). For biogenic silica SIL uses a method modified from Strickland and Parsons (1976). For Site 1, 0-39 cm, ~11 mg of dry, crushed sediment was digested in a 0.1M sodium hydroxide (NaOH) solution at 85°C and sampled at hours 2, 3, and 4. Mass for all remaining samples was increased to ~15 mg to reflect the low biogenic silica values measured in the first run. After sampling, 2 ml of molybdate reagent was added to each vial, followed 10 minutes later by 3 ml of reducing solution. The samples were allowed to sit for a minimum of three hours, then analysed using a Hitachi U-2001 spectrophotometer with wavelength set to 812 nm. Each run included replicates from the previous sample group and from within the run, and was controlled by 10 standards and a blank with concentrations ranging from 0 µM to 1200 µM.

At both sites, sedimentary organic matter (SOM) $\delta^{13}C$ is enriched by ~2‰ relative to water column suspended particulate organic matter (POM) $\delta^{13}C$, reflecting recycling and remineralization of organic matter.

With the exception of the uppermost sample, $\delta^{13}C$ of POM at Site 2 is slightly enriched relative to Site 1. This pattern may reflect the greater abundance of fresh organic matter (both detritus of the prymnesiophyte algae *Phaeocystis antarctica* and material bound within intact diatom frustules) observed in slide-mounted filters from Site 2.

Although the character of the cores from the two sites is very different, their surface sediments have similar C and N isotopic values, confirming that they share a modern biogenic sediment source. The carbon isotopic values are only slightly lighter than the surface sedimentary $\delta^{13}C$ mapped adjacent to Ross Island by Villinski et al. (2000).

The relative depletion of $\delta^{13}C$ moving upcore from older sediments to younger sediments coincides with an increase in the abundance of the sea-ice affiliated diatom *Fragilariopsis curta* in the diatom assemblage at both sites. While the shift in carbon isotopes could be attributed entirely to early diagenesis of the sedimentary organic matter, it is nevertheless interesting to note that it is coupled with a change in the community.

Weight percent opal is unexpectedly high at both sites, with maxima of 13.8% at Site 1 and 28.5% at Site 2 (Figure 28). The absence of biogenic debris seen at Site 1 in Unit 5 and the trace amounts in Unit 7, suggest that around 8% of the opaline silica estimated has come from another source, possibly the fine volcanic glass that is common in these sediments. The same might also be true of sediments from Site 2. Especially at Site 2, however, the structure of the opal curve closely mirrors changes in the concentration of diatom valves and fragments per gram of sediment.

SOM $\delta^{13}C$ is lowest near the surface and exhibits enrichment in ^{13}C down core, reflecting the release of labile carbon through decomposition of organic matter. An atomic C:N ratio of 7 to 8 at Site 2 likely reflects relatively fresh organic material

preserved in the sediments. An assessment of Site 1 organic material is complicated by down core sedimentary N concentrations, particularly in the diamict, which are so high that they seem to reflect a non-biological contribution. This contribution may be from nitrates dissolved in the pore waters and/or from ammonium adsorbed onto clay particles.

Table 14. Table of the biogenic component in Windless Bight sediments.

Depth	% Carbonate	% Opal (hour 4)	Wt. % C	Wt. % N	$\delta^{13}C$	$\delta^{15}N$
0	0.12	18.39	0.66	0.10	-26.26	4.58
2	0.12	17.85	0.71	0.11	-26.83	4.46
4	0.10	21.67	0.63	0.09	-26.43	3.99
6	0.08	24.61	0.46	0.08	-25.46	4.78
8	0.08	27.61	0.45	0.08	-24.70	5.68
10	0.08	27.44	0.46	0.08	-24.75	5.86
12	0.08	28.14	0.50	0.09	-24.98	5.80
14	0.10	25.71	0.46	0.08	-25.11	6.21
16	0.10	28.28	0.61	0.08	-25.59	6.07
18	0.09	28.47	0.55	0.09	-25.21	5.84
20	0.10	26.71	0.63	0.10	-25.44	5.85
22	0.12	24.21	0.69	0.10	-25.75	5.77
24	0.13	23.26	0.55	0.09	-25.39	5.33
26	0.13	22.26	0.50	0.08	-25.40	5.56
28	0.13	20.91	0.61	0.08	-25.39	5.09
30	0.13	21.35	0.56	0.09	-25.47	5.14
32	0.12	22.00	0.64	0.09	-25.45	4.79
34	0.13	22.62	0.59	0.09	-25.29	5.24
36	0.12	21.29	0.49	0.08	-25.03	5.86
38	0.14	20.24	0.42	0.07	-24.69	5.91
40	0.15	19.97	0.47	0.07	-25.01	5.51
42	0.15	20.03	0.48	0.07	-24.94	5.23
44	0.15	19.79	0.45	0.07	-24.72	5.48
46	0.16	19.15	0.44	0.07	-24.85	5.66
48	0.16	19.29	0.41	0.06	-24.79	6.43
50	0.17	19.20	0.37	0.06	-25.02	6.22
52	0.21	19.43	0.40	0.06	-25.24	6.01
54	0.22	19.17	0.39	0.06	-25.09	5.63
56	0.24	19.29	0.35	0.05	-24.75	5.67
58	0.28	19.13	0.36	0.05	-25.32	5.62
60	0.40	17.21	0.28	0.04	-25.05	5.38
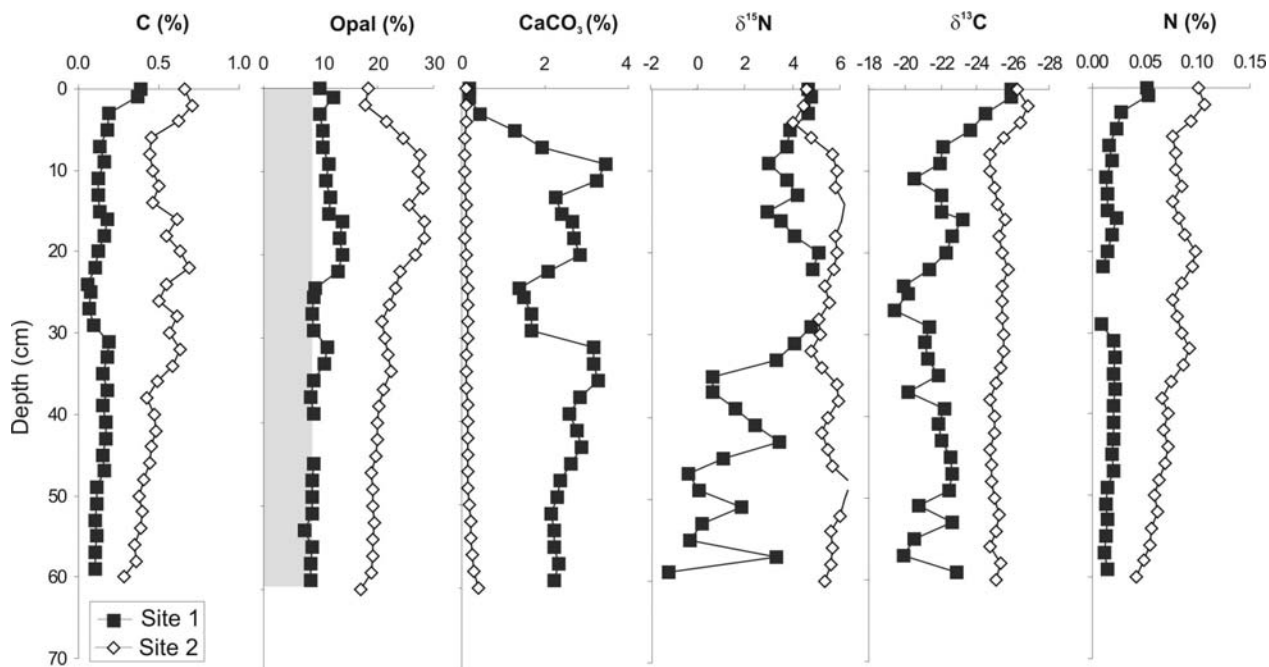
Figure 28. Down core variability in the biogenic fraction of Windless Bight cores from Sites 1 and 2.

4.4.1 References

Strickland, J.D. and Parsons, T.R. 1976. Practical handbook of seawater analysis. *Bulletin Fish. Res. Board Can*. (Ottawa) 167, 311p.

Villinski, J.C., Dunbar, R.B., and Mucciarone, D.A. 2000. Carbon 13/Carbon 12 ratios of sedimentary organic matter from the Ross Sea, Antarctica: A record of phytoplankton bloom dynamics. *Journal of Geophysical Research* 105, C6, 14,163-14,172.

4.5 Sediment ages

Peter Barrett and Gavin Dunbar

Ten samples were taken for dating and ^{14}C ages obtained from bulk organic carbon in acid insoluble organic (AIO) residues at the Rafter Radiocarbon Laboratory, Lower Hutt. Analytical data are presented in Table 15.

Ideally, these ages should be presented in a form comparable with ages from other marine and terrestrial records, i.e. in calendar years before present (cal BP). However, correcting and calibrating AIO ^{14}C ages from the Ross Sea region has proven difficult due to two factors unique to the region. First, the marine reservoir correction, at 1200-1300 years is substantially greater than for most of the world's oceans as a consequence of enhanced upwelling of "old" deep waters in the region (Gordon and Harkness, 1992; Andrews et al. 1999). Second, reworking of sediment containing ^{14}C from organic matter that is "dead" (i.e. >50 ka in age, when all ^{14}C has decayed) appears to be significant in the Ross Sea (Licht et al., 1998). Incorporation of such material into the bulk AIO content of sediment increases its apparent ^{14}C age in proportion to the ratio of "dead": contemporaneous AIO material. Thirdly, to convert conventional ^{14}C ages to their calendar year equivalent, a correction also needs to be made for variable production of ^{14}C over time. The approach to applying these corrections to our samples is based largely on the findings of Licht et al. (1998) and Andrews et al. (1999), who suggest that within relatively uniform post-glacial sediments "…a reasonable radiocarbon chronology can be obtained by (a) dating the sediment/water interface and (b) subtracting this age from subsequent dated samples." This process effectively applies two corrections to the "raw" AIO ages. 1) A marine reservoir correction of 1300 years (assuming all the AIO material is of marine origin) and; 2) a "dead" carbon correction which accounts for contamination of the *in situ* organic material with some old (>50ka) material reworked from elsewhere in the Ross Sea. (For Sites 1 and 2 this is 3040 and 1400 yrs respectively). This process leaves the core tops with a "0" age in ^{14}C years and ignores the possibility of a depositional hiatus at the water/sediment interface. It is further assumed that the magnitude of the reservoir correction and the proportion of dead: contemporaneous carbon remains constant downcore, though we cannot verify this. A further correction for variable ^{14}C production is then applied using the calibration of Fairbanks et al. (2005). Analytical data and calibrated ages are presented in Table 15.

The oldest sediment cored is Unit 7, Site 1, a 30-cm-thick diamicton (Figure 19). This unit provided a cluster of ages between 21800 to 25700 years BP, which are not in stratigraphic order, but indicate deposition of the whole unit approximately within this time range. Ages above this and from Site 2 are in stratigraphic order, and indicate more or less continuous sedimentation since the Last Glacial Maximum.
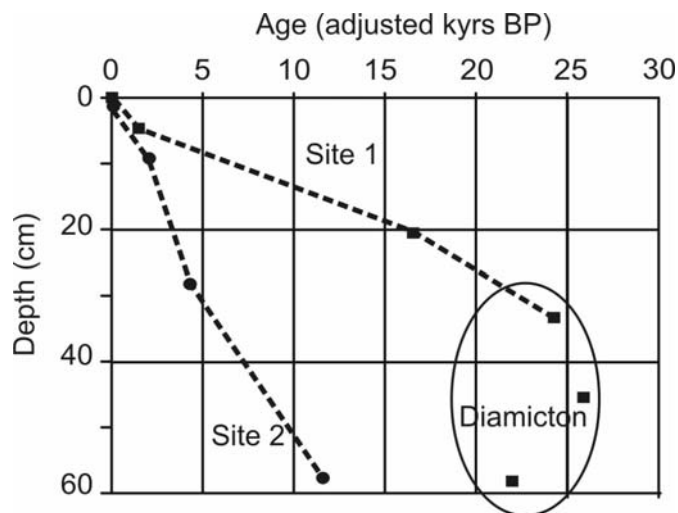

Figure 29. Age-depth curves for Sites 1 and 2, Windless Bight. Ages have been adjusted by subtracting 1300 years from those in Table 15.

From this we infer a sedimentation rate of 0.01 mm/year for Site 1 for Units 6-2, and 0.05 mm/year for Site 2 for Units 3 and 2 (Figure 29). These values are at the low end of the range in sedimentation rates for Holocene sediments in the Ross Sea shelf, typically in the range 0.05 to 0.25 mm/year (Domack et al., 1999).

Table 15. Analytical data for ^{14}C ages on cores from Sites 1 and 2 in Windless Bight.

Lab Code	CORE/DEPTH	Depth (cm)	Reported Age (^{14}C yrs)	Error (yrs)	Percent Modern	$\delta^{13}C$	$\delta^{14}C$	Calibrated age (yrs BP)	Std dev (yrs)
NZA18135	Site 1 0-1 cm	0.5	4343	55	58%	-27.2	-423.9	0*	-
NZA18846	Site 1 4-5 cm	4.5	5845	35	48%	-25.2	-520.3	1380	37
NZA18136	Site 1 20-21 cm	20.5	18080	100	10%	-24.9	-895.3	16480	182
NZA18137	Site 1 33-34 cm	33.5	24550	190	5%	-23.1	-953.1	24160	189
NZA18856	Site 1 45-46 cm	45.5	25750	190	4%	-22.6	-959.5	25750	294
NZA18857	Site 1 58-59 cm	58.5	22550	170	6%	-25.0	-939.6	21800	279
NZA18138	Site 2 1-2.5 cm	1.75	2701	50	71%	-26.9	-292.9	0*	-
NZA18847	Site 2 9-10 cm	9.5	4743	40	55%	-25.3	-449.8	2000	52
NZA18139	Site 2 28-29 cm	28.5	6562	45	44%	-25.7	-561.6	4280	85
NZA18140	Site 2 58-59 cm	58.5	12797	85	20%	-25.0	-798	11690	202

*assumed

4.5.1   References

Andrews, J.T., Domack, E.W., Cunningham, W.L., Leventer, A., Licht, K.J., Jull, A.J.T., DeMaster, D.J., Jennings, A.E. 1999. Problems and possible solutions concerning radiocarbon dating of surface marine sediments, Ross Sea, Antarctica. *Quaternary Research* 52, 206-216.

Domack, E.W., Jacobson, E.A., Shipp, S., Anderson, J.B. 1999. Late Pleistocene-Holocene retreat of the West Antarctic ice-sheet system in the Ross Sea: Part 2, Sedimentologic and stratigraphic signature. *Geological Society of America Bulletin* 111, 1517-1536.

Fairbanks, R.G., Mortlock, R.A., Chiu, T.-C., Cao, L., Kaplan, A., Guilderson, T.P., Fairbanks, T.W., Bloom, A.L., Grootes, P.M., Nadeau, M.-J. 2005. Radiocarbon calibration curve spanning 0 to 50,000 years BP based on paired 230Th/234U/238U and 14C dates on pristine corals. *Quaternary Science Reviews* 24, 1781-1796, doi:10.1016/j.quascirev.2005.04.007.

Gordon, J.E. and Harkness, D.D. 1992. Magnitude and geographic variation of the radiocarbon content in Antarctic marine life: Implications for reservoir corrections in radiocarbon dating. *Quaternary Science Reviews* 11, 697-708.

Licht, K.J., Cunningham, W.L., Andrews, J.T., Domack, E.W., and Jennings, A.E. 1998. Establishing chronologies from acid-insoluble organic 14C dates on Antarctic (Ross Sea) and Arctic (North Atlantic) marine sediments. *Polar Research* 17, 203-216.

4.6   Sediment texture
Peter Barrett

Grain size analyses were carried out in the Sedimentology Laboratory at Victoria University of Wellington. Care was taken not to sample across a unit boundary. The sand fraction and fine gravel fraction with sized by sieve and the mud fraction by settling using a Sedigraph 5100 as described by Barrett et al (2000). Sample sizes were small (typically between 5 and 10 g), and hence the proportions of the gravel fraction (>2 mm) can vary up to 20% from individual clasts. However the sand and mud fraction proportions should be replicable within 1-2%. The data are presented as both frequency percent and statistics in Appendix 7.4.

Figures 30 and 31 show the trends for cores from each site for % mud, reflecting sedimentation from suspension, and % coarser than 0.5 mm (coarse sand and gravel). In this setting such coarse sediment can be transported only by floating ice, as currents strong enough to move such sediments would also remove the sea floor mud. Typical histograms for each unit are also shown.

In Site 1 the soft clay-rich nature and the extreme textural range of the 30 cm of diamicton forming Unit 7 support the field interpretation of deposition from the basal debris layer when the grounding line of the Ross Ice Shelf was much deeper than today. The radiocarbon ages indicate this was slightly before or during the Last Glacial Maximum. The transition to Unit 6 represents the retreating of the grounding line and the resumption of more typical sub-ice shelf sedimentation. Most of the overlying sediment is a slightly fine sandy mudstone (more than 80% mud). However two features are unusual:

- The well-sorted fine sand that forms Unit 5. Fine sand sorting elsewhere on the floor of McMurdo Sound has been the result of sand blown by wind on to sea ice, but this is not a feasible explanation for a site covered by shelf ice. The sand might have been blown on to the surface during an unusual storm event and moved down through the shelf as more snow accumulated until it was released to the sea floor by basal melting. Alternatively the sand might have been transported to the site by sediment gravity flow, though it is hard to see how the nearby icy coast could permit a concentration of such sand as a source.
- The coarse sand and gravel that increases up through Unit 1 (discussed below).

Sediment texture at Site 2 suggests a quieter depositional environment, but there is nevertheless significant coarse sand and even fine gravel both in the lower 5 and the upper 15 cm of the core.

The coarse sand and gravel found in both cores requires explanation. Figure 32 shows the setting for sedimentation beneath the McMurdo Ice Shelf today, with average current flow eastward under the ice shelf from the open waters of McMurdo Sound. The slow current speed (average 7 cm/s, Robinson, 2005, submitted) can carry fine sediment beneath the shelf, but sediment of coarse sand grade or larger cannot be introduced this way because it rapidly sinks to the sea floor. Some coarse sediment is transported around McMurdo Sound today by ice bergs and sea ice, but there is no record of the McMurdo Ice Shelf edge retreating 12 km to expose both sites in the last 20,000 years (Kellogg et al. 1996). Coarse sediment might conceivably have been carried in by the ice shelf. This possibility is now being checked.
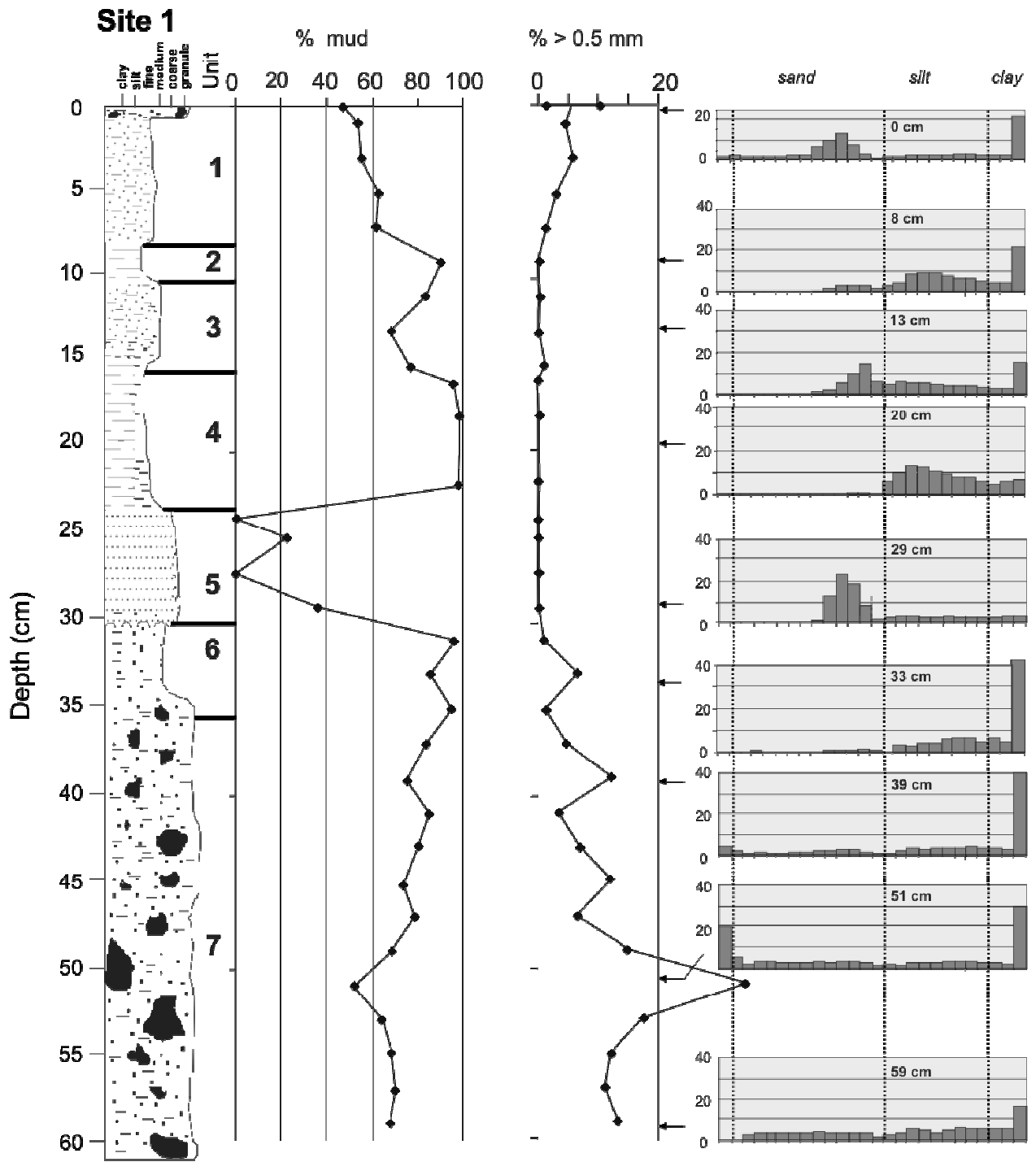
Figure 30. Log of Site 1 Core 4 with trends for % mud, % coarser than 0.5 mm, and representative histograms.
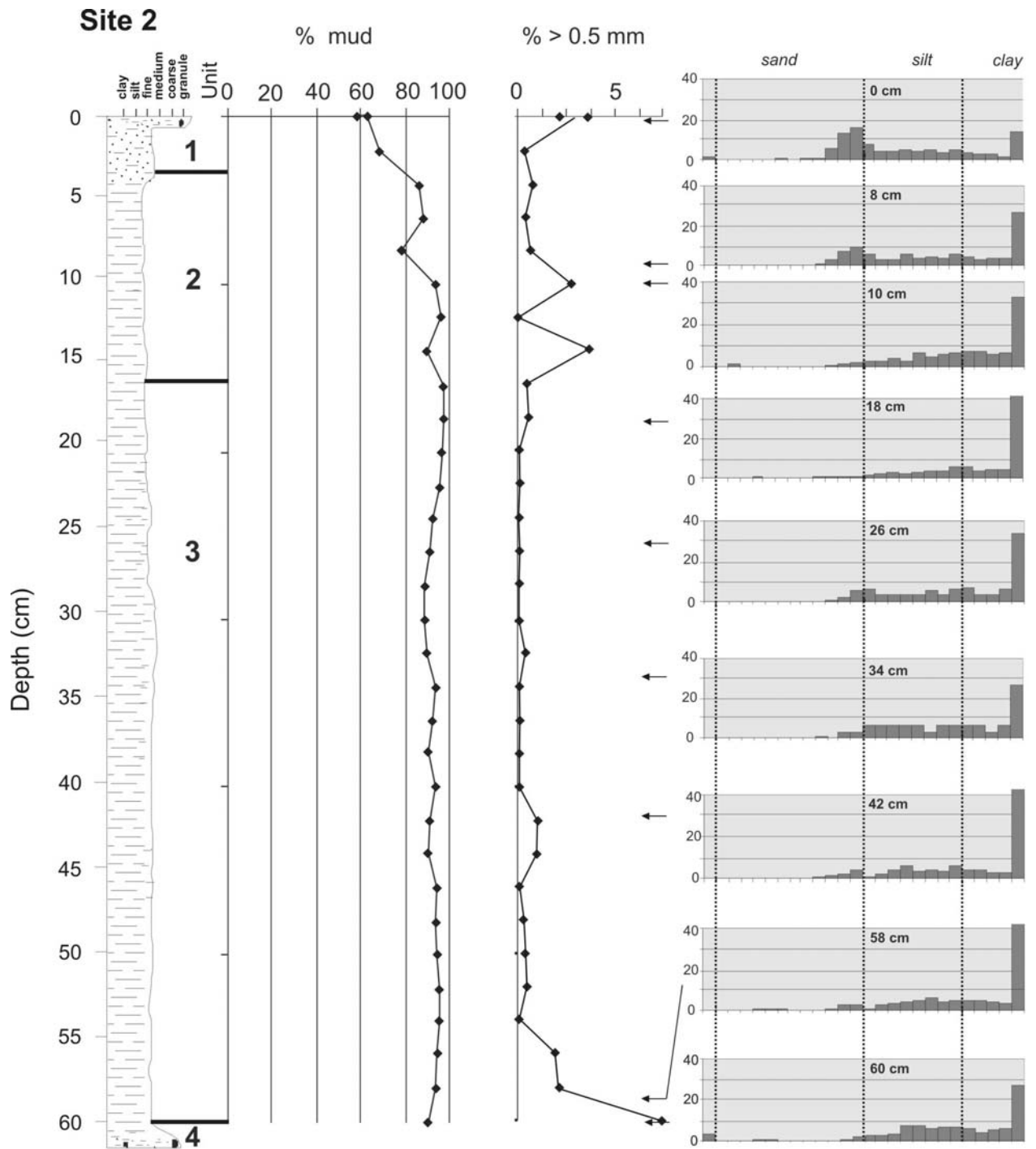
Figure 31. Log of Site 2 Core 4 with trends for % mud, % coarser than 0.5 mm, and representative histograms.

aeolian sand on sea ice

biogenic material from
near surface and sea floor

Site 1 Site 2

aeolian sand and gravel in shelf ice?

0

McMurdo Ice Shelf   Basal debris zone

300

IRD from W McM bergs
(gravel and sand)

Basal melting   Basal melting

600

<0.03 mm (silt and clay)

<0.125 mm (v fine sand)

<0.5 mm (medium sand)

900
metres

0   10   20   30   40 km

Size - mm	0.5	0.3	0.03
Material	Med sand	Bio pellets	Coarse silt
Settling velocity in cm/sec	6.5	0.46	0.05
Hours to settle 900 m	3.8	54	500
Km travelled in 7 cm/sec flow	1	14	126
Km travelled in 14 cm/sec flow	1.9	27	252

Ross Sea

Mt Terror

Ross
Island

Mt Erebus

Windless
Bight

Site 2

Ross Ice Shelf

Site 1

Figure 32. Section (left to right) from McMurdo Sound across the McMurdo Ice Shelf to the ice-covered slopes of Ross Island. Transport paths of various grain sizes and distances are shown for the eastward flowing current regime.

4.6.1   References

Barrett, P.J., Brooker, M.R., Anderson, J.J. 2000. Grain Size Analysis at VUW. *Unpublished Laboratory Manual*, 20pp.

Kellogg, T.B., Hughes, T., Kellogg, D.E., 1996. Late Pleistocene interactions of East and West Antarctic ice-flow regimes: evidence from the McMurdo Ice Shelf. *Journal of Glaciology* 42, 486-500.

Robinson, N.J., 2005. An Oceanographic study of the cavity beneath the McMurdo Ice Shelf. Unpublished MSc Thesis, Victoria University of Wellington, p.146.

4.7 Diatoms

Margaret Harper

This account summarises a report on diatoms from 29 samples taken from the two Windless Bight cores that are the subject of this report. A brief review of earlier work is followed by an outline of methods used, results and a discussion of their significance.

In the first comprehensive study of diatoms in McMurdo Sound, Leventer and Dunbar (1987) compared the diatom flora from sea ice, sediment traps and surficial sediment at various sites. In the sediment and most traps, heavily silicified *Thalassiosira* species of oceanic origin were most abundant and the only sea-ice form common was *Fragilariopsis curta*. Just under the sea ice thin-walled benthic species *Entomoneis kjellimani, Pleurosigma, Nitzschia stellata, Pinnularia quadratarea* were abundant. High flux rates in traps just above the sea floor indicated resuspension of sediments. In the only report on diatoms from beneath the Ross Ice Shelf, El-Sayed and Fryxell (1993), described material from the 237 m water column at the RISP J-9 site 400 km south of the shelf edge. At 37 m above the sea floor they only found a few valves of *Coscinodiscus* and *Trinacria* species. But *Fragilariopsis* and other pennate diatoms dominated the few microplankton remains strained from water 20 m below the 420 m thick ice shelf.

Dunbar and Leventer (1989) consider both oceanic diatoms and resuspended diatomaceous sediment have been carried under the shelf by ocean currents and have then settled in regions of deeper quieter water. They concluded that the Ross Sea gyre (Jacobs et al. 2002) and its cyclonic (clockwise) water circulation carries opal (mainly diatom remains) from open water in the Ross embayment to under the ice shelf. They found that sediments under the ice shelf were depleted in organic carbon compared with oceanic sediments. Organic carbon was lost during advection as currents carry remains of dead diatoms under ice. The Windless Bight sites are in a similar situation though only 5 and 12 km respectively from the shelf edge. Currents at the two Windless Bight sites described earlier in this report are influenced strongly by the tide in both speed (which reaches a maximum of 17 cm/s) and direction. However, they were found to have a net eastward flow eastward under the ice shelf from McMurdo Sound with a speed averaging 7 cm/s.

A recent study whose results are relevant to this report is that of Sjunneskog and Scherer (2005), who studied the diatom floras of short sediment cores from the Ross Sea. They found remains of diatoms common in the Ross Sea today (mainly *Fragilariopsis* species and dichaete *Chaetoceros* spores) were most abundant in the upper diatom rich muds. Fragments of stratigraphically long-ranging diatoms (not extant in the Ross Sea today, including some fossil and oceanic species) were dominant in basal diamictons. Earlier Scherer et al. (2004) devised a diatom fragmentation index to help distinguish between normal marine diatomaceous sediments and those that have been transported by grounded ice. This Scherer Index is the ratio of intact centric valves (not including *Chaetoceros* spp.) to intact pennate valves. They calibrated the index with a ring shear device. When the results were compared with diatom samples from glacial and pelagic sediments from the Ross Sea and they considered the index indicated relative subglacial stresses. (If over 90% of the intact valves are centric, the material is considered highly sheared and of subglacial origin; if less than 50% are centric then the material is unsheared and of pelagic origin, mainly from sea ice).

54

4.7.1 Methods
Sediment samples (3 gm) were air dried, oxidised with warm hydrogen peroxide (80°C), then simmered in concentrated hydrochloric acid and washed. Sand and clay were removed by repeated settling, (45 seconds twice discard sediment, 7 hours thrice discard liquid). Initial counts were over diametre transects of pipetted aliquots of suspended material. For Site 2 concentrations Battarbee trays were used which coat coverslips with known amounts of suspension (Battarbee, 1973). Samples from Site 1 were concentrated using heavy liquid separation (specific gravity 2.25).

Initial counts did not include fragments under 10 µm in size and these are less easily seen than original more concentrated mounts. Therefore assessment of fragmentation (fragments <10 µm %, >10 µm and whole valves %) is based on counts for Site 2 of a small area of Battarbee tray coated samples and in Site 1 on samples made from dilute aliquots. Three groups of remains were distinguished in initial counts: whole valves, significant remains (readily identified ends and middles of valves) and fragments over c.10 µm long axis. Later counts include small fragments from 10 to 5 µm in size.

4.7.2 Results
Figure 34 summarises the results of diatom counts giving the proportions of four major species, seven genera and three groups of minor species at each site. Three diatom units can be recognised based on the occurrence of contemporary Ross Sea species (termed here the Ross Sea flora), a mixture of these and oceanic species, and the dominance of oceanic species (see Sjunneskog and Scherer, 2005). The units, which are described below, also differ in the concentration of diatom remains, fossil content, and degree of fragmentation (Table 16). In Figure 33 the proportions of the Ross Sea flora through cores from both sites are compared. It should be noted that, according to the radiocarbon ages, the full 61 cm of Site 2 was deposited over roughly the same time period (the last 12,000 years) as the upper 12 cm of Site 1.

4.7.2.1 Unit A (Site 1, 0-5 cm; Site 2, 0-58 cm)
This unit is characterised by the percentage of contemporary Ross Sea species exceeding 50%. It includes only the top two samples in the Site 1 core but all except the basal one from the Site 2 core. Concentrations are high, and the proportion of fossil remains is low.

4.7.2.2 Unit B (Site 1, 4-36 cm; Site 2, 58-61 cm)
This unit is characterised by having 25 to 50% contemporary Ross Sea species. Samples from the middle of the Site 1 core and one from the base of the Site 2 core are in this unit. Concentrations of diatom remains are low. The proportion of small fragments is increased.

4.7.2.3 Unit C (Site 1, 36-61cm)
This unit is characterised by having less than 20% contemporary Ross Sea species. It includes all the diamicton (36-61 cm). Concentrations were extremely low except near the base of Site 1 (54-61 cm downcore). The amount of fragmentation is very high; which makes it harder to recognise fossil fragments. Fragments of modern species are easier to identify because there is more intact comparison material at the top of the cores. There were very few whole valves in this unit (16 in a total of 1164 remains including all relevant counts) and most of these were chipped.

Table 16. Diatom zones distinguished at Sites 1 and 2, Windless Bight (*whole valves may be chipped).

Unit (main flora)	Ross Sea flora (%)	Fossil (%)	Conc. (x 10^6 per gm)	Small fragments <10 µm (%)	*Whole valves (%)
A (Ross Sea)	Dominant (>50)	Rare (<4)	Medium (>10)	Abundant (<65)	Infrequent (2-8)
B (mixed)	Abundant (25-50)	Variable (2-5)	Low (0.1-3)	Dominant (65-97)	Variable (0-8)
C (oceanic)	Frequent (<25)	Infrequent (3-7)	Low (<4)	Predominant (>84)	Rare (0-1)

The most frequently identified diatom species at both sites are the modern species *Fragilariopsis obliquecostata*, *F. curta* and *Thalassiosira antarctica*. The commonest fragments had hexagonal areolae and are classified as "*Coscinodiscus* s.l." (*Coscinodiscus* sensu lato) although some of these fragments may come from other oceanic centric genera such as *Triceratium* and *Thalassiosira* (but not *T. Antarctica* or *T. gracilis)*. Next commonest are elongate fragments of pennates tentatively identified "*Thalassiothrix* etc*", occasional ends show this group also includes species of *Thalassionema* and *Trichtoxon*.

4.7.3   Discussion
Intact or whole valves form less than 10% of the remains even in the best preserved samples. This extremely fragmented condition is typical of sediment from under ice shelves (Leventer and Dunbar, 1987; El-Sayed and Fryxell, 1993). There are very few remains of vegetative valves of *Thalassiosira antarctica* and *Eucampia antarctica* although the thick-walled valves of their resting-cells are common. Similarly *Chaetoceros* resting spores are common in several samples but fragments of setae or vegetative valves were rare. Vegetative valves are much more common than resting forms where there is active growth. Frequent resting forms indicates deposition at a distance from where they grew.

4.7.3.1   Diatom Unit A (Site 1, 0-5 cm; Site 2, 0-58 cm)
This unit is dominated by the contemporary Ross Sea species. The commonest are *Fragilariopsis obliquecostata* and *F. curta*. Sjunneskog and Scherer (2005) consider a similar assemblage on the Pennell Bank in the Ross Sea indicates seasonal open water, but they have more *F. curta* which indicates presence of winter sea ice (Gersonde et al., 2005). *F. obliquecostata* only grows in very cold water (<-1°C, Gersonde et al., 2005) in the presence of summer sea ice. It resists dissolution so can indicate regional sea ice cover in areas of low sedimentation rates. There were rare fragments of some of the more fragile sea ice species *Entomoneis kjellerani, Nitzschia stellata* and *Pleurosigma* species that grow in the Ross Sea (Leventer and Dunbar, 1987). Diatom remains in Unit A come mainly from McMurdo Sound. Tidal currents carry sea ice species growing in McMurdo Sound over a 600 m deep sill and past Hut Point into the deeper waters and slower currents of Windless Bight (Figure 34), leading to diatom deposition. This unit also contains a small amount of glacial input. This is indicated at Site 2 by the fragmentation index of Scherer et al. (2004), which exceeds 50% (52-74%) in all but the top sample (0.5 cm only 47%) and also by the occurrence of occasional fossil forms. The Fragmentation Index is not used for the Site 1 as there too few intact valves at most levels.
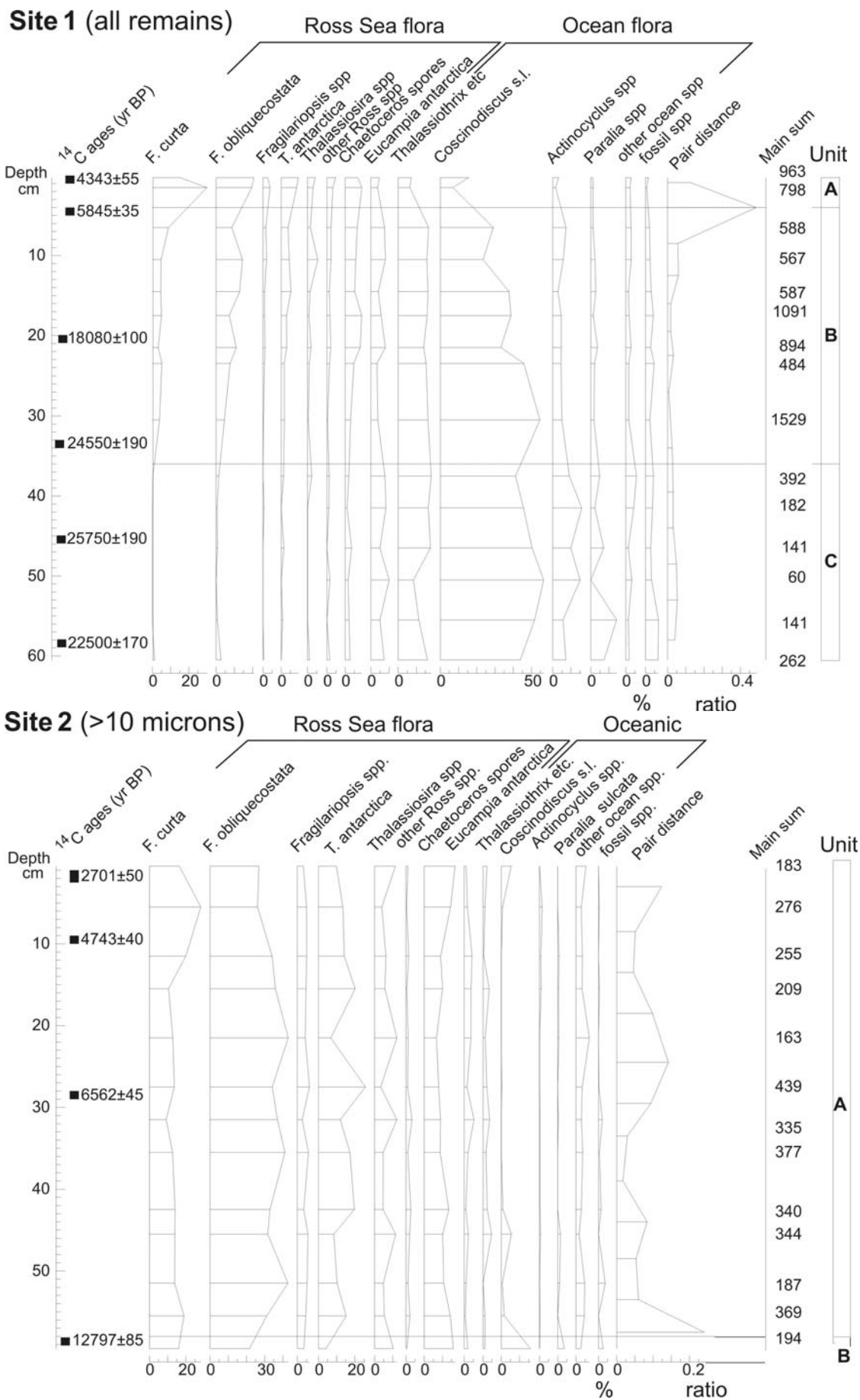
Figure 33. Diatom percentage variation in main taxonomic groups through Site 1 and 2 cores.
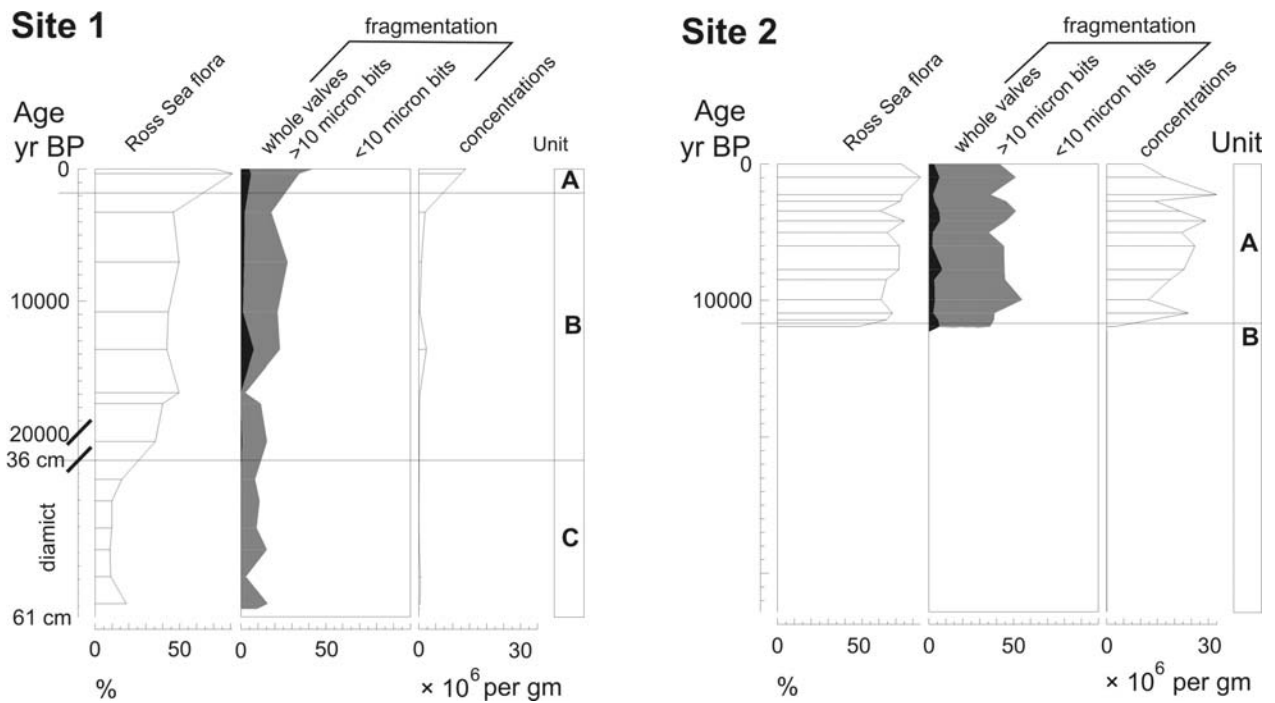
Figure 34. Diatom percentage variation in Ross Sea flora and fragmentation, also concentrations through cores from Sites 1 and 2, Windless Bight.

4.7.3.2 Diatom Unit B. (Site 1, 5-36 cm; Site 2, 58-61 cm)

Contemporary Ross Sea species are frequent in this unit but not dominant. Fragments of *Thalassiothrix,* a planktic genus become more abundant at Site 1. It is a long ranging genus extending back to the middle Miocene, but is still extant (Harwood and Maruyama, 1992). Fragments of *Coscinodiscus* sensu lato, a longer ranging genus, also become more abundant. An increase in fossil remains and in small diatom fragments (5-10 microns size) indicates a higher proportion of remains have been glacially reworked (Sjunneskog and Scherer, 2005) than in Unit A. This unit forms a transition between the other two. Sjunneskog and Scherer (2005) interpret a similar mixed assemblage as indicating nearby ice shelf breakup. Their mixed assemblage from mid-core (TC33 33-55 cm) in the central Ross Sea was radiocarbon dated as deposited between about 12.7 to 8.1 Ka (Sjunneskog and Scherer 2005), but dates from surface sediments indicate these dates may well be 3 Ka too old, suggesting deposition between 10 and 5 Ka (Andrews et al., 1999).

4.7.3.3 Diatom Unit C. (Site 1, 36-61 cm)

This is typical of samples of pebbly sandy mud (diamicton) at Site 1. It has the lowest percentage of contemporary Ross Sea species, and only *Eucampia antarctica* is present at all levels, its fossil range extends back to the middle Miocene. Some small fragments of this may be misidentified *Trinacria* species. However the presence of a few sea ice diatom remains suggests occasional water flow beneath the basal ice from which the sediment was being released. Diatom remains are sparse and most are fragments of *Coscinodiscus* sensu lato. Sjunneskog and Scherer (2005) found the commonest remains in their diamictons were fragments of *Paralia* (up to 50%). *Paralia* is relatively uncommon in the Windless Bight cores, but the proportion of its remains increases from a mean of c.1% in Unit A, to 2% in B and c.6% in C. The long-lived "oceanic" assemblage suggests reworking of pre-existing diatoms by grounded ice passing over higher topography to the south, with only the most robust frustule fragments

58

surviving to be released from the basal debris layer as the ice floats in the deeper water of Windless Bight during the Last Glacial Maximum.

4.7.4 Comparison of Sites 1 and 2

The floras at Site 1 except at the very top are sparse and highly fragmented, making identification and enumeration difficult even after the use of heavy liquid to concentrate material. The floral changes match the recognised range from glacially deposited diamicton (pebbly sandy mud, below 36 cm downcore) to the deposition of fine sandy mud largely from suspension, with no recognisable influence from bottom currents. The flora at Site 2 is better preserved and more concentrated than even at the top of Site 1. It is generally very consistent with relatively small variations in fragmentation (Scherers Index), concentration and the relative proportions of oceanic and sea ice species (Figure 34). Maximum current velocities at Site 1 are a little stronger than at Site 2 today, but not enough to explain the difference in the floral record. Does the better preservation and higher abundance of diatoms in Site 2 reflect its greater distance from the edge of the McMurdo Ice Shelf? This might be true today but is unlikely to be so prior to 7000 yr BP when the grounding line for the ice shelf lay at the same latitude as Ross Island (Conway et al., 1999), and the calving line was most likely hundreds of km north.

4.7.5 Diatoms in water column compared with core tops.

Nearly all the diatoms found in the water column were typical contemporary Ross Sea forms (with the exception of rare *Paralia* and *Denticulopsis*). Upper water column samples at Site 1 (110 and 370 m) contained more diatom colonies with remnants of cell contents. Flora from the lower part of the water column contained fewer colonies and more fragments. The lower floras still differed from those in the core tops (Table 17, 18). The sea-ice diatom *Fragilariopsis cylindrus* was dominant in the water at Site 1, but uncommon in the core top where *Fragilariopsis curta* was the most abundant form. *Fragilariopsis cylindrus* was less abundant in the water at Site 2 and again uncommon in the core. Valves of robust forms such as *Chaetoceros* spores and *Fragilariopsis obliquecostata* survive in the core tops when other forms have been fragmented by grazers. A camera lowered through a new hole nearby Site 1 showed grazers are active on the sea floor (Carter et al. 2007). Currents measured at both Sites 1 and 2 at times exceeded 17 cm/sec strong enough to resuspend diatoms (Robinson & Pyne, 2003). *(Information on diatoms in the water column comes from Christina Riesselman pers. comm. 2006 Stanford University).*

4.7.6 Summary

Three diatom units have been recognised in the Windless Bight cores, they are distinguished by the proportion of contemporaneous Ross Sea diatoms (>50%, 20-50% and <20%) in them. The units also differ in concentration, amount of fragmentation and fossil content. Most of the contemporaneous diatoms are derived from the sea ice in McMurdo Sound. The other diatomaceous material comes from glacial reworking and supports the presence of extensive grounded ice in the region during the Last Glacial Maximum. Site 1 records the transition from this state to the present with the shelf margin a short distance seaward of Windless Bight. Although Site 1 is 7 km from the ice margin and Site 2 is only another 5 km in, contemporaneous diatoms at the latter site are more abundant and better preserved.

Table 17. Diatom counts from the water column (Courtesy of Christina Riesselman, Stanford University).

	HWD03-1			HWD03-2				
Depth (m)	110	370	916	149	427	427	910	910
Cast number	S1C1	S1C1	S1C1	S2C11	S2C5	S2C13	S2C9	S2C2
Achnanthes sp.	-	-	-	-	1	-	-	-
Berkeleya sp.	-	-	-	-	-	-	-	1
Chaetoceros spores	12	4	4	25	18	13	3	29
Chaetoceros vegetative	19	4	7	20	10	20	2	28
Cocconeis costata	-	1	1	-	-	-	-	-
Cyclotella sp.	-	2	-	-	-	-	-	-
F. curta	21	12	4	47	46	14	19	65
F. cylindrus	319	46	97	311	85	197	34	299
F. kerguelensis	-	-	-	-	-	-	1	-
F. obliquecostata	-	-	2	5	-	-	-	-
F. pseudonana	3	-	-	-	-	-	-	-
F. rhombica	-	-	-	-	-	-	1	-
F. ritscheri	-	-	-	-	1	-	2	1
F. spp.	26	7	7	2	8	3	6	-
N. medioconstricta	-	1	-	-	-	-	-	-
N. stellata	2	-	-	2	-	-	-	-
N. stellata	-	-	-	-	-	-	-	1
Navicula sp.	-	-	-	-	1	1	-	-
Paralia sp.	1	-	-	-	-	-	-	-
Plagiotropis gaussi	-	-	1	1	-	1	-	2
Synedra sp.	-	-	-	-	-	1	-	2
T. gracilis	-	-	2	-	1	1	-	-
T. lentiginosa	-	1	-	-	-	-	1	-
T. sp.	-	-	1	-	-	-	-	-
T. tumida	-	-	-	1	-	-	-	-
Unknown centric (colony)	4	2	-	-	-	-	-	-
Dinoflagellate cyst	1	-	12	3	5	9	6	9
Total	407	80	126	414	171	251	69	428
Colonial cells	195	23	60	114	41	43	12	134

60

Table 18. Diatom taxa found in cores from Windless Bight, Antarctica.

v. cells. = vegetative cells, r. cells = resting cells. In curved brackets floral grouping: in upper case according to Sjunneskog and Scherer (2005), lower case assigned by M.A.H based on the literature. M = modern Ross Sea Flora, L = long-ranging oceanic species and F = fossil, t=terrestrial. N,N% = Site1, Site 2 % (>0.5% percent total, NA less than 0.5%). *only fragments present

Achnanthes cf. brevipes Ag. {m}

Actinocyclus spp {L} 4,1%

Actinocyclus actinochilus (Ehr.) Simon. {M} 1,1%

Actinocyclus cf. *ingens* Ratt. {f}

* *Actinoptychus* cf. *senarius* (Ehr.) Ehr. {L}

Anaulus cf. *simonsenii* Witk. & Metz. {f}

Asteromphalus sp. {f}

A. aff. *parvulus* Kar. {M}

Cestodiscus sp. {f}

Chaetoceros sect. *Dicladia* spores (>5 taxa) {M} 3,2%

C. aff. *bulbosum* (Ehr.) Heid. {M}

C. aff. *dichaeta* Ehr, setae {M}

C. cf. *dichaeta* Ehr, spores {M} 4,3%

C. cf. *neglectum* Kar., spore & setae {M}

Cocconeis cf. *pinnata* (Grev.) Greg. {m}

Corethron aff. *criophilum* Castra. {M}

Coscinodiscus spp. sensu lato {L} 69,18%

C. cf. *elliptopora* Dona. {f}

Dactyliosolen antarcticus Castra., copula {l}

Delphineis sp {l}.

Denticulopsis sp. {F}

Entomoneis cf. *kjellimanii* Cl. {M}

Eucampia antarctica (Castracane) Mang., r. cells {M} 10,7%

E. antarctica (Castr.) Mang., v. cells {M}

E. antarctica var. *recta* (Mang.) Fryx. et Pras. r & v. cells {M}

Fragilariopsis angulata Hasle {M} NA,1%

F. curta (Van Heurck) Hasle {M} 12,9%

Fragilariopsis cf. *cylindrus* (Grun.) Hasle {M}

F. cf. *kerguelensis* (Van Heu.) Hasle {M}

F. obliquecostata (Van Heu.) Heid. {M} 16,24%

F. cf. *ritscheri* Hust. {M}

F. separanda Hust. {m}

F. sublinearis Hasle {m} 1,NA%

Grammatophora cf. *marina* (Lyng.) Kütz. {l}

Liradiscus spp. [fossil *Chaetoceros* spores] {F}

Melosira cf. *sol* (Ehr.) Kütz. {m}

Navicula directa (W. Sm.) Ralfs {m}

N. gibbula Cl. {mt}

N. glacei Van Heu. {m}

Nitzschia spp. {m}

N. cf. *laevis* Hust. {m}

N. cf. *lineola* Cl. [*Pseudonitzschia*] {m}

N. cf. *stellata* Mang. {m}

N. cf. *turgiduloides* Hasle {m}

Paralia sulcata (Ehr.) Cl. {L} 5,1%

Pinnularia sp. {m}

P. cf. *cymatapleura* West & West {mt}

Pleurosigma spp. {M}

Poretzia sp {f} 1,NA%

Porosira glacialis (Grun.) Jorg. {m}

P. pseudodenticulata (Hust.) Zhuse {m} 1,1%

Proboscia spp. {l} 1,1%

P. alata (Bright.) Sund. {l}

Rhabdonema sp. septa {l}

Rhizosolenia spp ends {L} 1,1%

R. cf. *antennata* fo. *semispina* Sund. {l}

Rhizosolenia cf. *hebetata* fo. *hiemalis* Gran {l}

R. cf. *rhombus* Kar. {l}

Rouxia spp. {F} 2,NA%

R. cf. *antarctica* Heid. & Kolbe {f}

Sceptoneis cf. *grunowii* Aniss. {f}

Stellarima microtrias (Ehren.) Hasle & Sims {L}

Stephanopyxis spp. {F} 1,NA%

S. cf. *turris* (Grev.) Ralfs {l}

Stictodiscus cf. *hardmanianus* Grev. {f}

cf. *Suririella* sp {m}

Thalassionema cf. *nitzschioides* (Grun.) Hust.   {L} NA,1%

Thalassiosira spp. {l}

T. cf. *ambigua* Kozlova {m}

T. antarctica Comb. (r. cells) {M} 6,7%

T. cf. *antarctica* Comb. (v. cells) {M}

T. cf. *eccentrica* (Ehr.) Cl. {L}

T. gracilis var. *gracilis (*Kar.) Hust. {M} 1,2%

T. cf. *gracilis* var. *expecta* (Van Land.) Fryx. & Hasle {m}

Thalassiosira cf. *inura* Gers. {F}

T. cf. *oestrupii* (Ost.) Hasle {m}

T. oliverana var. *sparsa* Harw. & Maru. {f}

T. lentiginosa (Jan.) Fryx. {m} 1,NA%

T. cf. *leptopus* (Ehr.) Hasle {l}

T. cf. *maculata* Fryx. & Johan.)

T. cf. *trifulta* Fryx. {m}

T. tumida (Janisch) Hasle {M}

Thalassiothrix sp. {L}

Trichtoxon reinboldii (Van Heur.) Reid et Round {l}

Trinacria cf. *excavata* Heib. {F}

Non diatom: Silicoflagellate, *(Distephanus speculum speculum)* chrysophyte cysts, sponge

spicules (mainly flattened elongate with slight ridge) and rare testate amoebae scales.

4.7.7 References

Andrews, J.T., Domack, E.W., Cunningham, W.L., Leventer, A., Licht, K.J., Jull, A.J.T., DeMaster, D. J. and Jennings, A.E. 1999. Problems and possible solutions concerning radiocarbon dating of surface marine sediments, Ross Sea, Antarctica. *Quaternary Research* 52, 206-216.

Battarbee, R.W. 1973. A new method for estimating absolute microfossil numbers with special reference to diatoms. *Limnology and Oceanography* 18, 647-653.

Carter, L., Dunbar, G. McKay, R. Naish, T. 2007. Sedimentation and oceanography beneath the McMurdo Ice Shelf at Windless Bight, 2006. *Antarctica Data Series* No 32, p 30.

Conway, H., Hall, B.L., Denton, G.H., Gades, A.M., Waddington, E.D. 1999. Past and future grounding-line retreat of the West Antarctic Ice Sheet. *Science* 286, 280-283.

Dunbar, R.B. and Leventer, A.R. 1989. Biogenic sedimentation in McMurdo Sound, Antarctica. *Marine Geology* 85, 155-179.

El-Sayed, S.Z. and Fryxell, G.A. 1993. Phytoplankton. In Friedmann. E.I. (ed.), *Antarctic Microbiology*. Wiley: New York, 65-121.

Gersonde, R., Crosta, X., Abelmann, A., and Armand, L. 2005. Sea-surface temperature and sea ice distribution of the southern Ocean at the EPILOG Last Glacial Maximum – a circum-Antarctic view based on siliceous microfossil records. *Quaternary Science Reviews* 24, 869-896.

Harwood, D.M., and Maruyama, T. 1992. Middle Eocene to Pleistocene diatom biostratigraphy of ODP Leg 120, Kerguelen Plateau. *Proceedings of the Ocean Drilling Program, Scientific Results* 120, 683-733.

Jacobs, S.S., Giulivi, C.F., and Mele, P.A. 2002. Freshening of the Ross Sea during the Late 20th Century. *Science* 297 (5580), 386.

Leventer, A. 1992. Modern distribution of diatoms in sediments from the George V Coast, Antartica. *Marine Micropaleontology* 19, 315-333.

Leventer, A. and Dunbar, R.B. 1987. Diatom flux in McMurdo Sound,Antarctica. *Marine Micropaleontology* 12, 49-64.

Robinson N., Pyne A., 2003. Water column current profile analysis from beneath the McMurdo ice Shelf at Windless Bight and under the sea ice in Granite Harbour , Antarctica *Antarctic Data Series* No 26, p. 30.

Scherer, R.P., Sjunneskog, C.M., Iverson, N.R., and Hooyer, T.S. 2004. Assessing subglacial processes from diatom fragmentation patterns. *Geology* 32, 557-560.

Sjunneskog, C. and Scherer, R.P. 2005. Mixed diatom assemblages in glacigenic sediment from the central Ross Sea Antarctica. *Palaeogeography, Palaeoclimatology, Palaeoecology* 218, 287-300.

4.8 Foraminifera and radiolaria

Chris Hollis and Percy Strong

Foraminifera and radiolarians and are relatively common in surface sediments from both sites beneath Windless Bight (Table 19). Radiolarians are also relatively common in sediment samples from a short core in the southern, seaward Site 1. Radiolarian assemblages are dominated by *Prunopyle antarctica* and *Antarctissa* spp. Foraminiferal assemblages in surface sediments are dominated by agglutinated benthic species of the genera *Reophax*, *Miliammina*, *Portatrochammina*, *Hyperammina* and *Recurvoides*. Calcareous benthic species are rare in surface sediments but exhibit a down-core increase relative to agglutinated species in the Site 1 core (0-11.5 cm below sea floor). This is probably due to decomposition of organic bonds and break-up of agglutinated tests in subsurface sediments. The most common calcareous genera are *Globocassidulina*, *Trifarina* and *Astrononion*. A significant occurrence of common *Globocassidulina* is noted in the lower part of the core (6-10 cm below sea floor). Rare specimens of the planktic foraminifera *Neogloboquadrina pachyderma* occur in four of six core samples.

4.8.1 Material and methods

Wet sediment samples were provided by Gavin Dunbar. One surface sediment grab sample (HWD03-G2) at Site 2 and six sediment samples from one of the three short (11.5 cm) cores (Site 1-C3) from Site 1 were processed for radiolarians and foraminifera. The six samples were taken from 0-2, 2-4, 4-6, 6-8, 8-10 and 10-11.5 cm below the top of the core. Half of the core was sampled, providing c. 20 cc of wet sediment for each. All samples were washed with dispersant through a 63 μm sieve. After initial assessment of all sediment residues (>63 μm), heavy liquid separation (sodium polytungstate, SG = 1.65) was used to concentrate microfossils in the light fraction of the core sediments following the method of Hollis and Strong (2003).

Dried sample residues were split into size fractions using 150 and 300 μm sieves. A selective pick was carried out on the >150 μm fraction of the grab sample. Representative assemblages of radiolarians, foraminifera and sponge spicules were mounted on two faunal slides (>300 μm and 150-300 μm). Full faunal picks were carried out on the >150 μm light fractions of the six core samples. All radiolarians, foraminifera, ostracods and molluscan fragments, as well as selected sponge spicules and diatoms were mounted on faunal slides. Examination of the 63-150 μm fraction of the core samples revealed numerous radiolarians. A split of this fraction will be mounted as strewn slides for study of radiolarians under transmitted light microscope.

Quantitative analysis of the assemblages has not been undertaken because less than 100 specimens of radiolarians or foraminifera were recovered from subsurface core samples. Instead abundance is recorded as (Tables 20 and 21): Present (1 specimen), Rare (2-4 specimens), Few (5-10 specimens) and Common (>10 specimens).

Table 19. Samples for foraminiferal and radiolarian study from Sites 1 and 2, Windless Bight.

Sample	Depth	Rads	Diatoms	Sp. spics	Agg. forams	Cal. forams	Lithology
Site 1-Core 1	0 - 2 cm	few	few	common	common	rare	gravelly sand
	2 - 4 cm	few	rare	rare	few	rare	sandy mud
	4 - 6 cm	few	rare	rare	few	rare	sandy mud
	6 - 8 cm	few	rare	rare	few	few	sandy mud
	8 - 10 cm	rare	rare	rare	rare	common	sandy mud
	10 - 11.5 cm	rare	rare	rare	rare	none	sandy mud
Site 2 - Grab	Surface	common	common	common	common	rare	sandy mud

4.8.2   Results

Radiolarians and agglutinated foraminifera are common in the surface sediment sample from Site 2. The assemblages are typical of those known from modern surface sediments in Ross Sea (e.g. Fillon, 1973, 1974; Chen, 1975; Violanti, 1996). Calcareous foraminifera are very rare, with only three benthic specimens recorded.

Radiolarians and agglutinated foraminifera are common in the uppermost sample from Core Site 1-C3 (0-2 cm). As at Site 2, the assemblages are typical of those known from modern Ross Sea sediments. Calcareous foraminifera are relatively common and include rare *Neogloboquadrina pachyderma*.

Downcore, radiolarians remain relatively common, the most common species being *Prunopyle antarctica*. In contrast, agglutinated foraminifera decrease in abundance and diversity downcore, presumably due to breakdown of the organic compounds that hold the agglutinated tests together. The genera *Miliammina*, *Reophax*, *Hormisinella*, *Hyperammina* and *Textularia* appear to be most prone to breakdown in the sediment as they are common in the uppermost part of the core but absent or rare in the lower part. In contrast, trochamminids appear to persist in moderate numbers to the base of the core.

Calcareous foraminifera occur in all core samples except the lowermost sample (10-11.5 cm). Large specimens of *Globocassidulina* are relatively common in the lower part of the core; they are accompanied by rare specimens of the planktic species *Neogloboquadrina pachyderma*. Rare to few *Astrononion echolsi* and *Trifarina angulosa* occur throughout the core. It is likely that these calcareous foraminifera have been washed in or recycled into the sediments of Site 1.

All specimens of *Globocassidulina* appear to be the Pleistocene-Recent species *G. biora* or *G. crassa crassa* rather than the Pliocene species *G. crassa rossensis*. This indicates that if the calcareous assemblage is recycled it is recycled from Pleistocene sediments. Relict Pliocene assemblages containing *G. crassa rossensis* have been reported from several sites in Ross Sea (Fillon, 1974).

Table 20. Radiolaria from Sites 1 and 2, Windless Bight.

Sample	Grab	C3/0-2	C3/2-4	C3/4-6	C3/6-8	C3/8-10	C3/10-11.5
Antarctissa cyclindrica	F						
Antarctissa denticulata	F						
Antarctissa strelkovi	R						
Antarctissa spp.	R	R	F				P
Litheliidae indet.	R						
Lithelius minor gr.	R						
Prunopyle Antarctica	F	F	F	F	F	R	R
Schizodiscus sp.	R						
Spongodiscus spp.	R	F	R	R	P	R	R
Spongoplegma Antarctica	P	R	P	P		P	
Spongotrochus glacialis	F		P	R			P
Tricerospyris Antarctica	P						

Table 21. Foraminifera from Sites 1 and 2, Windless Bight.

Sample	Grab	C3/0-2	C3/2-4	C3/4-6	C3/6-8	C3/8-10	C3/10-11.5
Agglutinated benthic foraminifera							
Ammodiscus incertus		R	P				
Cribrostomoides jeffreysi	R	R	R	R		P	
Deuterammina grisea	?						
Haplophragmoides canariensis	?						
Hyperammina malovensis	F	F	P				
Hormisinella ovicula gracilis	R	F	P				
Lagenammina difflugiformis?	P						
Miliammina earlandi	F	F	R	P			
Miliammina lata	F	R	F				
Nodulina dentaliniformis	F	F	R				
Portatochammina malovensis	F	F	F	R	F	R	R
Psammosphaera parva	R	R					
Pseudotrochammina bullata		R	P				
Recurvoides contortus	F	F	P	R		P	
Reophax bilocularis	R	R	P	R	R	P	
Reophax scorpiurus	C	F	R	R			
Reophax spiculifer	F	F	R	R			
Reophax spp.			P				
Rhabdammina spp.	F	R			R		P
Textularia earlandi	R	R					

Table 21 (continued).

Calcareous benthic foraminifera						
Astrononion echolsi		R	P		R	F
Cassidulina porrectus				P		
Cibicides spp.						R
Globocassidulinoides biora		P				C
Globocassidulinoides crassa		P			F	
Ehrenbergina glabra		P				
Epistominella exigua?		R				
Miliolid spp.		R				
Nonionella? sp.	P	P				
Stainfortha concave	P		R			
Trifarina angulosa	P	F		R	R	R
Planktic foraminifera						
Neogloboquadrina pachyderma		R	P		R	R
Other						
Ostracoda		P				
Bivalvia		P				
Gastropoda		P				

4.8.3   References

Chen, P.-H. 1975. Antarctic radiolaria. *Initial Reports of the Deep Sea Drilling Project* 28, 437-514.

Fillon, R.H. 1973. Radiolarian evidence of late Cenozoic oceanic paleotemperatures, Ross Sea, Antarctica. *Palaeogeography, Palaeoclimatology, Palaeoecology* 14(3), 171-185.

Fillon, R.H. 1974. Late Cenozoic foraminiferal paleoecology of the Ross Sea. *Antarctica. Micropaleontology* 20(2), 129-150.

Hollis, C.J. and Strong, C.P. 2003. Biostratigraphic review of the Cretaceous/Tertiary Boundary transition, mid-Waipara River section, North Canterbury, New Zealand. *New Zealand Journal of Geology and Geophysics* 46, 243-254.

Violanti, D. 1996. Taxonomy and distribution of recent benthic foraminifers from Terra Nova Bays (Ross Sea, Antarctica), Oceanographic Campaign 1987/1988. *Palaeontographia Italica* 83, 25-71.

4.9 Sedimentary petrography
Robert McKay

4.9.1 Introduction
Sand grains recovered in the Windless Bight cores are likely to be sourced from either the Transantarctic Mountains (TAM) to the southwest and west of Ross Island, or from the surrounding volcanoes of the late Cenozoic McMurdo Volcanic Group (MVG). The MVG centres to the south (i.e. Minna Bluff, Mt Discovery, Black and White Islands) are mostly basaltic shields, whereas to the north, Ross Island consists of the anorthoclase-phonolite Mt Erebus overlying the older basaltic shields of Mt Terror, Mt Bird and Hut Point Peninsula. The MVG are glassy basaltic rocks with micolites and microphenocrysts of feldspar, olivine and kaersutite as common mafic minerals. They have no quartz. The TAM are characterised in this region by a basement of Late Precambrian-Early Paleozoic metasediments and granitoids (quartz, feldspar, lithics), overlain by Devonian-Triassic Beacon Supergroup (largely quartzose and quartzofeldspathic sandstone) and Ferrar Dolerite (clinopyroxene, pigeonite and plagioclase), all distinctive mineralogies.

4.9.2 Methods
The 63-500 μm fraction of each sample was saturated in epoxy to produce pellets for sectioning. The pellets were cut into thin sections to give a maximum quartz birefringence colour of white. The textural and compositional characteristics of each slide were described and point counts of 400 grains were undertaken (Tables 22 and 23). Sand grains were grouped into one of the following categories:

- *Organic remains:* Dominated by sponge spicules (especially at Site 2), although diatoms, foraminifera, organic pellets and radiolarians are also present.

- *Calcite:* Mostly organic in origin, although rare grains of metamorphic calcite with twinning and zoning were noted in the basal unit of Site 1.

- *Volcanic lithics:* Volcanic lithics vary from unweathered, angular basaltic groundmass with K-feldspar, plagioclase, olivine or pyroxene phenocrysts to reworked volcanic grains (epiclasts). The epiclasts are normally well rounded and display significant quantities of clay minerals enclosing feldspars, olivine and pyroxenes (Figure 35). They are inferred to be the result of significant weathering of volcanic source rocks, probably a result of glacial erosion and exposure during ice sheet retreat. The volcanic lithics are all inferred to be sourced from the MVG, although no distinction of individual volcanic centres (i.e., Ross Island, Black Island) is made.

- *Volcanic glass:* Vary from colourless/light brown to red brown. They are angular to subrounded and are often highly vesicular. Rare olivine/plagioclase phenocrysts.

- *Plagioclase:* Angular to rounded grains, with a tabular form and cleavage at ~90°, multiple twinning or local alteration to sericite.

- *Altered Feldspar:* Angular to rounded grains, displaying significant alteration (visible in plain polarised light) to sericite or albite(?).

- *K-Feldspar:* Tabular grains with simple twinning

- *Microcline:* Feldspar with cross hatched twinning, indicative of a granitic source (Figure 35)

- *Quartz:* Varies from angular to well-rounded. Most grains are mono-crystalline with straight to strong undulose extinction. Some grains have fluid inclusions. Smaller grains

of quartz lacking distinguishing features may have been identified as feldspar. Polycrystalline quartz grains were also included in this group. Likely sources of this quartz are from Beacon Supergroup sediments, basement granitoids, and basement metasediments (esp. polycrystalline quartz)

- *Beacon quartz:* Rounded to well-rounded quartz with overgrowths are inferred to be derived from Devonian Beacon Supergroup sediments (Korsch 1974). (Figure 35)

- *Sedimentary grains:* Range from quartz arenite to arkose lithics. (Figure 35)

- *Pyroxene with exsolution lamellae:* Pyroxenes sourced from the Ferrar include Pigeonite, which displays distinctive exsolution lamellae. Pigeonite is not observed in pyroxenes derived from the McMurdo Volcanic Group (Smellie, 1998). (Figure 35)

- *Heavy minerals:* Many of the heavy minerals were broken grains that lacked distinguishable features. However, pyroxenes, amphiboles and biotite were noted.

Table 22. Proportions of the various sand grain types (63 to 250 µm) through Windless Bight, Site 1 Core 4, by point counting from thin sections.

Depth (cm)	0	5	11	13	15	20	24	29	31	43	53
Organics	X	2	1	X	2	X	X	0	0	0	0
Calcite	X	1	1	1	1	2	1	1	X	3	3
Volcanic glass	25	26	19	18	23	20	29	22	16	3	14
Volcanic lithics	46	47	61	69	55	61	50	64	43	22	29
Heavy minerals	6	3	4	2	2	4	8	4	1	4	2
K-feldspar	X	X	3	X	X	X	1	1	X	X	1
Altered feldspar	7	6	6	3	6	2	5	5	4	10	13
Plagioclase	2	7	4	5	9	8	3	X	8	16	3
Quartz	10	4	1	X	1	1	1	2	18	27	26
Rounded quartz	3	1	0	0	0	0	0	0	6	9	8
Sedimentary lithics	X	X	0	0	0	0	0	0	2	5	1
Microcline	0	0	X	0	0	0	X	X	0	1	1
Pigeonite	X	X	X	0	0	0	0	0	X	0	1

Table 23. Proportions of the various sand grain types (63 to 250 µm) through Windless Bight, Site 2 Core 4, by point counting from thin sections.

Depth (cm)	0	14	36	58
Organics	4	8	2	0
Calcite	1	0	1	0
Volcanic glass	14	21	25	24
Volcanic lithics	51	44	51	46
Heavy minerals	4	1	2	5
K-feldspar	1	3	0	1
Altered feldspar	9	11	7	8
Plagioclase	12	9	12	14
Quartz	4	3	1	2
Rounded quartz	0	0	0	0
Sedimentary lithics	0	0	0	0
Microcline	0	0	0	X
Pigeonite	X	0	0	0
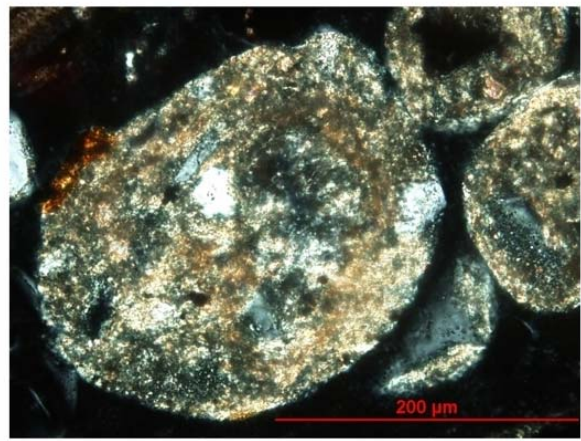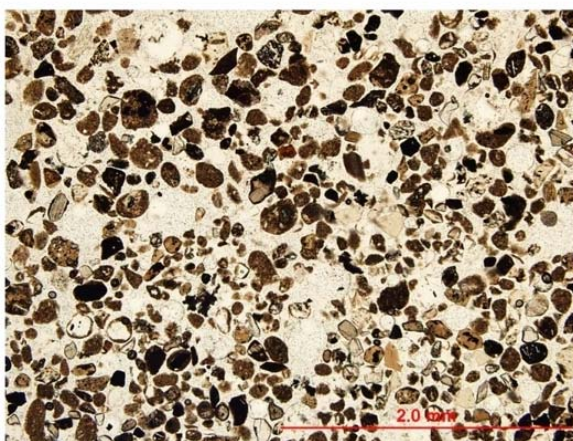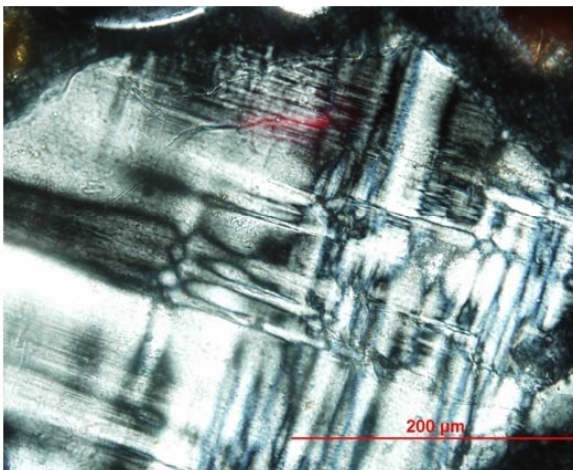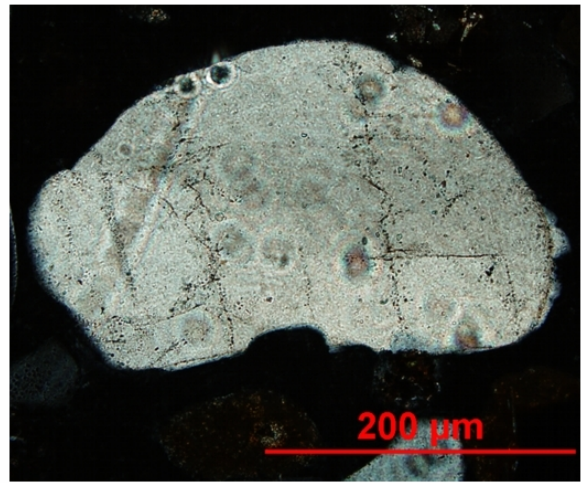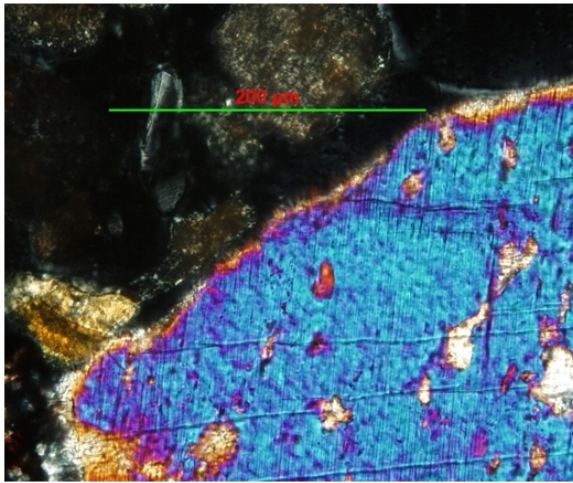
Figure 35. Photomicrographs showing sand grain types from different sources in Windless Bight cores. Top left: Pigeonite from Ferrar Dolerite (Site 1, 3 cm). Top right: Rounded Quartz with overgrowth from Devonian Beacon Supergroup (Site 1, 0 cm). Centre left: Microcline from granitoid (Site 1, 0 cm). Centre right: Sedimentary lithic from Transantarctic Mountains. Bottom left: Well-sorted grains from black sand (Site 1, 29 cm). Bottom right: Volcanic epiclast from black sand (Site 1, 29 cm)
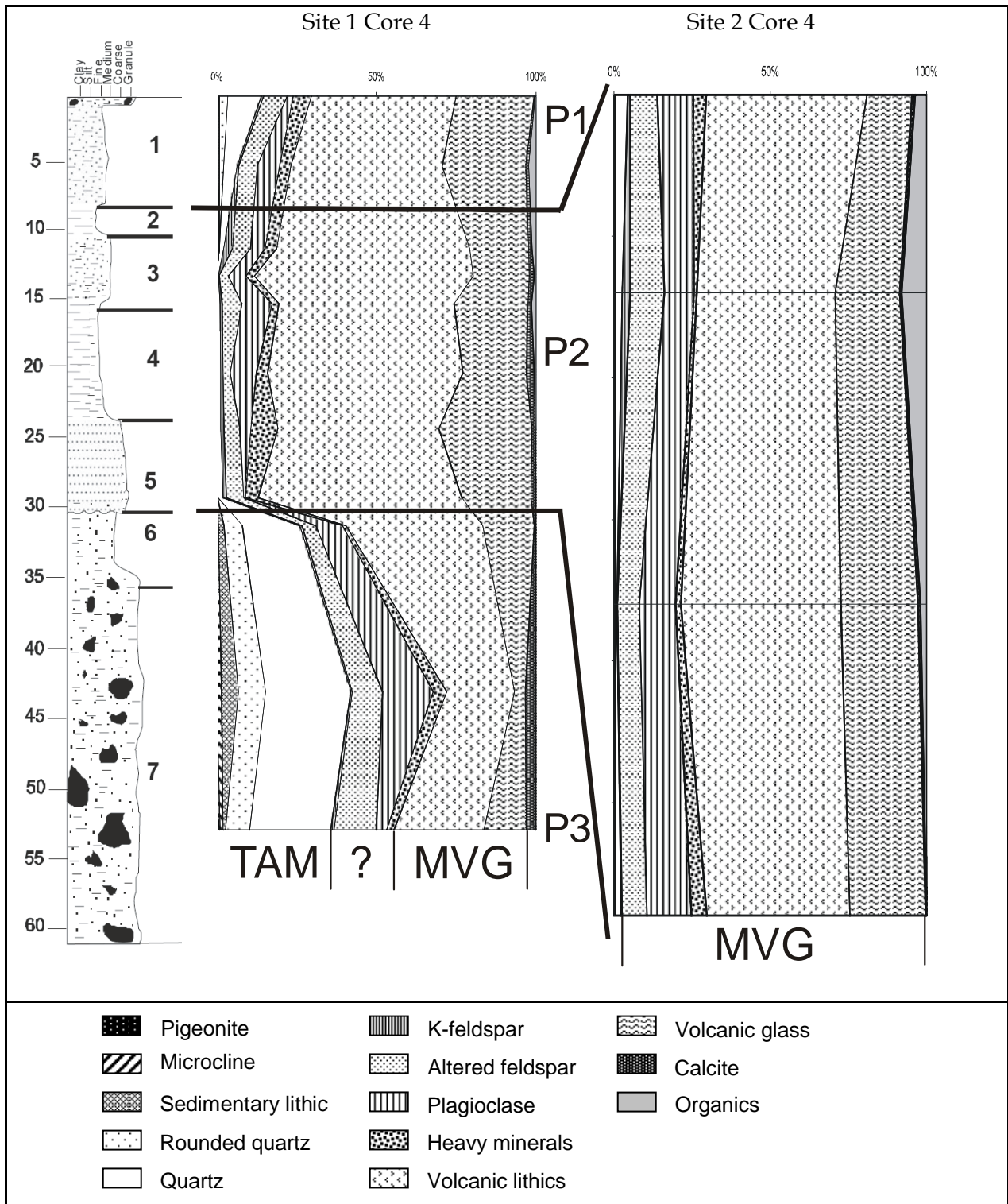
Figure 36. Staked area charts showing percentage contribution of sand grains. Petrofacies (P1, P2 and P3) are based largely on the proportion of TAM sediments. The petrofacies boundaries were constrained by the lithological units from Site 1 (shown in stratigraphic column to the left). Note that the entire length of the core from Site 2 represents ~12ky, which is only the upper 15 cm of core from Site 1.

4.9.3   Results

Using the relative abundance of TAM grains, three distinct petrofacies are observed at Site 1 (see Figure 36). They record the transition from a regionally grounded ice sheet through to a sub-ice shelf environment and the approach of the receding calving line. Because petrographic data were not obtained for every interval, lithological boundaries have been used as a guide to likely petrofacies boundaries.

4.9.3.1   *Petrofacies 3 (Units 6-7: 31-60 cm)*

The basal unit of Site 1 is characterised by a larger grain size, poor sorting, and a high quartz (18-27%) and feldspar (13-28%) content. Rounded quartz (6-9%) is also relatively common, while volcanic glass (4-16%) and lithics (21-43%) are significantly lower than the younger units. This strong TAM signal, combined with the presence of gravel clasts up to 48 mm in length (some of which are striated), supports the interpretation that both Units 6 and 7 were transported in the basal glacial debris zone of a greatly expanded and regionally grounded Ross Ice Shelf.

4.9.3.2   *Petrofacies 2 (Site 1: Units 2-5 (7-31 cm); Site 2: (0-62 cm))*

Petrofacies 2 (P2) is characterised by a complete dominance of MVG grains, with volcanic lithics constituting 50-69% of the assemblage, while volcanic glass represents 19-29%. A high proportion of the volcanic lithics are rounded. Weathered volcanic lithics are particularly well sorted and rounded in Unit 5 (24-31 cm), and is likely the result of sediment gravity flow processes. This interpretation does not apply to Units 2-4, which do not display the same degree of sorting. However, the provenance of these units is still from a local source. It is likely these units are the result of local reworking with moderate levels of oceanic circulation following the regional development of a floating ice shelf.

The petrology at Site 2 is consistent throughout the core and is dominated by MVG grains, indicating that the entire core was deposited by reworking of local sediments with moderate sub-ice shelf currents. As at Site 1, the upper 3 cm of Site 2 is characterised by a sandy, granular layer. However, it is less pronounced and the grain provenance is consistent with the rest of the core. Organic remains are more abundant at this site, especially sponge spicules.

4.9.3.3   *Petrofacies 1 (Unit 1: 0-7 cm)*

Petrofacies 1 (P1) corresponds to the upper 7 cm of soft sandy mud (with minor coarse sand and clasts up to 16 mm in length). Sponge spicules, forams and radiolarians are noted, but biogenic content is still relatively minor compared to Site 2. Although dominated by volcanic lithics and glass (69-73%), there is a significant TAM component, notably rounded quartz from Devonian Beacon Supergroup sediments (1-3%). There is also a notable increase in quartz (4-10%) and sedimentary lithics (1-5%). Microcline and pigeonite are also noted in this assemblage, which also suggests an active sediment source from the TAM during the Holocene. This petrofacies may represent the break-up of the ice shelf in McMurdo Sound (with the TAM grains being associated with ice rafting). Despite evidence of increased sea-ice diatom taxa in this unit (esp. *Fragilaropsis curta*), as noted by Harper (this volume), the increase in pelagic sedimentation is not high enough to be associated with sustained periods of seasonally open water above this site. There is also an increase grain size in the upper 3 cm at Site 2 that may also be indicative of an open McMurdo Sound during this period. However, an increase in sub-ice shelf currents during the mid to late Holocene may have resulted in the reworking of locally exposed diamict on the seafloor, which is likely to consist of ridges, hummocks and furrows commonly associated with glacial deposition.

4.9.4 Conclusions

The provenance of Units 6-7 (31-61 cm) at Site 1 show a strong TAM signal, supporting the lithological interpretation that these units are derived from basal glacial debris when Ross Ice Shelf was grounded in the immediate vicinity. Unit 5 (24-31 cm), a well-sorted reworked volcanic sand, appears to be a sediment gravity flow. Units 2-4 do not have any significant input of sediments sourced from the TAM and likely represent the reworking of local sediments by moderate sub-ice shelf currents. An increase in TAM grains in Unit 1 (0-7 cm) at Site 1 is likely the result of localised reworking of the older diamict unit exposed of the seafloor. Site 2 does not show any significant shifts in provenance, indicating that the calving line of McMurdo Ice Shelf has not retreated further than its present position during the Holocene.

4.9.5 References

Korsch, R.J. 1974. Petrographic comparison of the Taylor and Victoria groups (Devonian to Triassic) in South Victoria Land, Antarctica, New Zealand. *Journal of Geology and Geophysics* 17(3), 523-541.

Smellie, J.L. 1998. Sand grain detrial modes in CRP-1: Provenance variations and influence of Miocene eruptions on the marine record in the McMurdo Sound region. *Terra Antartica* 5(3), 579-587.

4.10 Sedimentary geochemistry

Giovanna Giorgetti

Samples were taken every 2 cm through Core 4 from Sites 1 and 2. Major and trace elements were determined on fused glass discs by X-ray fluorescence (XRF) spectrometry using a Philips MagiX-Pro with Rh tube for major minor and trace elements. The estimated accuracy is better than 7% for all elements, except for Nb, Zn, and Co, which range from 8 to 12%. Loss on ignition (LOI) was evaluated by gravimetry with a muffle furnace at 960°C for an hour. Fe_2O_3 represents total Fe. The analytical results are presented as Al-normalised values to minimise dilution effects associated with biogenic components. The data are shown in Figures 37 and 38.

4.10.1 Site 1 Core 4

The variations of some element/Al ratios with depth have been analysed. Major changes in elemental ratios of Mg, Si, Sr and Rb occur at the boundaries of the different units. The laminated Unit 5 shows peculiar characteristics with respect to the other units. Mg/Al, Ca/Al, Fe/Al, Sr/Al ratios all increase in the lower part of the core (Units 6-7) while Rb/Al ratio decreases.
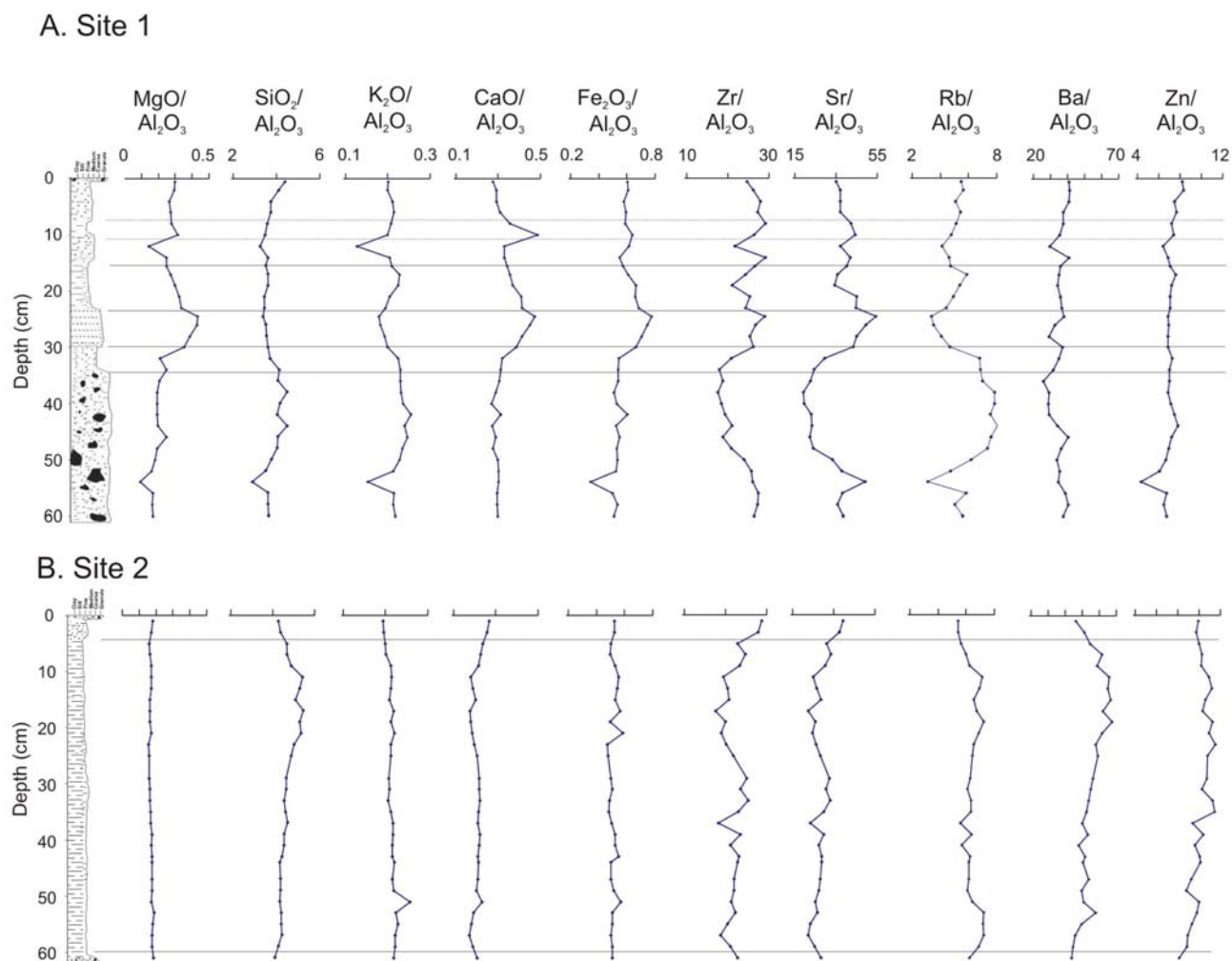

Figure 37. Plots of element/Al ratios for cores from Windless Bight. Horizontal lines are unit boundaries from the visual core descriptions. A. Site 1. B. Site 2.

K/Al ratio shows an opposite trend with respect to Ca/Al; the same opposite relation exists between Sr/Al and Rb/Al. Ca/Al ratio reflects the Sr/Al trend such as K/Al ratio reflects the Rb/Al ratio. Consequently, Ca and Sr are related to the same mineral phase (carbonate) and K and Rb to micas.

4.10.2 Site 2 Core 4

The element/Al ratios show smooth trends and no sharp changes can be noticed downcore, showing that the chemical composition of these sediments is quite homogeneous. Si/Al and Ba/Al ratios show the same trend and they reach higher values in the upper part of Unit 2. They are probably related to biogenic productivity.

Usually, Ti, Al (Nb, Y) are considered immobile elements and their ratios remain constant in sediments having the same source area. If Al_2O_3 and TiO_2 were immobile and fractionated in a similar manner in sediments, data points in a TiO_2 vs Al_2O_3 diagram should plot along a line with constant slope.

4.10.3 Comparison of cores from Sites 1 and 2

Figure 38 shows the TiO_2 vs Al_2O_3 diagram for samples from the two cores. Units 1-3 (0-16 cm) and Units 6-7 samples (below 31 cm) from Site 1 define two sub-parallel linear arrays suggesting different source rocks for these intervals. Samples from the intervening interval show considerable spread of TiO2 and little variation in Al_2O_3. This distribution is due to sorting: the constant Al_2O_3 values indicate that feldspars (the main Al-bearing phase) is separated from Ti-bearing phase (volcanic grains) by sorting. Most samples from Site 2 plot along the same trend as those from the upper 16 cm of Site 1. However the deepest samples share the same trend as those from Unit 7 in the Site 1 core.

The chemical mobility and hydraulic sorting of Zr can be explored with a ratio diagram involving Ti-Zr-Al (Figure 38). If Zr were chemically mobile data points would have scattered rather display a linear trend. In fact, data points from Units 1-3 of Site 1 (and all of Site 2), and from Units 6-7 in Site 1 define two sub-parallel linear trends as they do in Figure 38. Data points from Units 4 and 5 from Site 1 are scattered. Mt Erebus volcanics (mugearite and benmoreite), Beacon sandstone, and Ferrar dolerite analyses have been plotted for comparison. Mt Erebus volcanics overlap with the linear trend of sediments from the Site 2 core and from the diamicton of the Site 1 core, indicating their dominance as the source rocks of the sediments.
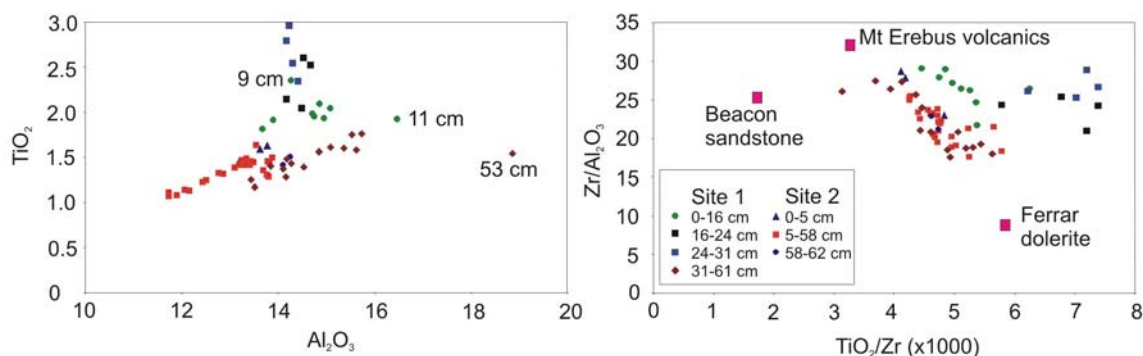

Figure 38. Crossplots of elemental ratios for Sites 1 and 2. (Left). TiO_2 vs Al_2O_3. (Right). Zr/ Al_2O_3 vs TiO_2/Zr.

4.11 Quartz surface textures
Damiano Damiani

Past studies of continental and marine sediments have linked the textural features of quartz grain morphology with processes of grain transport and diagenesis (eg. Krinsley and Doornkamp, 1973; Margolis and Krinsley, 1974; Mahaney, 1995). To study the grain morphology of quartz grains from the Windless Bight cores 13 representative samples were taken from Site 1 Core 4, dried, and sieved to collect the fraction between 63 μm and 2 mm. Thirty grains typically in the range 100 to 400 μm were selected randomly, and observed by Scanning Electron Microscopy (10 kV). Quartz composition was verified by energy dispersive spectrometry (EDS).

Four types of quartz grains have been distinguished (Figures 39 and 40):

- Type 1. These grains are angular, with sharp edges and a high relief. The grains bear numerous mechanical breakage features of various sizes that include conchoidal fractures, arc and straight steps, parallel to semi parallel striations, breakage blocks and fractured plates. The forms of chemical alteration are absent or very moderate, usually in the form of solution pits. These features are indicative of glacial erosion and/or transport.

- Type 2. These grains are characterised by surfaces extensively modified by high chemical activity. The predominant silica precipitation features are silica globules and overgrowth, present in various stages of formation. Some grains show solution pits. These textures are generally representative of grains which sat in a high-chemical diagenetic environment. They are interpreted as grains from sandstones of the Devonian-Triassic Beacon Supergroup.

- Type 3. These grains exhibit the same microfeatures as Type 1 grains, but they are sub-angular to sub-rounded in outline with medium to low relief and smoothed edges. Some surfaces show chemical features as solution pits and silica pellicles. These quartz grains exhibit features representative of glacial grains that were later exposed to subaqueous transport.

- Type 4. These grains are well rounded and show few, if any, relict features. The common shape is spherical, but many grains may show a certain grade of elongation (inherited from the original grain shape). Upturned plates (a series of small plates protruding from the surface) often cover the entire surface of grains. They are representative of an eolian environment.

The high amount of quartz grains derived from the sandstone rocks of the Beacon Supergroup characterises the higher part of the core. The absence of superimposed features underlines a poor modification due to transport processes.

These grains have been eroded, deposited in the near sea and subjected a short transport by ice and marine currents.

In Unit 5 (well sorted sandstone) quartz grains from glacial deposits and quartz grains of glacial origin modified by a subaqueous transport prevail.

The lower part of the core (Unit 7) shows a higher percentage of quartz grains affected by glacial abrasion. This evidence indicates the rapid deposition of material subjected to glacial erosion and/or transport as the predominant process.

4.11.1 References

Krinsley, D.H. and Doornkamp, J.C. 1973. *Atlas of Quartz Sand Surface Textures*. Cambridge University Press: London, 91 pp.

Mahaney, W.C. 1995. Pleistocene and Holocene glacier thicknesses, transport histories and dynamics inferred from SEM microtextures on quartz particles. *Boreas* 24, 293-304.

Margolis, S.V. and Krinsley, D.H. 1974. Processes of formation and environmental occurrence of microfeatures on detrital quartz grains. *American Journal of Science* 274, 449-464.
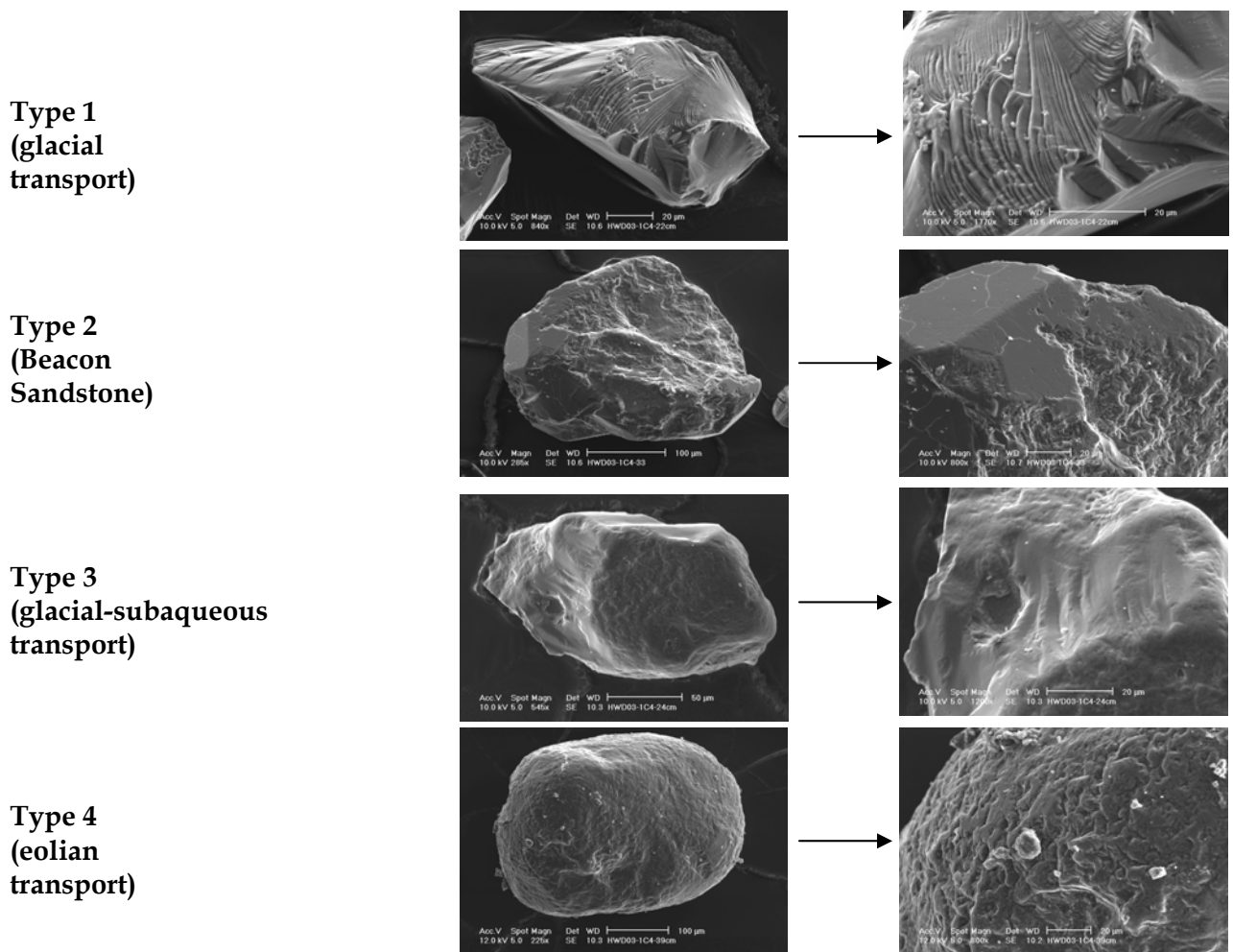
**Type 1
(glacial
transport)**

**Type 2
(Beacon
Sandstone)**

**Type 3
(glacial-subaqueous
transport)**

**Type 4
(eolian
transport)**

Figure 39. Features of the four types of quartz surface textures (see text for descriptions).
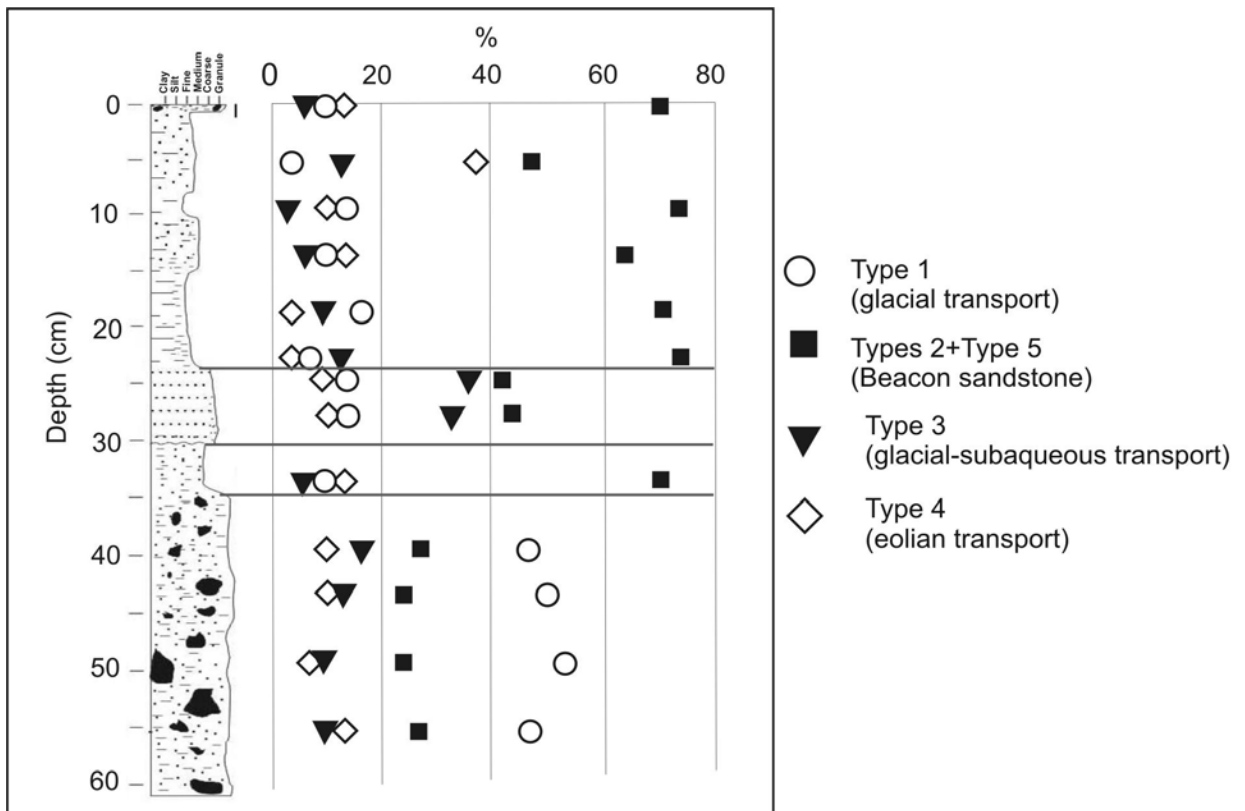
Figure 40. Distribution of quartz surfaces textures through the core from Site 1, Windless Bight.

4.12 Physical Properties

Frank Niessen

High-resolution physical properties such as Magnetic Susceptibility (MS), Wet Bulk Density (WBD), P-wave Velocity (Vp) and Sediment shear strength were determined in sediment cores retrieved from both sampling locations at Windless Bight. Physical properties of marine sediments are important parameters for core correlation and can function as tools to identify stratigraphic pattern in the sediment column (Fütterer, 1994; Rachor, 1997).

MS is commonly used as an indicator of lithological changes (e.g. Nowaczyk, 1991). In marine sediments, changes in magnetic susceptibility are normally controlled by variation in the content of magnetite. Magnetite has a significant higher susceptibility ($K = +10^{-2}$) than most common minerals ($K = -10^{-6}$ to $+10^{-6}$). In the McMurdo Sound area, for example, increased MS is observed in sediments younger than 19 Ma of the Cape Roberts Project core 1 and is indicative for sediment input from the Erebus Volcanic Province (Niessen et al. 1998). Thus for the sediment cores of the two locations in Windless Bight, MS may function as first indicator of changes in sediment provenance with time. For depositional environments under shelf ice, sediment shear strength is an important parameter to state whether or not the shelf ice was grounded at times. In case of grounding, significant overconsolidation of the sedimentary record must have occurred. Also, overconsolidation leaves a clear imprint on porosity and thus WBD. The latter is usually controlled by porosity, which is related to sediment composition, grain size and compaction. In case of non-cemented siliciclastic sediments, Vp normally depends on porosity and grain size (Erickson & Jarrard, 1998).

4.12.1 Methods

Core measurements of physical properties were carried out by logging of magnetic susceptibility, gamma-ray attenuation, p-wave travel time, sediment thickness, and temperature using a GEOTEK Multi Sensor Core Logger (MSCL) operated in a laboratory container at Scott Base during event K042 in 2003. Logging and sensor specifications are summarised in Table 24. Whole cores were logged in plastic liners (external diameter of 63 mm and a wall thickness of 2 mm). Logging intervals were 1 mm for Site 1 Cores 1 to 3 and 2 mm for all other cores.

Magnetic susceptibility (MS) is defined as the dimensionless proportional factor of an applied magnetic field in relation to the magnetisation in the sample and is directly measured in SI units. However, because the loop and point sensors used (Table 24) have specific responses to core diameter and sediment volume, all MS values determined on whole gravity cores and split cores are corrected as follows:

$K_l = K_{lm} / K_{rel}$,

where K_l is the corrected susceptibility of loop-sensor data (10^{-5} SI), K_{lm} is the measured susceptibility and K_{rel} is a constant for gravity cores of 59 mm sediment diameter (Table 24).

In order to directly compare MS measured on whole cores with point-sensor data obtained on split cores the following correction was applied:

$K_p = 4.41 * K_{pm} + 73.9$,

where Kp is the corrected susceptibility of point-sensor measurements.

This correction is an approximation and is based on empirical correlation of MS data of core Site 1 Core 4 (this study), where both loop and point sensor data are available. The correlation coefficient of both data sets is 0.944. MS data obtained from the same core measured with different sensors at similar depth intervals cannot match exactly because loop sensor and point sensor measure different sediment volumes.

Gamma-ray absorption is calibrated to wet bulk density (WBD) using different proportions of aluminum and freshwater together in a liner of the same material and dimensions as the sediment core liners. The calibration is described in detail by Best & Gunn (1999). Fractional porosity (Phi) is calculated from WBD assuming constant grain density (dg) and pore water density (dw) of 2.7 and 1.03 g cm^{-3}, respectively:

$$Phi = (dg-WBD) / (dg-dw).$$

Total P-wave travel time (TT) was measured using acoustic plate contact transducers (GEOTEK Ltd., UK) and converted to measured p-wave velocity (Vpm) as follows: Vpm = ST / (TT-PTO), where ST is the measured sediment thickness assuming constant liner wall thickness, and PTO is the travel time offset through the core liner wall and transducer plus electronic delay (Table 24).

PTO was determined empirically using a liner filled with water of known temperature and salinity and thus velocity. All measured velocities (Vpm) were normalised to 20°C using the MSCL temperature logs:

$$Vp = Vpm + 3 * (20 - tm),$$

where Vp is the P-wave velocity at 20°C and tm is the measured temperature.

Sensor orientation during gamma-ray, travel time and sediment thickness measurements were horizontal as shown in Figure 41. Data from the above sensors refer to a plane located in the centre of the core (along A to B as illustrated in Figure 41). In order to record differences in WBD and Vp at different core orientations, the cores were measured at different angles of rotation (Figure 42). Therefore, different data sets exist for each core of which only one data set each is shown in this report (except for Cores 4 from Site 1 and Site 2). Loop-sensor magnetic susceptibility is independent of core rotation. Point-sensor magnetic susceptibility was logged on the surfaces of the archive halves of split cores. A summary of different core orientation and data acquisition is summarised in Table 25.

In addition to whole and split core logging sediment shear strength was measured on split cores using a Haake Rotovisco RV-12/500M. The vane used with the instrument was inserted 1 cm deep into the sediments and rotated. Shear strength was measured at peak failure recorded on a graphic recorder and is expressed in kPa. The resolution of the sheared sediment volume is approximately 0.25 cm^3. Depth intervals were selected using the WBD logs to allow shear strength measurements in sediments of different physical property character (except for lone stones).

4.12.2 Results and preliminary interpretation
Physical properties of WBD, porosity, Vp, MS and shear strength (split cores only) of Cores 1 to 6 from Site 1 are presented in Figures 42 to 44 and of Cores 1 to 4 from Site 2 are presented in

Figures 45 to 48, respectively. Note that fractional porosity is calculated from density and therefore shows mirror-imaged pattern of the WBD records.

4.12.2.1 Site 1
There is a distinct down-core variability of physical properties in all cores retrieved from Site 1. This suggests a definition of up to 10 physical property units for Site 1 (PP1-1 to PP1-10), particular well defined in the longer Cores 4, 5 and 6 (Figures 42 to 44). From top to bottom PP1-1 to PP1-8 are defined by a more or less regular cyclicity of WBD, porosity and Vp where PP1-1, -3, -5, -7 exhibit generally lower porosity and higher velocity than the interbedded layers of PP1-2, -4, -6 and -8. Within the above record PP1-7 is outstanding because it is characterised by distinctly increased MS of up to $2000 * 10^{-5}$ SI, whereas MS in overlying and underlying units ranges between 500 and $1000 * 10^{-5}$ SI. PP1-7 consists of well-sorted black sand, which appears to be enriched in magnetic components probably derived from local sources within the Mt Erebus Volcanic Province. In the lowermost Units PP1-9 and -10, the pattern of WBD, porosity and Vp is characterised by distinct peaks of very low porosity and high velocity superimposed on stronger small-scale variability compared to the units above (Figures 42 to 44). The peaks have WBD of up to 2.15 g cm^{-3} and Vp up to 3700 m s^{-1} typical for rocks and are associated with large pebbles found in Units PP1-9 and -10. Because lone stones of different sizes are randomly distributed in a muddy matrix, Units PP1-9 and -10 exhibit the largest variability of porosity obtained at different angle of core orientation. The distinction of Units PP1-9 and -10 is based on MS which is increased in PP1-10 muds up to more than 1000 (10^{-5} SI), whereas it is lowest in PP1-9 (<500 10^{-5} SI).

Sediment shear strength of Cores 1, 4 and 5 generally range between 0 and 20 kPa with a weak trend of increase observed downcore. The maximum shear strength of 30 kPa is measured relatively close to the sediment surface in stiff mud (PP1-3 of Core 4, Figure 42). All measurements indicate relatively weak consolidation typical for near surface sediments. Overconsolidation by a considerable load of ice (e.g. grounded shelf ice) would result in shear strength much higher than determined here. For example, Jakobsson et al. (2001) describe overconsolidated sediments from the Arctic Ocean which have shear strength on the order of 100 kPa possibly associated with grounding of massive ice during the Quaternary. The relatively low shear strength measured in all cores from Site 1 and 2 is consistent with the deep acoustic penetration observed by 3.5 kHz sediment echo-sounding at Site 1.

The physical property pattern described above is consistently measured in all cores from Site 1, except for the very short Cores 1 to 3 where only the upper units are found. However, the presented pattern (Figures 42 to 44) suggests that the top layer (Unit PP1-1) is missing in Cores 1, 2, 5 and 6. Also, it is interesting to note that the thicknesses of units can vary from core to core. For example, almost exactly the same pattern and unit thicknesses are observed in Cores 4 and 5 down to 62 cm subbottom (Figures 42 and 43), whereas a similar pattern is observed in Core 5 but only down to 51 cm subbottom (Figure 43). In particular, Unit PP1-3 appears to be variable in thickness from core to core (Figures 42 and 43). It is too early to state whether this variability is caused by the coring technique or related to variability in sedimentation rates in space and time.

4.12.2.2 Site 2
Down-core variability of physical properties of cores from Site 2 is less pronounced than observed at Site 1 although cores of similar length up to 63 cm were retrieved (Figures 45 to 48). In total only 3 units (PP2-1 to PP2-3) are distinguished, and of these PP2-3 appears not to be

recovered in Cores 2 and 3. In Unit PP2-1, Vp and MS are slightly higher and porosity is lower. Unit PP2-2 exhibits the highest porosity of 0.8 (or slightly above), the lowest Vp of 1500 m s^{-1} or lower and the lowest MS (500 * 10^{-5} SI or lower) of all sediments retrieved from both locations. PP2-3 is characterised by a significant decrease in porosity, and slight increase of Vp and MS. This gradient suggests that of this unit only the top end has been cored at Site 2.

Sediment shear strength is generally well below 20 kPa in all PP2 units of Cores 3 and 4 (Figures 47 and 48) and thus generally lower at Site 2 than at Site 1. There is a minor increase notable at the boundary between Units PP2-1 and PP2-2 but no trend of increased shear strength downcore is obvious as was observed in sediments at Site 1.

Like Site 1, thickness of individual PP2 units can vary significantly from core to core. For example, Unit PP2-2 extends from 7.5 to 36.5 cm in Core 1 and from 9.5 to 57.5 cm in Core 4 (Figures 45 and 48).

4.12.3 References

Best, A.I. and Gunn, D.E. 1999. Calibration of marine sediment core loggers for quantitative acoustic impedance studies. *Marine Geology* 160, 137-146.

Erickson, S.N. and Jarrard, R.D. 1998. Velocity-porosity relationships for water-saturated siliciclastic sediments. *Journal of Geophysical Research B* 103(12), 30,385-30,406.

Fütterer, D.K. 1994. Die Expedition ARCTIC ´93, Der Fahrtabschnitt ARK-IX/4 mit FS "Polarstern" 1993. *Berichte zur Polarforschung* 149, 244 pp.

Jakobsson, M., Loevlie, R., Arnold, E.M., Backmann, J., Polyak, L., Knutsen, J.-O., Musatov, E. 2001. Pleistocene stratigraphy and paleoenvironmental variation from Lomonosov Ridge sediments, central Arctic Ocean. *Global Planetary Change* 31, 1-22.

Niessen, F., Jarrard, R.D., Bücker, C. 1998. Log-Based Physical Properties of the CRP-1 Core, Ross Sea, Antarctica. *Terra Antartica* 5(3), 299-310.

Nowaczyk, N.R. 1991. Hochauflösende magnetostratigraphie spätquatärer sedimente arktischer meeresgebiete. *Berichte zur Polarforschung* 78, 187p.

Rachor, E. 1997. Scientific Cruise Report of the Arctic Expedition ARK-XI/1 of RV "Polarstern" in 1995. *Reports on Polar Research* 226, 157 pp.
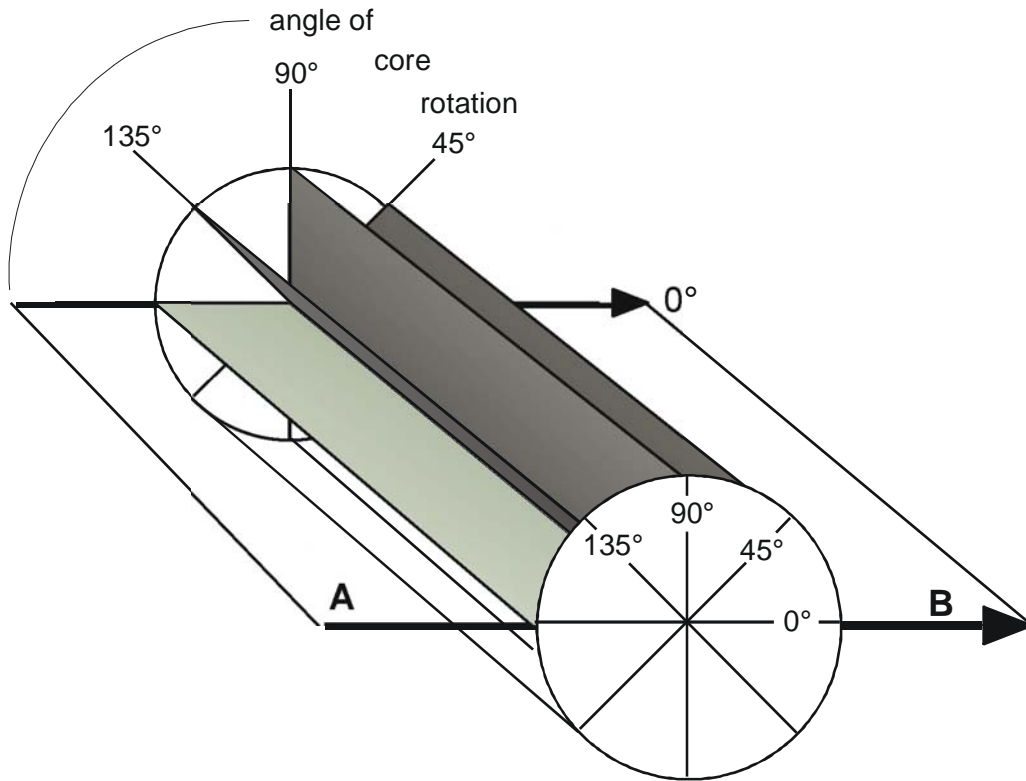
Figure 41. Sensor orientation of Multi-Sensor-Core-Logger (MSCL) along A-B as used in this report, and logging planes at different angles of core rotation.
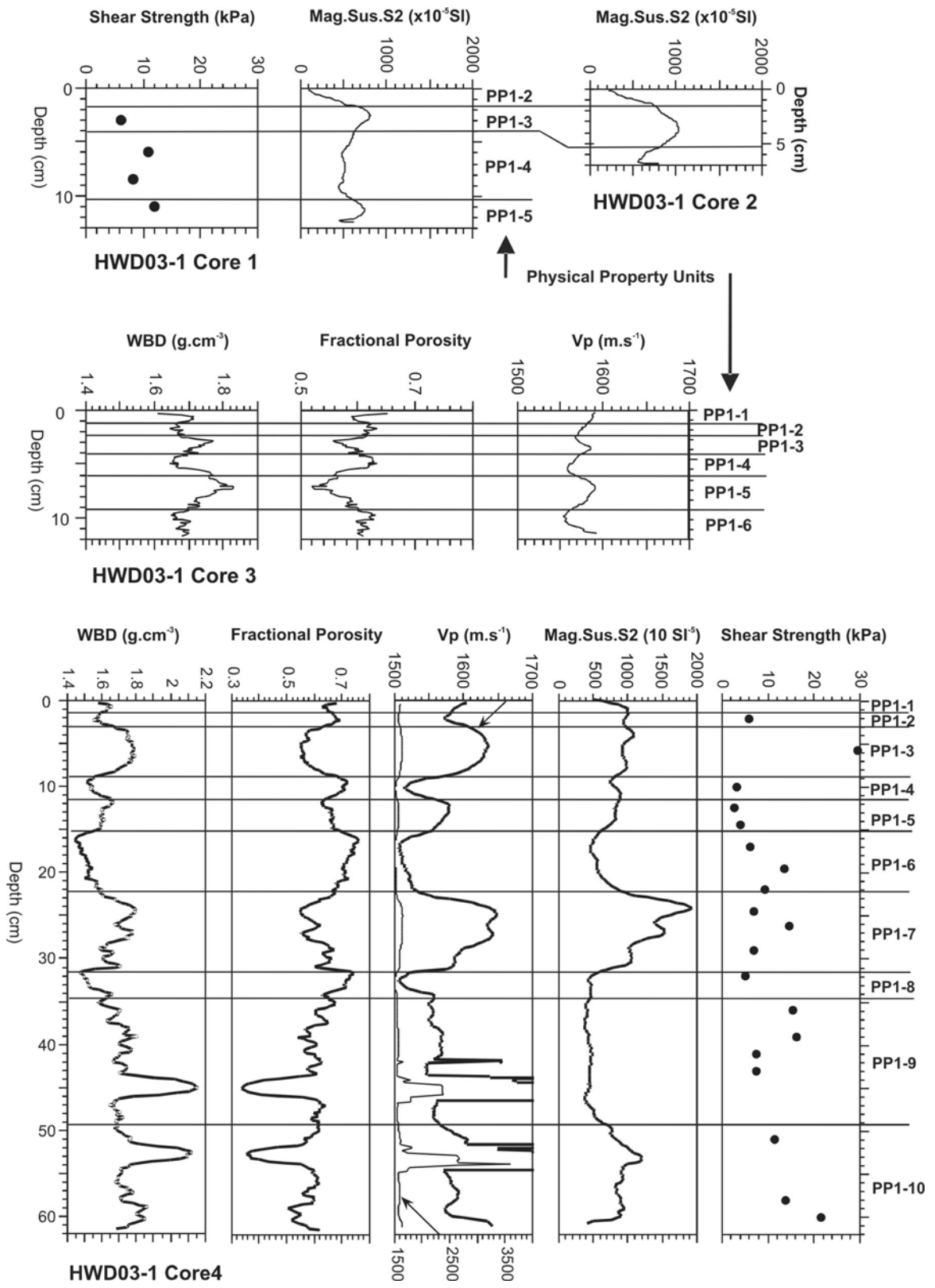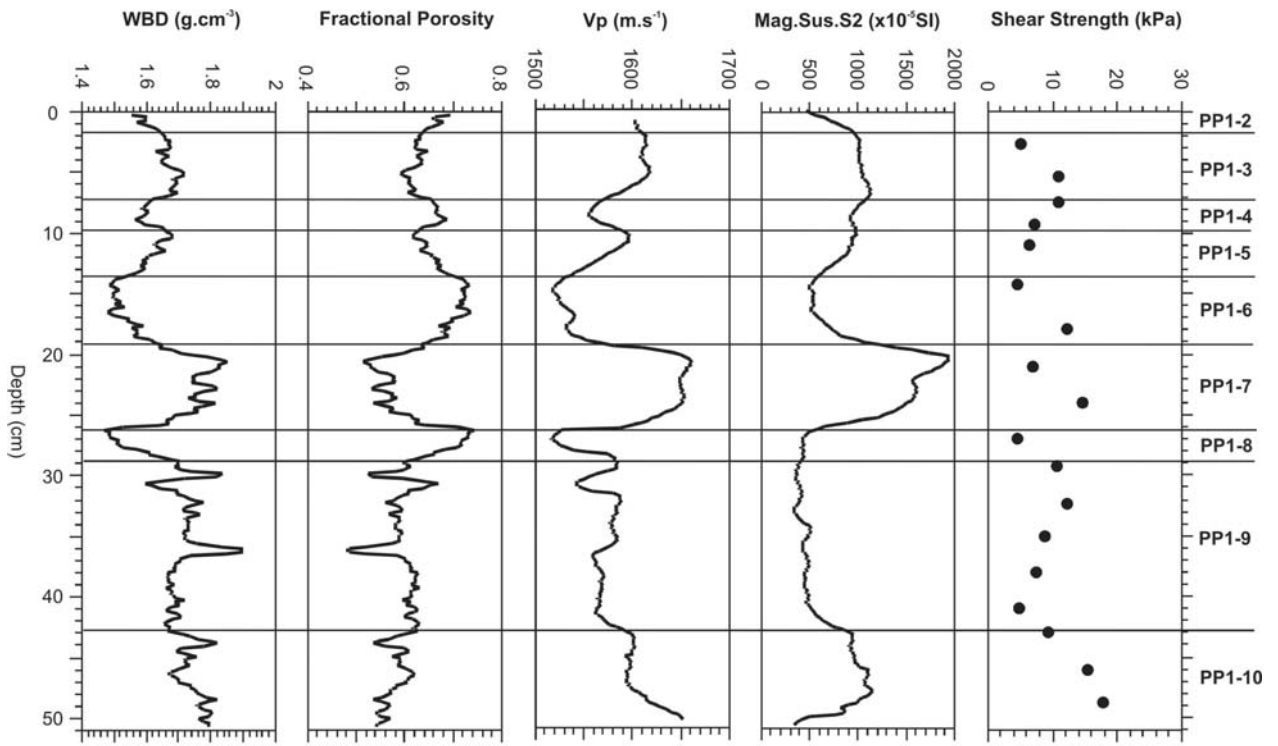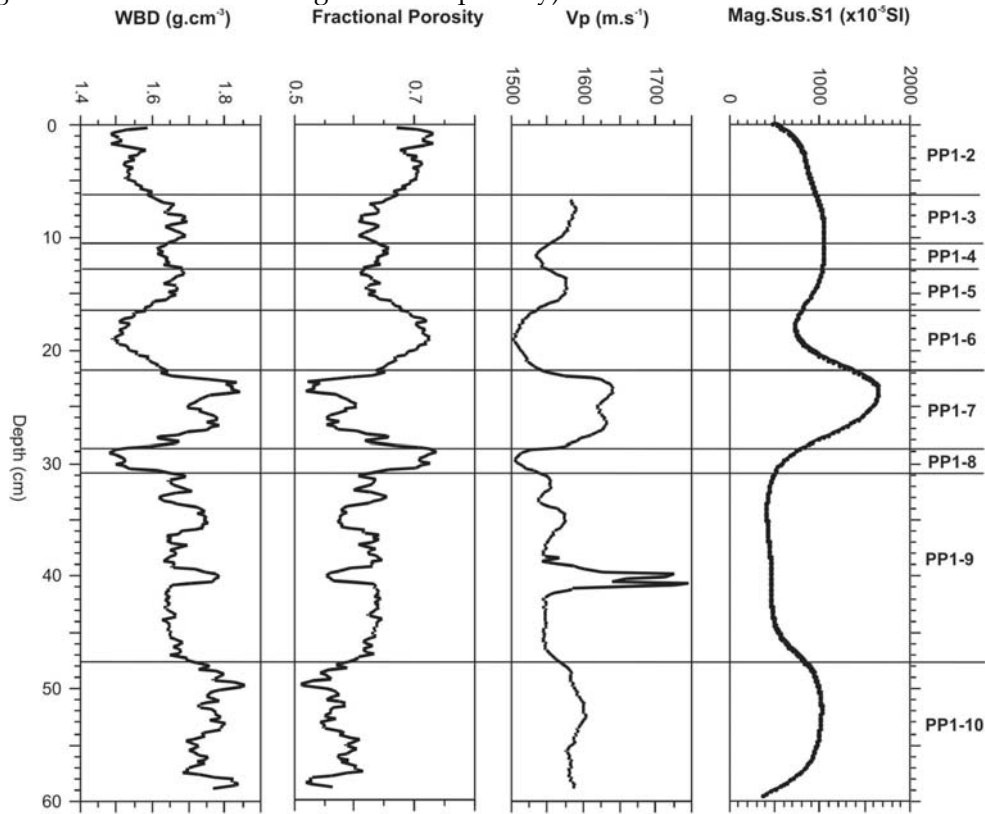
Figure 42. Physical properties and units of Cores 1 to 4 from Site 1 (WBD = Wet Bulk Density, Vp = P-wave velocity, Mag.Sus.S2 = Point-Sensor Magnetic Susceptibility). Note that Vp data for Core 4 are plotted on two different scales.

HWD03-1 Core 5

*Figure 43.*Physical properties and units of Core 5 from Site 1 (WBD = Wet Bulk Density, Vp = P-wave Velocity, Mag.Sus.S2 = Point Sensor Magnetic Susceptibility).

HWD03-1 Core 6

*Figure 44.*Physical properties and units of Core 6 from Site 1 (WBD = Wet Bulk Density, Vp = P-wave Velocity, Mag.Sus.S1 = Loop-Sensor Magnetic Susceptibility).
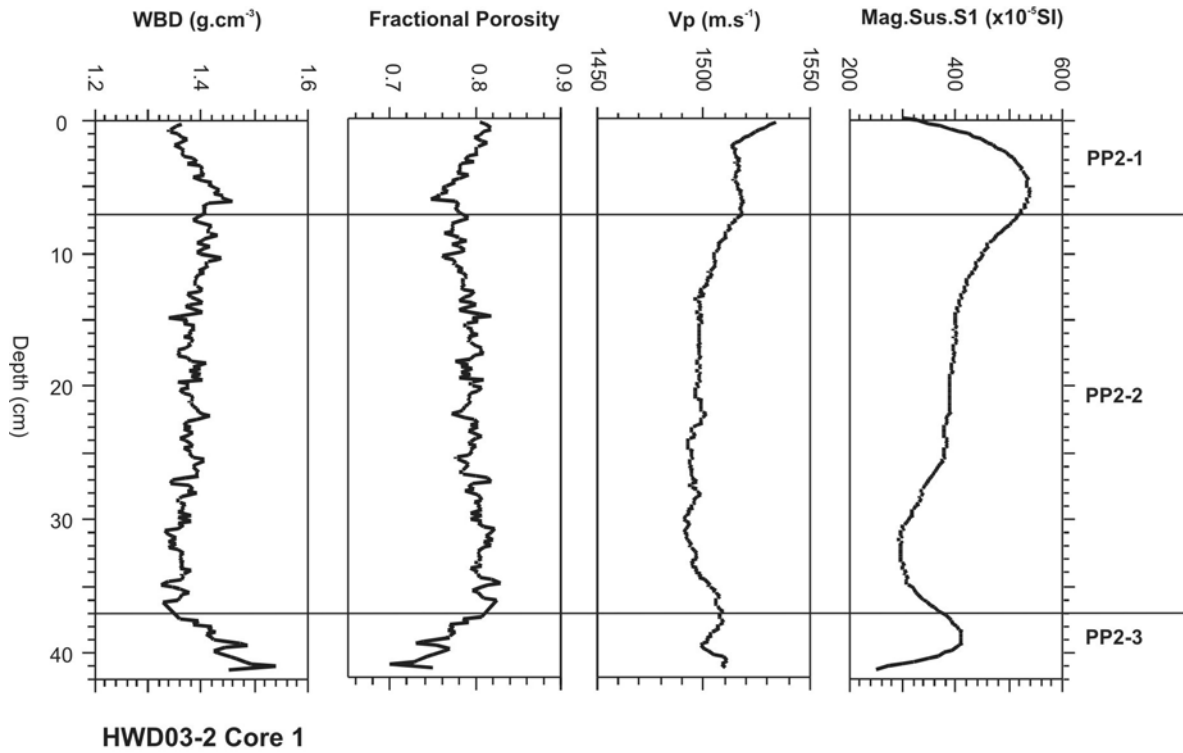
86

Figure 45. Physical properties and units of Core 1 from Site 2 (WBD = Wet Bulk Density, Vp = P-wave Velocity, Mag.Sus.S1 = Loop Sensor Magnetic Susceptibility).
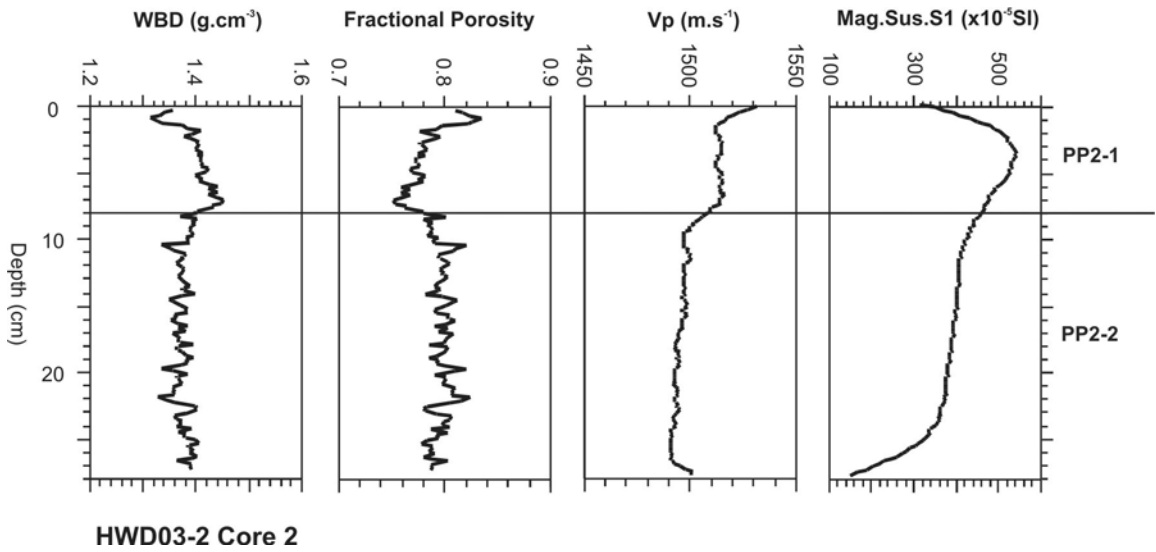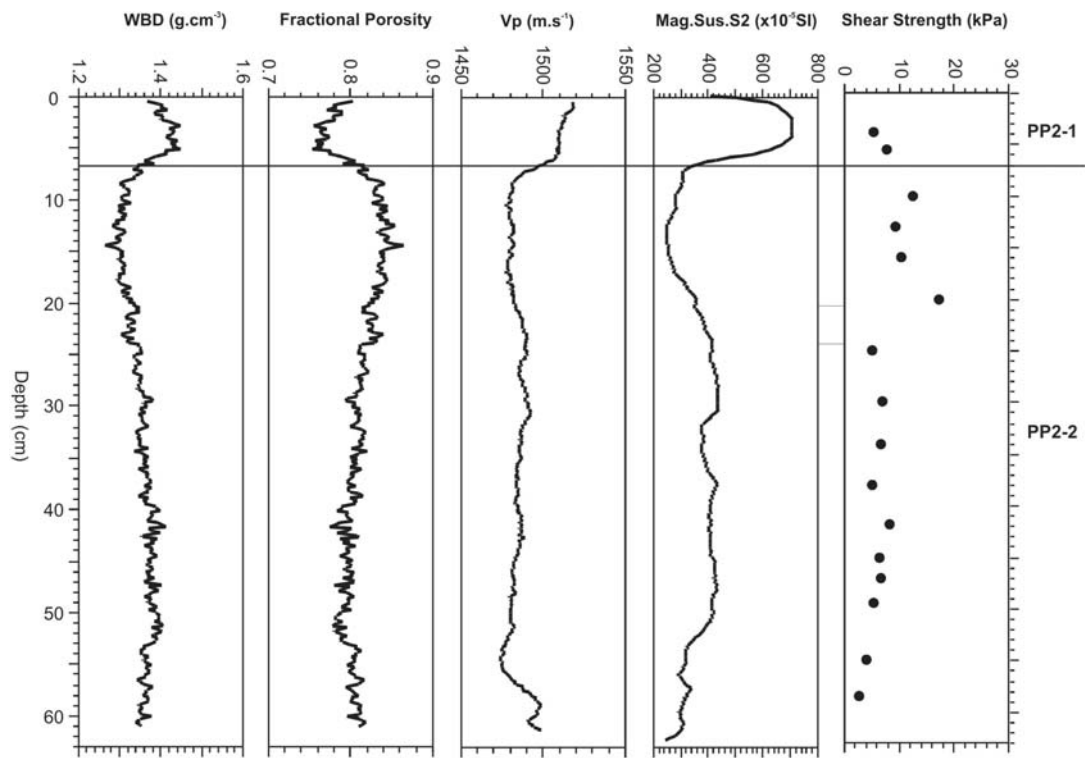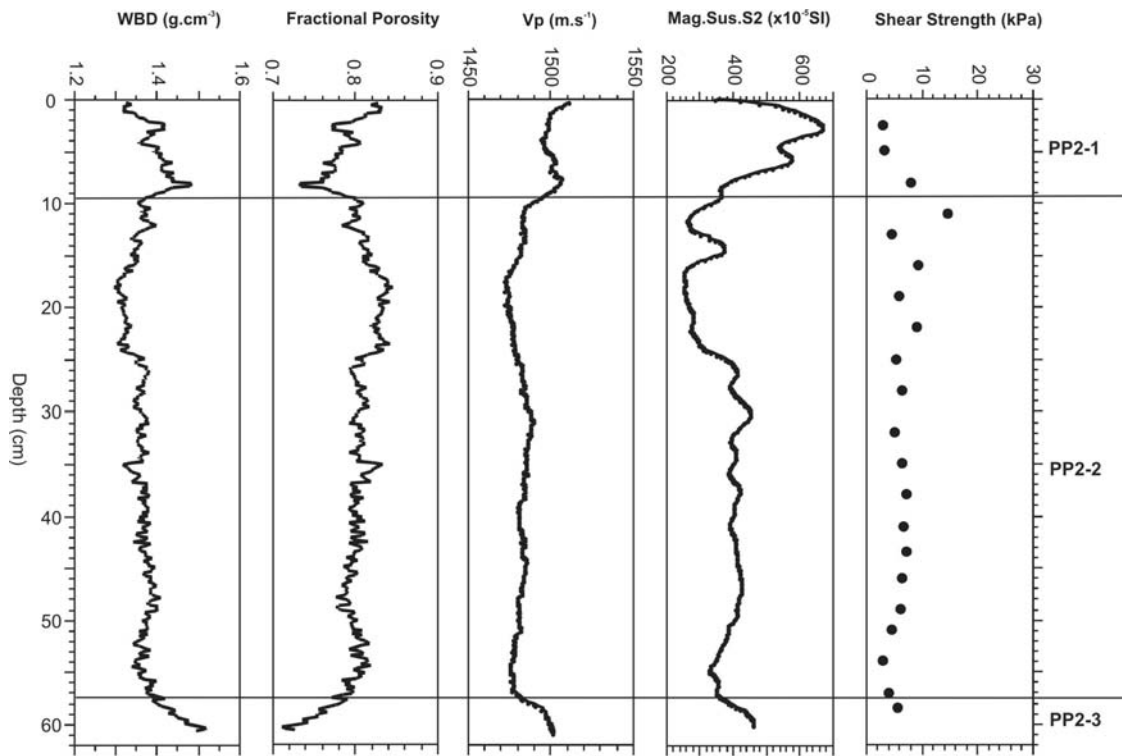

Figure 46. Physical properties and units of Core 2 from Site 2 (WBD = Wet Bulk Density, Vp = P-wave Velocity, Mag. Sus.S1 = Loop-Sensor Magnetic Susceptibility).

Figure 47. Physical properties and units of Core 3 from Site 2 (WBD = Wet Bulk Density, Vp = P-wave Velocity, Mag. Sus.S2 = Point Sensor Magnetic Susceptibility).

Figure 48. Physical properties and units of Core 4 from Site 2 (WBD = Wet Bulk Density, Vp = P-wave Velocity, Mag. Sus.S2 = Point Sensor Magnetic Susceptibility).

Table 24. Multi-Sensor-Core-Logger (MSCL) specifications for event K042, 2003.

P-wave Velocity and Core Diameter	
Transducer diameter	50 mm
Transmitter pulse frequency	250 kHz
Transmitted pulse repetition rate:	1 kHz
Received pulse resolution	50 ns
P-wave travel-time offset (PTO)	5.56 µs

Wet Bulk Density	
Gamma ray source	Cs-137
Source activity	356 MBq
Source energy	0.662 MeV
Collimator diameter	2.5 mm
Gamma detector	Scintillation Counter, Type 2 (John Count Scientific Ltd.)

Magnetic Susceptibility	
Loop sensor type	MS-2C (Bartington Ltd.)
Loop sensor nominal diameter	80 mm
Alternating field frequency	0.565 kHz
Magnetic field intensity	approx. 80 A/m rms
Loop sensor correction coeff. (Krel)	0.38
Point sensor type	MS-2F (Bartington Ltd.)
Point sensor tip diameter	15 mm

Table 25. MSCL data acquisition summary (top line = core number, y = yes, n = no, WBD = Wet Bulk Density and angle of core orientation according to Figure 41, Vp = P-wave velocity and angle of core orientation according to Figure 41, MS1 = Magnetic Susceptibility loop sensor, MS2 = Magnetic Susceptibility point sensor, s = counting time in seconds).

*VB03 --> *	1/1	1/2	1/3	1/4	1/5	1/6	2/1	2/2	2/3	2/4
Core split	y	y	n	y	y	n	n	n	y	y
WBD 0°	n	n	15s	15s	15s	15s	15s	15s	15s	15s
WBD 45°	n	n	n	5s	15s	15s	10s	10s	10s	10s
WBD 90°	n	n	15s	15s	15s	15s	15s	15s	15s	15s
WBD 135°	n	n	n	5s	15s	15s	10s	10s	10s	10s
Vp 0°	n	n	y	y	y	y	y	y	y	y
Vp 45°	n	n	n	y	y	y	y	y	y	y
Vp 90°	n	n	y	y	y	y	y	y	y	y
Vp 135°	n	n	n	y	y	y	y	y	y	y
MS1	n	n	n	1s	1s	1s	1s	1s	1s	1s
MS2	1s	1s	n	1s	1s	n	n	n	10s	10s

5   SUMMARY

This report summarises data and results from the first exploratory probe beneath the McMurdo Ice Shelf (MIS) in the western Ross Sea. Two holes were cut by hot-water drill through the MIS, approximately 5 and 12 km east of the shelf edge. A third site was cut through 3 m of sea ice at the edge of the ice shelf, 5 km south of Scott Base.

	Site 1	*Site 2*	*Sea Ice*
Ice shelf thickness	70.5 m	143.7 m	-
Water depth	926 m	923 m	~600 m
Distance to shelf edge	5 km	12 km	-
Date occupied	Jan. 10-22	Jan. 23-Feb. 2	Jan. 10–Feb.3
CTD casts (time, #)	36 hrs (14)	24 hrs (10)	-
ADCP (duration)	87 hrs	47 hrs	24 days
Grab (#)	2	2	-
Core (#, max. length)	6, 61cm	4, 62cm	-

CTD - Conductivity Temperature Depth sensors.
ADCP-Acoustic Doppler Current Profiler.

The main scientific goals were to (1) survey the water column to establish the present oceanographic regime (water column structure, current speed and direction, tidal influence) and (2) sample the Quaternary sediment cover to investigate the recent ice shelf retreat history. Each HWD site was chosen on the basis of existing seismic survey data, which indicated a substantial thickness of sediment suitable for deep drilling as part of the ANDRILL project.

Current velocity, as measured by ADCP, is strongly influenced by diurnal tidal cycles, with higher current speeds occurring on flood tides. Under the ice conditions that prevailed during the data collection period, flood tides tended to flow in an anti-clockwise direction around Hut Point Peninsula and into Windless Bight, whilst ebb tides flow in the opposite direction, albeit at slower speeds. The resulting net flow is therefore from McMurdo Sound into Windless Bight. This is consistent with the composition of the seafloor sediment, which contains many diatom fragments, presumably advected under the ice shelf from the open water and seasonal sea ice cover in McMurdo Sound. Maximum current speeds of ~50, 22 and 20 cm.s^{-1} were recorded at the sea ice site, Site 1 and Site 2 respectively. The direction and speed of ocean currents is remarkably consistent throughout the water column.

Sub-bottom profiling at Site 1 was carried out using a 3.5 kHz transducer placed 2 m below the base of the shelf ice. Between the sea floor and a sub-bottom depth of 320 m 38 distinct reflectors are visible and indistinct reflectors are visible to 640 m sub-bottom depth. The unusual degree of penetration for a single transducer in depth water may be attributable to a substantial thickness of unconsolidated, muddy, sediment. However, further acoustic measurements are planned to check on this result.

Sediment cores up to 61 and 62 cm long were recovered from Site 1 and Site 2, respectively. At Site 1 the lowermost 30 cm is diamicton – a sandy terrigenous mud with scattered pebbles up to 4 cm long some of which are striated. Radiocarbon dating of acid-insoluble organic material from the diamicton yielded 3 ages, not in stratigraphic order, but grouped around 24 Kyr BP, consistent with deposition during the Last Glacial Maximum (LGM). The diamicton grades up into sandy mud with an increasing amount of biogenic silica, including a relatively diverse

90

assemblage of ocean and sea ice diatoms and sponge spicules. The lower part of this interval includes an 8-cm-thick sharp-based unit of laminated well-sorted sand that may represent a sediment gravity flow, or aeolian sediment that has melted through the ice shelf. The core is topped by a 2-cm-thick muddy sand with pebbles up to 16 mm long. Above the diamict three ^{14}C ages suggest a relatively constant sedimentation rate of ~1.6 cm/kyr. At Site 2 the entire core but for the lower 2 cm is sandy mud like the upper part of the core from Site 2 but with more (~20%) biogenic silica. The lowermost 2 cm is a pebbly diamicton with a ^{14}C age of 12 kyr BP. Above this, three additional ^{14}C ages indicate a relatively constant sedimentation rate of ~5 cm/kyr.

The pattern of sedimentation from these two cores is consistent with that observed elsewhere in the Ross Sea, where diamicton representing the last phase of deposition beneath a grounded Ross Ice Sheet grades over 1-2 cm into a relatively thin Holocene biogenic mud blanket that formed under open water (or near -open water) conditions. However, here in 900 m of water in Windless Bight the diamicton is not over-consolidated (unlike the Ross Sea sites). This suggests that although basal debris was being transported and released from glacier ice, the ice was not grounded. These findings suggest that a long, relatively complete stratigraphic record of ice sheet advance and retreat will be recovered from Windless Bight.

More detailed studies of the biogenic (silica and carbonate) content and geochemistry of these sediments have subsequently been undertaken. Diatoms are the most abundant skeletal remains and three diatom units have been recognised in the Windless Bight cores and are characterised by varying concentration, fragmentation and proportions of contemporaneous Ross Sea diatoms (>50%, 20-50% and <20%), in them. Most contemporaneous diatoms are derived from blooms under the sea ice in McMurdo Sound. Other diatomaceous material comes from glacial reworking and supports the presence of extensive grounded ice in the region during the LGM. Site 1 records the transition from this state to the present with the shelf margin a short distance seaward of Windless Bight. Although Site 1 is 5 km from the ice margin and Site 2 is only another 7 km in, contemporaneous diatoms at the latter site are more abundant and better preserved.

Radiolarians and foraminifera are relatively common in surface sediments from both Sites 1 and 2. Radiolarian assemblages are dominated by *Prunopyle antarctica* and *Antarctissa* spp., whilst foraminiferal assemblages in surface sediments are dominated by agglutinated benthic species of the genera *Reophax*, *Miliammina*, *Portatrochammina*, *Hyperammina* and *Recurvoides*. Calcareous benthic species are rare in surface sediments but exhibit a down-core increase relative to agglutinated species in the Site 1 core (0-11.5 cm below sea floor), probably due to poorer preservation of agglutinated tests in subsurface sediments. The most common calcareous genera are *Globocassidulina*, *Trifarina* and *Astrononion*. A significant occurrence of common *Globocassidulina* is noted in the lower part of the core (6-10 cm below sea floor). Rare specimens of the planktic foraminifera *Neogloboquadrina pachyderma* occur in four of six core samples.

Sediment composition, based on detailed studies of sediment geochemistry and sand fraction petrography, suggests the provenance of lithogenic material in Windless Bight is mixed. Diamict dating from the LGM contains abundant quartz, feldspar and volcanic lithic fragments. The presence of quartz, a common mineral in the Beacon Sandstone on the Trans-Antarctic Mountains, but absent in volcanoes bounding Windless Bight supports the lithological interpretation that these units are derived from basal glacial debris when the Ross Ice Shelf was grounded in the immediate vicinity. By contrast, Holocene sediments are dominated by volcanic

lithic fragments and glass with only trace amounts of quartz, indicating a predominance of material derived from volcanic rocks surrounding the Bight.

6   ACKNOWLEDGMENTS

7 APPENDICES

Only available at www.victoria.ac.nz/antarctic/

7.1 APPENDIX 1 – CTD data

HWD03-1	CAST 6	15.01.03	2151 nzdt
Depth (m)	T Deg C	S psu	Sigma T
1.595	-1.1064	20.2414	16.2047
3.563	-1.2357	22.5627	18.0827
5.497	-1.2705	23.2999	18.6795
7.378	-1.3103	23.8139	19.0957

Note: Start time and data are New Zealand Daylight Time (NZDT).

7.2 APPENDIX 2 – ADCP data

These data are provided in RD Instruments format only (although ASCII data may be added at a later date). RDI software is required to read these files.

7.3 APPENDIX 3 – Water column chemistry

Data are stored in a single EXCEL spreadsheet with filename APP4 Water column chemistry.xls

Worksheet 1 - Suspended sediment

Cast/depth range	Depth	Site	Wt (mg)	Amp(V)	Amp(V)	d15N	d13C	C:N	mg N/L	mg C/L	Run
				N	C	Air	PDB	Atomic			
P7 75-80m	75	HWD03-1	1.50	0.18	1.16	3.07	-28.35	7.81	6.89	46.13	16
P6 110-115m	110	HWD03-1	1.50	0.14	1.07	2.71	-29.29	9.54	5.19	42.49	15
P5 370-375m	370	HWD03-1	1.50	0.08	1.02	8.20	-28.30	15.68	2.98	40.06	14

Worksheet 2 – Water

Cast/ Depth range	Depth (m)	SITE	Wt (mg)	Amp(V)	Amp(V)	d15N	d13C	C:N	mg N/L	mg C/L	Run
				N	C	Air	PDB	Atomic			
P7 75-80m	75	HWD03-1	1.50	0.18	1.16	3.07	-28.35	7.81	6.89	46.13	16
P13 75-80m	75	HWD03-1	1.50	0.14	0.97	3.19	-28.95	8.30	5.29	37.70	22
P1 75-80m	75	HWD03-1	1.50	0.34	4.16	3.81	-27.81	16.20	12.18	169.19	11

7.4 APPENDIX 4 – Core grain size data

Data are stored in a single EXCEL ver 5.0 spreadsheet with filename APP5 Grain size.xls Samples from each core are reported as rows of data, and then rows of statistics (see example below from Site 1).

Frequency																
Class midpts			-2.00	-1.25	-0.75	-0.25	0.25	0.75	1.25	1.75	2.25	2.75	3.25	3.75	9.75	12.00
Class limits		-2.00	-1.50	-1.00	-0.50	0.00	0.50	1.00	1.50	2.00	2.50	3.00	3.50	4.00	10.00	Rest
00cm grab3		0.0	0.0	0.1	0.1	0.2	0.4	0.7	1.1	3.4	4.4	9.2	10.4	10.4	2.6	28.6
00cm		1.4	2.1	1.1	1.2	1.1	1.4	2.3	2.6	6.7	9.8	12.5	6.9	3.5	2.2	22.0

Statistics										Graphic (Folk)			Proportions			
		5%	16%	25%	50%	75%	84%	95%		Mean	StDev	Skew	Gravel	Sand	Silt	Clay
00cm grab3		1.9	2.8	3.3	5.9	10.7	12.8	17.1		7.2	4.8	0.4	0.1	40.2	19.8	39.8
00cm		-0.8	1.7	2.3	3.6	9.3	11.6	16.1		5.6	5.0	0.5	4.6	48.0	15.9	31.5

7.5 APPENDIX 5 – Core geochemistry data for C, $\delta^{13}C$, N, $\delta^{15}N$, SiO_2 and $CaCO_3$

Data are stored in a single EXCEL ver 5.0 spreadsheet with filename APP6 Core CNSi geochemistry.xls
See example below.

SITE 1							SITE 2						
Depth	% CO3	% Opal	Wt. % C	Wt. % N	d13C	d15N	Depth	% CO3	% Opal	Wt. % C	Wt. % N	d13C	dN15
0	0.17	10.03	0.39	0.05	-25.92	4.65	0	0.12	18.39	0.66	0.10	-26.26	4.58

| 1 | 0.20 | 12.25 | 0.37 | 0.05 | -25.87 | 4.75 | | 2 | 0.12 | 17.85 | 0.71 | 0.11 | -26.83 | 4.46 |